

The Reactivity of Mineral Dust and Soot Surfaces Towards NO₂, SO₂ and H₂O in the Temperature Range 180 to 670 K

Dissertation

submitted to

**Fachbereich Chemie
Universität Duisburg – Essen**

in partial fulfilment of the
requirements for a

**Doctor of Natural Sciences
(Dr. rer. nat.)**

**Aneta Pashkova
from
Asenovgrad/Bulgaria**

December 2006

Tag der mündlichen Prüfung: 18. 12. 2006

Vorsitzender: Prof. Dr. R. Boese

1. Gutachter: Prof. Dr. R. Zellner

2. Gutachter: Prof. Dr. A. Schönbacher

Acknowledgements

Here is the place where I would like to thank Prof. Zellner, first of all for the opportunity that he gave me to write my PhD thesis in the University of Essen, and then for his continuous support and guiding advice. These almost five years in Essen were for me fulfilled with new experience. I have learnt so much, and I am still learning. Thank you.

My very sincere thanks also to Dr. Sabine Seisel. She is the other “Doktorvater” for me and she is the person who helped me so much not only for the work but also for all the difficulties as a foreigner in Germany. Thank you, Sabine, for your patience and help.

Many thanks to all of my work colleagues from the research group of Prof. Zellner, who helped me always with good advice when I needed it, and also to my bulgarian colleagues and friends Yanka and Atanas who were always there for me.

I would also like to thank the Max-Buchner Forschungstiftung (DECHEMA e.V.) for the financial support of my work.

CONTENTS

1	INTRODUCTION	1
1.1	The Atmosphere – a dynamic system	1
1.1.1	Trace gases in the atmosphere.....	2
1.1.1.1	Nitrogen oxides (NO _x).....	4
1.1.1.2	Sulphur dioxide (SO ₂).....	8
1.1.1.3	Water vapour (H ₂ O).....	10
1.1.2	Aerosol surfaces.....	11
1.1.2.1	Mineral dust aerosols.....	13
1.1.2.2	Soot aerosols.....	14
1.2	Heterogeneous processes in the atmosphere	15
1.3	State of the art	17
1.3.1	Adsorption of water on mineral dust and soot surfaces.....	17
1.3.2	Reaction of NO ₂ with soot surfaces.....	18
1.3.3	Reaction of SO ₂ with soot surfaces.....	22
1.4	Aims of the work	23
2	EXPERIMENTAL PART	26
2.1	Knudsen cell reactor	26
2.1.1	Description of the apparatus.....	26
2.1.2	Main calculations and measurement principle.....	30
2.1.2.1	Steady state measurements.....	31
2.1.2.2	Pulsed valve measurements.....	36
2.2	Diffuse Reflectance Infrared Fourier Transformation Spectroscopy (DRIFTS)	40
2.3	Scanning Electron Microscopy (SEM)	42
2.4	Ion Chromatography	44
2.5	Substances and sample preparations	46
2.5.1	Gas phase species.....	46
2.5.2	Solid species.....	48
2.5.3	Sample preparations.....	54
2.5.4	Calibration of the mass spectrometer signals.....	55

Contents

3	RESULTS AND DISCUSSION.....	59
3.1	Adsorption of H₂O on mineral dust and soot surfaces	59
3.1.1	Adsorption of water on kerosene soot surfaces.....	60
3.1.1.1	Kinetic approach.....	60
3.1.1.2	Thermodynamic approach.....	71
3.1.2	Adsorption of water on mineral dust surfaces.....	77
3.1.2.1	Kinetic approach.....	77
3.1.2.2	Thermodynamic approach.....	83
3.1.3	ESEM measurements.....	86
3.1.4	Discussion.....	91
3.2	Reactions of SO₂ and NO₂ with soot surfaces	93
3.2.1	Reactions of SO ₂ with soot surfaces.....	93
3.2.2	Reactions of NO ₂ with soot surfaces.....	96
3.2.2.1	Sample pre-treatment.....	98
3.2.2.2	General calculations.....	100
3.2.2.3	Signal evaluation and product study.....	104
3.2.2.4	Ion chromatography (IC) results.....	108
3.2.2.5	Mechanistic interpretation of the reactions.....	109
3.2.3	Discussion.....	111
4	SUMMARY AND CONCLUSIONS.....	112
	REFERENCE LIST	114

ABSTRACT

The chemistry of atmospheric aerosol surfaces is currently not well understood. Important remaining questions concern the modification of the aerosol surfaces during ageing, the removal of trace gases from the gas phase and the processing in the hydrological cycle. Mineral dust and soot have been chosen as typical heterogeneous surfaces, which are ubiquitous in the atmosphere, and the role of which is still not very well understood. In this work these surfaces have been characterized in terms of two important issues:

Hydrophilicity of atmospheric surfaces: Hydrophilicity is a critical but difficult to quantify parameter, characterizing the possibility of aerosol particles to act as cloud/ice condensation nuclei. Therefore, adsorption and desorption rates together with the amount of water adsorbed, are important parameters in the assessment of the hydrophilicity. Regarding this issue we have studied the interaction of mineral dust and kerosene soot surfaces with water vapour in the temperature interval $203\text{ K} < T < 298\text{ K}$ using a Knudsen cell reactor. A comparison of the uptake kinetics and adsorption enthalpies of water on mineral dust and soot leads to the conclusion that water is interacting with mineral dust much stronger than with soot. In terms of the hydrophilicity concept the results suggest, that mineral dust may be regarded as hydrophilic whereas soot is hydrophobic and that fundamental kinetic and thermo-chemical parameters may be used to quantify this concept.

Reactivity of atmospheric surfaces: We have investigated two different types of soot samples (kerosene and ethene) and their behaviour towards NO_2 and SO_2 (as typical atmospheric pollutants) in a wide temperature interval between $180\text{ K} < T < 670\text{ K}$. It has been found that under these conditions SO_2 undergoes only reversible adsorption/desorption on the surface, whereas for temperatures above 300 K NO_2 adsorbs irreversibly on the surface and reacts further leading to the formation of NO and HONO as gas phase products with strongly temperature dependent yields. Complementary, for temperatures above 470 K , the formation of CO_2 as gas phase product is observed. For the mechanistic interpretation of the reaction we have found that NO_2 adsorbs irreversibly on the surface, followed by further formation of HONO or reduction to NO (depending on temperature). Additionally, due to the reduction to NO , a new oxidised surface site is formed at higher temperatures, which releases CO_2 into the gas phase, indicating the ability of NO_2 to oxidize the soot sample followed by the consumption of soot.

1 INTRODUCTION

1.1 The Atmosphere – a dynamic system

In the last century anthropogenic emissions of trace gases and aerosol particles have risen sharply and are now having a significant effect on climate, with consequences for the functioning of the Earth System [Granier et al., 2004]. In Figure 1.1-1 is summarized the global radiative forcing effect of the major pollutants in the atmosphere (source: IPCC, Intergovernmental Panel on Climate Change):

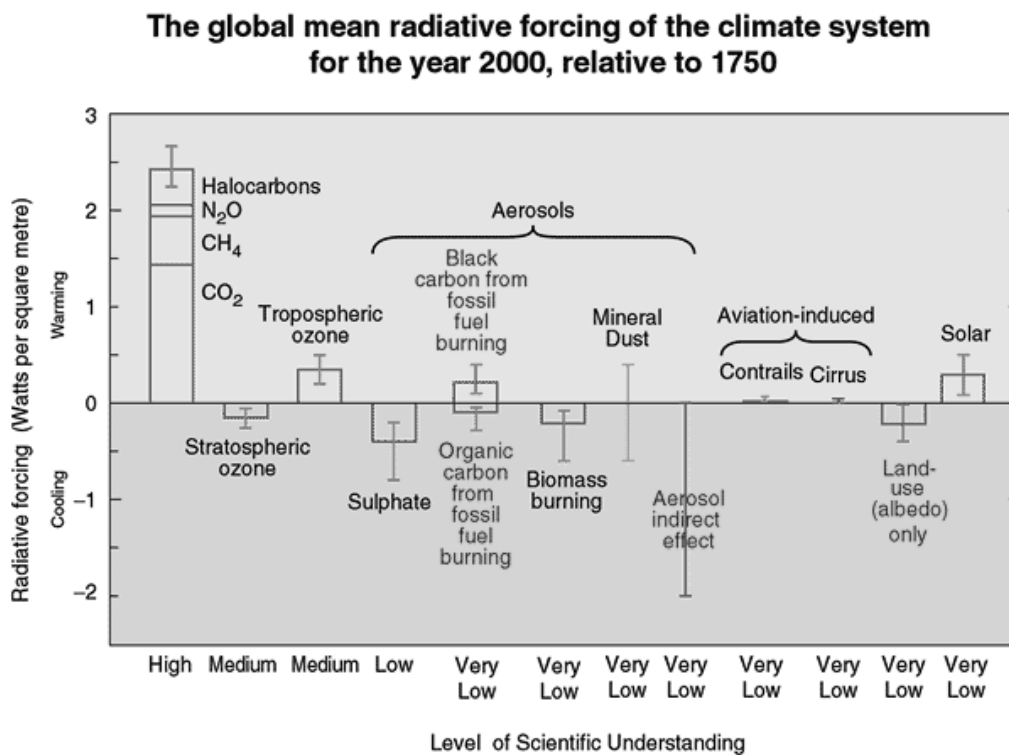


Figure 1.1-1: Global, annual mean radiative forcing (Wm⁻²) for the period from pre-industrial (1750) to present (IPCC, 2001)

Global-mean radiative forcing is a valuable concept for giving at least a first-order estimate of the potential climatic importance of various forcing mechanisms. It is basically a change imposed on the planetary energy balance, which has the potential to alter global temperature. As can be seen from Figure 1.1-1 the greenhouse gases (CO₂, CH₄, N₂O, Halocarbons), for

1. Introduction

example, intercept some of the outgoing radiation and thereby act to force the Earth's surface to come to a higher equilibrium temperature and therefore have a strongly positive radiative forcing effect.

In contrast to greenhouse gases, for example, which act only on outgoing infrared radiation, aerosol particles (AP) can influence both directions of the energy balance. The aerosol radiative effect can be *direct* or *indirect*. The *direct* effect is due to scattering and absorption of solar radiation by AP. The *indirect* effect comes from the action of AP as cloud condensation nuclei (CCN). For the latter, of great importance is the hygroscopicity of the particles, or their behaviour towards water under atmospheric conditions. Furthermore their action as CCN can increase the occurrence of clouds and change their properties. For example, an increased number of CCN modifies the size and number concentration of cloud droplets since smaller and more numerous droplets increase the cloud albedo. Another aspect of the indirect effect, concerning atmospheric chemistry, is the possibility of aerosol particles to participate in heterogeneous reactions, affecting the concentrations of trace species in the atmosphere, such as greenhouse gases and stratospheric ozone depleting compounds. Stratospheric ozone loss has been estimated to have a cooling effect [Global NEST, 2006].

Of these both effects, the direct effect is the best understood and studied. Estimates of the indirect effect are very uncertain and significant research efforts are directed toward its quantification, including ours.

1.1.1 Trace gases in the atmosphere

Throughout most of the atmosphere air acts as a carrier for a large number of trace gases. [Zellner, 1999] But the natural atmosphere is also not a stable body of gases of fixed composition. Material exchange with adjacent geochemical reservoirs, such as the oceans or the biosphere, causes a steady influx of trace gases, which are balanced by corresponding losses, either by a return flow to the same (or another) geochemical reservoir or by chemical reactions within the atmosphere. These processes keep the atmosphere in a dynamic equilibrium.

1. Introduction

One aim of atmospheric chemistry is to determine for any particular trace substance the origins (sources) and the removal mechanisms (sinks). Table 1.1-1 presents a summary of the trace gases mainly occurring in the troposphere, their mixing ratios in the air, and their origin and behaviour.

<i>Trace gas</i>	<i>Mixing Ratio</i>	<i>Distribution</i>	<i>Major Sources (Tg yr⁻¹)</i>	<i>Major Sinks (Tg yr⁻¹)</i>	<i>Residence time</i>
Methane, CH₄	1.7 ppmv rising	uniform	rice paddy fields, 70 domestic animals, 100 swamps/marshes, 200 biomass burning, 40 fossil sources, 100	reaction with OH, 490 to the stratosphere, 40 soil uptake, 30	8 yr
Hydrogen, H₂	0.5 ppmv	uniform	CH ₄ oxidation, 15 oxidation natural HC, 10 biomass burning, 10 fossil fuel use, 20	reaction with OH, 25 soil uptake, 40	2 yr
Carbon monoxide, CO	0.2 ppmv 0.05ppmv	NH SH	anthropogenic, 440 biomass burning, 770 CH ₄ oxidation, 860 oxidation natural HC, 610	reaction with OH, 2400 to the stratosphere, 100 uptake by soils, 400	1.5 m
Ozone, O₃	15-50 ppvb	low near equator rising to the poles	influx from stratosphere, 600 photochemical production, 1300	dry deposition, 650 photochemical loss, 1300	2 m
Nitrous oxide, N₂O	0.3 ppmv rising	uniform	emission from soils, 10 emission from oceans, 6 anthropogenic, 9	loss to stratosphere, 19	110 yr
Nitrogen oxides, NO_x (NO, NO₂)	30 pptv 300 pptv 5 ppb	marine air continental- remote continental- rural	fossil-fuel derived, 21 biomass burning, 8 emissions from soils, 10 lightning, 5	oxidation to HNO ₃ by OH and O ₃	2 d
Ammonia, NH₃	100 pptv 5 ppbv	marine air continental air	domestic animals, 26 emission from vegetation, 6 emissions from oceans, 9 fertilizer use, 8	dry deposition, 17 conversion to NH ₄ ⁺ aerosol and wet deposition, 36	5 d
Carbonyl sulfide, OCS	500 pptv	uniform	emission from soils, 0.3 ocean, 0.3 oxidation of CS ₂ and DMS, 0.5	uptake by vegetation, 0.4 loss to the stratosphere, 0.15	7 yr
Hydrogen sulfide, H₂S	50-90 pptv	marine air continental rural, higher in urban air	emissions from soils, 0.5 emission from vegetation, 1.2 volcanoes, 1	reaction with OH	3 d
Dimethyl sulfide, CH₃SCH₃	5-70 pptv similar	marine air continental, rural higher in urban air	emissions from oceans, 68 emissions from soils and vegetation, 2	reaction with OH reaction with NO ₃	2 d
Sulphur dioxide, SO₂	20-90 pptv 5 ppbv	marine air continental, rural	fossil fuel-derived, 160 volcanoes, 14 oxidation of sulfides, 70	dry deposition, 100 oxidation to SO ₄ ²⁻ aerosol and wet deposition, 140	4 d
Isoprene, C₅H₈	0.6-2.5 ppbv	continental surface air	emissions from deciduous trees, 570	reaction with OH	0.2 d
Terpenes, C₁₀H₁₆	0.03-2 ppbv	continental surface air	emissions from coniferous trees, 140	reaction with OH	0.4 d

Table 1.1-1: Approximate molar mixing ratios, global distribution, sources and sinks, and residence times of several important trace gases in the troposphere [Zellner, 1999]

1. Introduction

Because the substances occur in traces, mixing ratios (in dry air) are equivalent to mole fractions. For our work we are interested in the NO_x species, SO_2 , and also H_2O , which is not a trace gas due to its higher local concentrations in different parts of the atmosphere.

1.1.1.1 Nitrogen oxides (NO_x)

Nitrogen oxides (NO and $\text{NO}_2 = \text{NO}_x$) play an important role in polluted and unpolluted areas. They do not primarily act as fuel for tropospheric chemistry, but rather as a catalyst, promoting the tropospheric formation of O_3 and controlling the concentration of the OH radical, the most important oxidizing agent in the troposphere [Hernandez, 1996], [Zellner, 1999]. Both of these functions are effective in polluted as well as in background atmospheres. In their role as a catalyst, NO and NO_2 are rapidly interconverted – during daytime within a period of a few minutes. Concerning their budget and transport they are treated together as NO_x . Because of their important role in tropospheric chemistry, it is essential to know the sources and distributions of NO_x and the possible reaction mechanisms it undergoes in the atmosphere.

Sources and distribution of NO_x :

Summarized the global budget of NO_x in the troposphere is given in Table 1.1-2:

Sources	TgN yr ⁻¹	Sinks	TgN yr ⁻¹
Fossil fuel combustion	19.9 (14 – 28)	Wet deposition of NO_3^- (land)	19.0 (18 – 30)
Biomass burning	12.0 (4 – 24)	Wet deposition of NO_3^- (ocean)	8.0 (4 – 12)
Release from soils	20.2 (4 – 40)	Dry deposition of NO_x	16.0 (12 – 22)
Lightning discharges	8.0 (2 – 20)		
NH_3 oxidation	3.0 (0 – 10)		
Ocean surface	< 1.0		
Aircraft	0.5		
Injection from the stratosphere	0.1 (0.5 total NO_y)		
Total sources	64.0 (25 – 112)	Total sinks	43.0 (24 – 64)

Table 1.1-2: Global budget of NO_x in the troposphere [Brasseur et al., 1999]

The largest production of NO_x in the present atmosphere most likely results from fossil fuel combustion (approximately 20 TgN yr⁻¹), biomass burning (12 TgN yr⁻¹) and emission from

1. Introduction

soils (20 TgN yr^{-1}). NO_x is also formed by lightning. The magnitude of this source, however, is uncertain and estimated to vary from 2 to 20 TgN yr^{-1} . The release of NO_x by aircraft engines in the troposphere and lower stratosphere leads to an additional source of approximately 0.5 TgN yr^{-1} (in 1990). As the size of the fleet of subsonic aircraft is increasing and as development of high-altitude (15 to 20 km) supersonic transport is planned, this source is likely to increase in the future.

Major sinks of the NO_x species are the so called wet and dry deposition processes. NO_x is rapidly oxidized in the troposphere to nitrates that are soluble and removed from the atmosphere by wet deposition. The NO_x species are also directly taken up by plants over the continent which is the so called dry deposition [Brasseur et al., 1999].

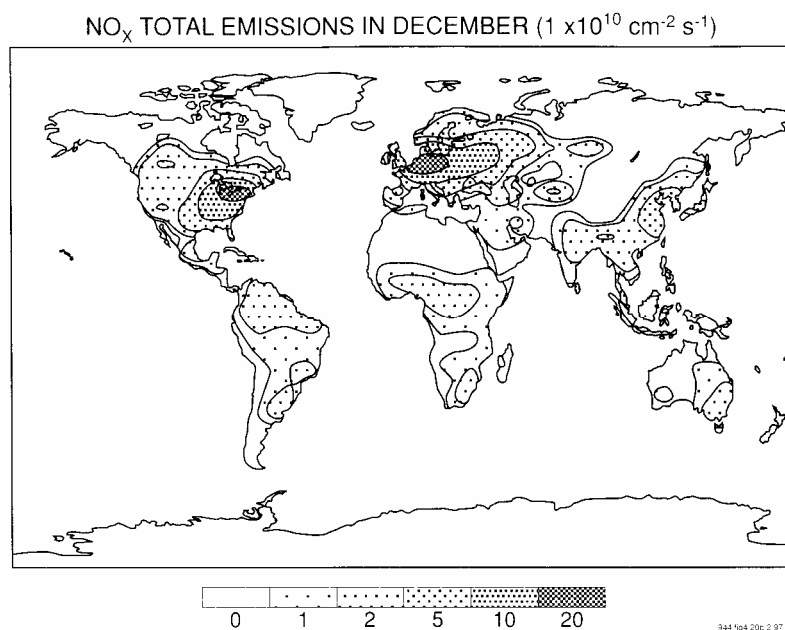


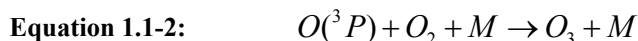
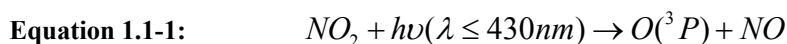
Figure 1.1-2: Surface emission ($10^{10} \text{ molecules cm}^{-2} \text{ s}^{-1}$) of NO_x on the global scale in December 1992. Contributions of fossil fuel combustion, biomass burning and soil emissions are included at spatial resolution $5^\circ \times 5^\circ$ [Brasseur et al., 1999]

In Figure 1.1-2 is represented the global distribution of surface NO_x emissions for December 1992. It can be clearly seen that the contours of the highest emissions outline the areas with high industrial activity in North America, Europe, and the Far East. It can also be seen the strong emissions from large sources in the tropics. On the contrary, the oceans are only a minor source of NO_x and it is assumed that emissions from the oceans are vanishing small, and all the sources are located on the continents.

1. Introduction

Tropospheric chemistry of nitrogen monoxide (NO):

Nitric oxide (NO) is mostly emitted and transformed in the atmosphere into NO₂, whose photolysis is the only known way of producing O₃ in the troposphere, according to the reactions [Finlayson-Pitts and Pitts, 1986]:

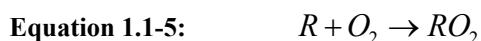


where M is the collisional stabilizer (mainly N₂ and O₂). However, NO is also the main sink of O₃:

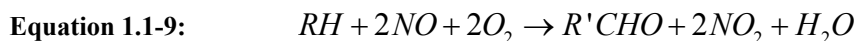


These three reactions (Equation 1.1-1, Equation 1.1-2 and Equation 1.1-3) achieve a steady state (the Leighton relationship) within a timescale of minutes, which does not lead to any net formation of O₃.

If the conversion of NO to NO₂ takes place in the presence of organics, deviations from the equilibrium mechanism (Equation 1.1-1, Equation 1.1-2 and Equation 1.1-3) occur [Nelson and Haynes, 1994]. The organic compounds are normally attacked by OH radicals, whereupon carbon containing radicals are formed:



where R is a general organic radical and R' has one H less than R, RO₂ is peroxy radical, RO is oxy radical. The net reaction can be given with:



The OH radical is not consumed in this process, so the rate is determined essentially by the steady state concentration of OH, determined by sources (O₃) and sinks (largely NO and NO₂).

A complementary mechanism of destruction of O₃ is observed in NO poor environments. When the ratio of the NO/O₃ concentrations is less than about 2·10⁻⁴, ozone is consumed and CO₂ is generated, due to the chain reactions:



1. Introduction

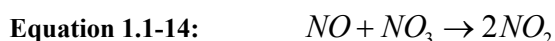


A possible reaction for a net source of NO₂, and respectively of O₃, is the termolecular reaction [Hernandez, 1996]:



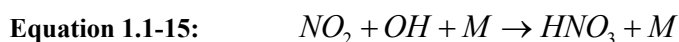
Although too slow (second order in NO of the reaction rate), to be of an importance for the atmosphere, this reaction might be possible at higher concentrations of NO for instance in uncontrolled power plant emissions.

NO reacts also very rapidly with the NO₃ radical, which has a significant role for the chemistry of the troposphere at night [Hernandez, 1996]:

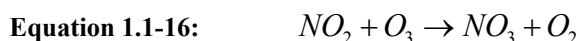


Tropospheric chemistry of nitrogen dioxide (NO₂):

NO₂ is mainly formed from NO oxidation, and represents a small proportion of the NO_x emissions. Once in the atmosphere, it can undergo different processes. During daylight hours the most important reactions are photolysis (Equation 1.1-1, Equation 1.1-2 and Equation 1.1-3) and the reaction with the OH radical leading to HNO₃:

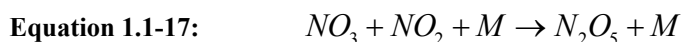


The nitrate radical is formed from the reaction of NO₂ with O₃:



NO₃ is rapidly photolysed ($560 < \lambda < 650$ nm), but at night time and in the absence of NO, it is an active oxidizing agent. It can react with variety of organics by addition to the unsaturated bonds and by hydrogen abstraction, being in the latter case the precursor of nitric acid [Hernandez, 1996].

The NO₂ reaction with the NO₃ leads to nitric acid:



The last (hydrolysis of N₂O₅) is a rapid process [Russel et al., 1985], [Wayne et al., 1990] that can take place in the liquid water present in fog or aerosols. It can also take place on ice surfaces [Seisel et al., 1998], [Wayne, 1991]

1. Introduction

One of the most important reservoirs of NO_2 is peroxyacetyl nitrate (PAN). It is the product of the temperature dependent reaction of NO_2 with the peroxyacetyl radical, formed from the OH attack on acetaldehyde and subsequent oxygen addition:



The rate constant for PAN decomposition is strongly temperature dependent. PAN is removed only slowly by dry and wet deposition processes, and by chemical attack. Once formed in polluted areas and if transferred above the boundary layer where the temperatures are low enough to prevent its decomposition, it can be transported over long distances. An increase in the temperature as a consequence of downmixing, for example, causes the release of NO_2 , which is then effectively transported [Singh, 1987]. Other organic nitrate products formed following a similar mechanism are peroxypropionyl nitrate (PPN) and peroxybenzoyl nitrate (PBzN).

Kinetically the most important processes which lead to a permanent loss of NO_2 are the HNO_3 forming reactions, with OH during the day and with O_3 and NO_3 at night.

1.1.1.2 Sulphur dioxide (SO_2)

Sources and distribution of SO_2 :

Sulphur dioxide is emitted by three main sources [Hernandez, 1996]:

- *Anthropogenic* - direct emission of sulphur dioxide from *anthropogenic activities*, primarily the combustion of fossil fuels in power plants and the smelting of non-ferrous metal ores. In EDGAR 3.2 the total global anthropogenic emissions of SO_2 for 1990 have been estimated at about 155 Tg, with a slowly decreasing trend in subsequent years (141 Tg for 1995, represented in Table 1.1-3).

The decrease is mainly due to controlled measures implemented in the EU and the USA and to declining economy of the former SU countries. Decreases in power generation and industrial combustion in the former SU countries, compensates for the higher growth of SO_2

1. Introduction

emissions in Asia, which showed an average 5-year growth rate of about 30% in the 1990 – 1995 timeframe.

	Total	Canada	USA	EU	Oceania	Japan	Eastern Europe	Former SU	Latin America	Africa	Middle East	South Asia	East Asia	South East
Fossil fuel	111.2	2.2	17.1	11.4	1.0	1.5	8.9	13.0	4.9	3.8	5.1	5.4	34.0	3.0
Biofuel	2.9	0.0	0.0	0.0	0.0	0.0	0.0	0.0	0.1	0.6	0.0	1.5	0.5	0.1
Industr. processes	25.0	0.4	1.0	5.0	0.5	0.6	1.6	3.0	4.4	1.3	0.5	0.5	5.7	0.5
Agriculture	0.2	0.0	0.0	0.0	0.0	0.0	0.0	0.0	0.0	0.0	0.0	0.0	0.0	0.0
Biomass burning	2.5	0.2	0.0	0.0	0.1	0.0	0.0	0.0	0.7	1.1	0.0	0.0	0.0	0.2
Waste handling	0	0.0	0.0	0.0	0.0	0.0	0.0	0.0	0.0	0.0	0.0	0.0	0.0	0.0
Total	141.9	2.8	18.1	16.5	1.7	2.2	10.5	16.0	10.1	6.9	5.7	7.5	40.2	3.8

Table 1.1-3: Sources and regional contribution of emissions of SO₂ in 1995 (Tg). Source: EDGAR 3.2

-Volcanoes – significant natural source of SO₂ to the troposphere. Part of the emitted SO₂ is converted into sulphuric acid upon entering in the atmosphere, as a result of the reaction with the hot volcanic gases with oxygen. Estimates of SO₂ emissions from volcanoes are based on correlation of direct flux measurements with the intensity of volcanic activity and an extrapolation to the active volcanoes in the world. [Berresheim and Jaeschke, 1983] estimated a total average annual emission of 7.5 Tg of sulphur.

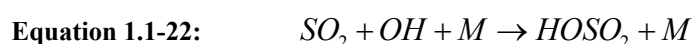
-Oxidation of organic sulphides – carbonyl sulphide (COS), carbon disulphide (CS₂) and dimethyl sulphide (DMS), by reaction with radicals. The mechanisms and the effectiveness of the formation processes are still a subject of investigation.

Tropospheric chemistry of SO₂:

Gas phase SO₂ is removed by deposition, oxidation and heterogeneous reactions with aerosols or clouds. The oxidation of SO₂ can occur in the gas phase, in fog and cloud droplets and on the surface of aerosol particles. Due to the very low vapour pressure of the sulphuric acid produced in this oxidation, it is transferred to the aerosol or cloud phases. These two types of oxidation are briefly described:

a/ Gas phase reactions

Potential SO₂ oxidants are the radicals OH, HO₂, RO₂ and the intermediates produced in the reaction of ozone with alkenes [Hernandez, 1996]. The best known and probably the only fast and efficient of these gas phase processes is the reaction of SO₂ with OH radicals:



1. Introduction

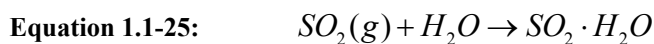


The reactions of SO_2 with O_3 and excited O_2 molecules, as well as its direct gas phase photooxidation are insignificant under typical tropospheric conditions.

b/ Aqueous phase reactions

Since clouds, fogs and rain have much higher liquid water content than particles, they contribute more to atmospheric aqueous phase oxidations. However, the rate of oxidation can increase in the liquid phase of the particles, as a consequence of the possibility of higher concentrations of solutes.

In the presence of a liquid phase, a part of SO_2 is dissolved:



and the HSO_3^- and SO_3^{2-} formed can be oxidized by O_2 , O_3 , H_2O_2 or Fe^{3+} ions.

1.1.1.3 Water vapour (H_2O)

Water vapour enters the atmosphere by evaporation from the ocean and transpiration of land plants and leaves it through various types of precipitation. Water is also unique among atmospheric molecules because it changes phase at terrestrial temperatures. This means that it can transfer energy from its frozen form at the poles to its liquid and vapour forms in the atmosphere. The distribution of water in the atmosphere varies strongly with time, location and height. It is also mainly driven by physical processes and only slightly affected by human activities, which makes it difficult to model [Brasseur et al., 1999]. On the average the mixing ratio of H_2O is typically 1% at the surface (in the troposphere), but is only a few ppmv in the stratosphere [Brasseur et al., 1999]. The dryness of the stratosphere arises from the fact that, as air is transported upward by the Hadley cell in the tropics, condensation and precipitation provide an efficient dehydration mechanism.

Water vapour condenses to form liquid drops when its vapour pressure exceeds the saturation point. In the troposphere, where the temperature decreases with increasing altitude, an air parcel nearly saturated with moisture will lose water by condensation and become

1. Introduction

increasingly drier as it rises from the ground to the tropopause. The lowest temperature in the troposphere of about 210 K occurs at the tropical tropopause. This temperature essentially determines the mixing ratio of water vapour in the lower stratosphere. The mean mole fraction of water vapour consequently decreases with altitude from about 7% over the tropical oceans to about 3 ppm in the lower stratosphere [Zellner, 1999].

Water plays also an important role for the chemistry of the atmosphere [Raschke and Warrach, 2001]. For example the water vapour molecules are the major source of the hydroxyl radical (OH) – one of the most important oxidation agents in the atmosphere. Water vapour affects the budget of ozone in the troposphere, lower stratosphere and mesosphere. In the troposphere, chemistry and photochemistry are directly affected by water droplets within clouds, while in the stratosphere, polar stratospheric clouds initiate heterogeneous chemical reactions that lead, for example, to the formation of the Antarctic ozone hole [Wayne, 1999].

1.1.2 Aerosol surfaces

In addition to trace gases the atmosphere contains a mixture of solid and liquid materials in the form of finely dispersed particles – aerosols [Zellner, 1999]. Aerosols in the atmosphere have several important environmental effects [Jacob, 1999]. In urban environments, they are a respiratory health hazard at the high concentrations found. They scatter and absorb visible radiation and hence limit visibility. They affect the Earth's climate both directly (by scattering and absorbing radiation) and indirectly (by serving as nuclei for cloud formation). They provide sites for surface chemistry and condensed-phase chemistry to take place in the atmosphere.

Primary aerosols are solid or liquid particles that are ejected directly into the atmosphere by processes like wind suspension, wave breaking and bubble bursting, leaf abrasion, burning of vegetation and of fossil fuels (eg. diesel smoke), volcanoes, agriculture industry. *Secondary* aerosols are solid or liquid particles that are created in the atmosphere after chemical or physical transformations of precursor gases. The precursor gases become particles by phase changes (condensation from gas to liquid), adsorption onto pre-existing particles, chemical reactions with other gases that produce particles, and absorption into water droplets.

1. Introduction

In Figure 1.1-3 illustrates the different processes involved in the production, growth and eventual removal of secondary aerosol particles [Jacob, 1999]. Gas molecules are typically in $10^{-4} - 10^{-3}$ μm size range. Clustering of gas molecules (nucleation) produces ultrafine aerosols in the $10^{-3} - 10^{-2}$ μm size range. These ultrafine aerosols grow rapidly to the $0.01 - 1$ μm fine aerosol size range by condensation of gases and coagulation. Growth beyond 1 μm is much slower because the particles are by then too large to grow rapidly by condensation of gases, and because the slower random motion of large particles reduces the coagulation rate. Aerosol particles originating from condensation of gases tend therefore to accumulate in the $0.01 - 1$ μm size ranges, often called the accumulation mode (as opposite to the ultrafine mode or coarse mode). These particles are too small to sediment at a significant rate, and are removed from the atmosphere mainly by scavenging by cloud droplets and subsequent rainout or direct scavenging by raindrops. These particles are too small to sediment at a significant rate, and are removed from the atmosphere mainly by scavenging by cloud droplets and subsequent rainout or direct scavenging by raindrops.

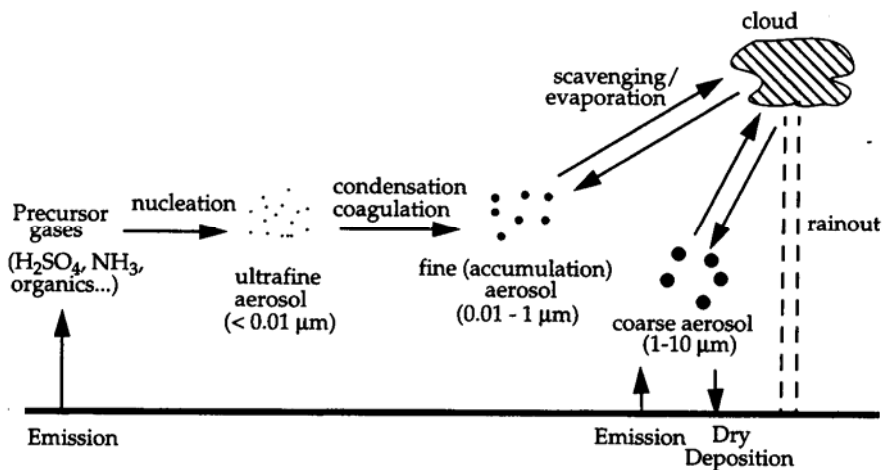


Figure 1.1-3: Production, growth and removal of secondary aerosol particles [Jacob, 1999]

The bulk of the atmospheric aerosol mass is present in the lower troposphere, reflecting the short residence time of aerosols against deposition (~ 1 to 2 weeks). Aerosol concentrations in the upper troposphere are typically 1 to 2 orders of magnitude lower than in the lower troposphere. In Table 1.1-4 summarized are given the typical number and mass concentrations of the ground level atmospheric aerosol in different tropospheric regions [Jaenicke, 1993].

The stratosphere contains, however, a ubiquitous $\text{H}_2\text{SO}_4\text{-H}_2\text{O}$ aerosol layer at $15 - 25$ km altitude, which plays an important role for the stratospheric ozone chemistry. The lifetime of the stratospheric aerosols is also much longer than in the troposphere because of the lack of precipitation.

1. Introduction

Normally, due to the scattering ability of the small droplets formed from the aerosol particles in clouds, they contribute to the cooling of the atmosphere. However, some aerosol particles, like soot and large amounts of mineral dust, may absorb solar and long wave radiation and have the potential to retain energy in the lower atmosphere, thus contributing to the greenhouse effect [Schulz, 2001]. Therefore, for our work we have chosen to investigate mineral dust and soot as typical abandoned aerosol surfaces, but with still not in details studied effects from an atmospheric point of view.

Aerosol location	Number density (m ⁻³)	Mass concentration (µg m ⁻³)	Mean particle radius (µm)
Urban	10 ¹¹ – 10 ¹²	~ 100	0.03
Rural continental	1.5·10 ¹⁰	30 – 50	0.07
Marine background	(3-6)·10 ⁸	~ 10 ^b	0.16
Arctic (summer)	2.5·10 ⁷	~ 1	0.17
Stratosphere	1·10 ⁶		

^b includes 8 µg m⁻³ sea salt

Table 1.1-4: Typical mass and number concentrations of different atmospheric aerosols, and corresponding mean particle radius, assuming an average mass density of 1.8 kg dm⁻³ and spherical particles [Jaenicke, 1993]

1.1.2.1 Mineral dust aerosols

The mineral dust aerosol represents one of the largest fractions of the global aerosol. It contains mainly windblown soil from the arid areas of the planet – the great deserts. Indeed, it consists mainly of different nonsoluble soil minerals such as quartz, calcite, gypsum, and clays. [Desboeufs et al, 1999]. Its annual emission rate is estimated from 200 to 5000 Tg [Schulz, 2001], [Jonas and Rohde, 1995], [d’Almedia, 1986], [Tegen and Fung, 1994], [Ginoux et al, 2001]. Because of its small size the fraction under 2 µm can be transported over long distances [Gomes and Gilette, 1993], [Husar et al.2001] and into higher altitudes by convection. In the source regions it can remain for several days in the atmosphere [Tabazadeh et al., 1998], [Guelle et al. 2000].

Although the dust particles are very abundant in the atmosphere, the role of mineral aerosol in atmospheric chemistry is currently not well understood. Dust aerosols may be potential reactive surfaces for heterogeneous chemistry as well as a vehicle for transportation of trace gases through the atmosphere. [Umann et al. 2005], [Karagulian et al. 2006], [Bian and

1. Introduction

Zender, 2003]. It is also found to be efficient nuclei for inducing cloud droplet and cirrus cloud formation [De Mott et al., 2003], [Hung et al., 2003].

1.1.2.2 Soot aerosols

Soot is emitted into the atmosphere from a wide range of combustion sources, of which engine emissions and biomass burning are the largest [Seinfeld and Pandis, 1998], [Rose et al., 2005], [Johnson et al., 2005], [Hendricks et al., 2004]. In the lower troposphere, especially in urban areas, mass densities of up to $10 \mu\text{g m}^{-3}$, mainly emitted by diesel engines, can be found [Israel et al., 1996]. In the upper troposphere soot particles, emitted by aircraft engines, have low average mass densities of 1ng cm^{-3} , corresponding to a number density of 0.1cm^{-3} [Blake and Kato, 1995], [Petzold et al., 1998]. However in the exhaust plume of jet aircraft number concentrations of $3 \cdot 10^7$ can be reached [Petzold et al., 1999], leading to extremely high local loads.

Soot is one of the most important components in atmospheric aerosols. The reason for this fact is manifold. It affects the optical properties of the aerosol, because it is the most efficient particulate light absorber [Horvath, 1993] which may decrease the single scattering albedo of the aerosol leading to atmospheric warming [Haywood and Shine, 1995]. There is also some evidence that soot can act as an efficient nucleation site for ice formation in the atmosphere (formation of persistent contrails [Project PAZI, Cologne 2003]) and hence it plays a significant role in the development of the ice phase in clouds, again influencing the planetary reflectance and also precipitation processes. [Hagen et al., 1989], [Popovitcheva et al., 2003a], [Popovitcheva et al., 2004], [Lammel and Novakov, 1995].

On the other hand, soot is believed to play a significant role in aerosol-induced health effects [Pope and Dockery, 1999], [Donaldson et al., 2001], [Ye et al., 1999]. Soot particles are neither water- nor lipid-soluble and have thus a completely different effect on health than water-soluble compounds [Kreyling and Scheuch, 2000].

1.2 Heterogeneous processes in the atmosphere

Gas phase chemistry is much better studied in terms of the processes contributing to the degradation and eventual removal of environmental chemicals from the atmosphere (in previous chapters discussed in some detail for NO₂ and SO₂) than heterogeneous chemistry. Heterogeneous processes of atmospheric relevance were first discovered to be important in the polar winter stratosphere, where they occur on either solid or supercooled liquid aerosols. These reactions convert chlorine and bromine reservoir species into photoactive halogen compounds, and N₂O₅ into particle bound nitric acid, thus setting the scene for the well known chlorine and bromine catalysed destruction of ozone under the action of sunlight. [Schurath and Naumann, 1998], [Zellner, 1999].

Heterogeneous reactions of trace gases on particulate matter must also be considered in the troposphere, particularly in the polluted boundary layer where aerosol particles are most abundant [Warneck, 1988]. As heterogeneous should be considered only those trace gas reactions, which involve adsorption of reactants at phase boundaries, i.e. on solid surfaces of dry particles at low relative humidities, or on ice crystals, or at the gas/liquid interface, although examples for the latter type of heterogeneous interaction are scarce [Mertes and Wahner, 1995]. Furthermore, some non-volatile environmental chemicals already exist in the atmosphere as aerosols, or adsorbed on the surface of particulates [Weingartner et al., 1997].

Table 1.2-1 combines, in the form of a matrix, various reactive species in the gas phase with various types of condensed particulate matter which may be important under atmospheric conditions. The entries in the table give short-hand information about the state of knowledge (or ignorance) with respect to each interaction [Schurath and Naumann, 1998].

From Table 1.2-1 is clear that in the case of heterogeneous atmospheric processes some questions still remain uncertain:

- i. Can the heterogeneous processes modify the surface of the particulate matter in order to change (shorten) their residence time in the atmosphere;
- ii. Can the particulate matter be degraded (e.g. oxidised and/or volatilised) by surface chemical reactions with species from the gas phase

In the case of the two types of surfaces – mineral dust and soot – which are considered here, the following points have been specifically addressed:

1. Introduction

i. We have tried to estimate how the interaction with water would change the surface of the particles in terms of hydrophilicity, in order to activate these particles for further nucleation processes.

ii. We have also tried to estimate if it is possible for NO₂ and SO₂ to oxidise soot particles and remove them from the atmosphere

substrate reactant	Diesel or aircraft soot	Mineral dust	Particles coated with organics	Sulphates, nitrates, bisulphates	Deliquescent sea salt particles	Sulphuric acid droplets	Cloud droplets, ice particles
OH	reactive loss, likely	unknown	H abstraction, addition	unknown	reactive loss likely	uptake?	uptake?
HO₂	reactive loss	unknown, may depend on composition	uptake and reaction?	unknown	uptake and reaction, likely		uptake, loss on surface
RO₂	reactive loss, likely	unknown	uptake	unknown	solubility limited uptake?		solubility limited uptake
O₃	reactive loss, surface ageing, competition?	unlikely to be important but unknown	reaction depending on structure	unknown	importance of direct uptake to be established		fast reactive loss, solubility limited
NO₂	chemisorption, reduction, HONO formation	HONO formation?	nitration, more likely by N ₂ O ₅ /NO ₂ ⁺	unknown	CINO formation on dry NaCl		HONO formation on ice? On water?
NO₃	reactive loss	unlikely to be important but unknown	reaction, e. g. with aromatics	unknown	solubility limited reaction with I, etc.		solubility is low
N₂O₅	hydrolysis or reaction as NO ₂ ⁺ depending on the substrate, reaction probabilities seem to be very variable, formation of particulate nitrate or gaseous HNO ₃				CINO ₂ , other halogen compounds formed	hydrolysis	
SO₂	catalytic oxidation, slow	catalytic oxidation, likely			oxidation in polluted marine atmosphere	unimportant	oxidation by H ₂ O ₂ , ozone, etc.
other relevant processes	chemisorption of radicals at radical sites	solubilisation of catalytic metals	gas to particle conversion, particle coating	pH dependent uptake of acidic/alkaline gases		uptake of ammonia, change pH	aerosol processing, interface phenomena

Table 1.2-1: Possible reactions of reactive gaseous species with various types of condensed particulate matter

1.3 State of the art

1.3.1 Adsorption of water on mineral dust and soot surfaces

For the interaction of water with natural mineral dust only one kinetic study at 298 K by [Seisel et al., 2004a] exists. In this study a high first-order adsorption rate constant of 6 s^{-1} and low desorption rate constant of $1.7 \cdot 10^{-3} \text{ s}^{-1}$ have been derived, indicating substantial water flux to the surface. In addition, a high number of surface sites for water adsorption is inferred. These observations lead to the conclusion that mineral dust may be regarded as hydrophilic. To our knowledge, however, the interaction of water with mineral dust has not yet been studied at temperatures below 298 K.

Instead, several studies under equilibrium condition at $273 \text{ K} \leq T \leq 298 \text{ K}$ have been reported for the interaction of water with individual clay minerals [Cases et al., 1992], [Dios Cancela et al. 1997], [Kalafi and Blanchard, 1999], [Cantrell and Ewing, 2001]. Mechanistically it was found, that the adsorption of water onto clay minerals consists of water adsorption on the external surface of the minerals at low relative humidity followed by sorption of water into the interlamellar space of the clay mineral. The first of these processes may be accompanied by a strong increase of the surface area of the clay mineral, since aggregates of particles (tactoids) may break up into smaller sized particles upon water adsorption [Cases et al., 1992]. The filling of the interlamellar space on the other hand strongly depends on the exchangeable cations present in the clay mineral [Dios Cancela et al. 1997]. As a consequence, measured adsorption isotherms have a complex shape [Cases et al., 1992] and differential heats of adsorption and desorption vary with the amount of water adsorbed by up to one order of magnitude [Dios Cancela et al. 1997], [Kalafi and Blanchard, 1999], [Cantrell and Ewing, 2001]. In addition, Monte Carlo simulations of the interaction of water with different clay minerals [Hensen et al., 2001], [Delville, 1995] show that the adsorption energies as well as the structure of the adsorbed water strongly depend on the counter ion in agreement with the experimental studies.

A number of studies on the interaction of water with soot surfaces at room temperature have been reported in the literature [Rogaski et al., 1997], [Chughtai, 1999a; 1999b; 2002], [Popovitcheva et al., 2001; 2003b], [Alcala-Jornod et al. 2000, 2002], [Seisel et al., 2004a]. From measurements performed under equilibrium conditions important information on the

1. Introduction

adsorption mechanism could be inferred [Chughtai, 1999a, 1999b, 2002], [Popovitcheva et al., 2003b]. At low relative humidities chemisorption is the dominant adsorption process which is strongly increasing with the number of oxidised surface groups [Chughtai, 2002]. Once a monolayer is completed, further water adsorption occurs in the micropores of the soot followed finally by multilayer adsorption at relative humidities above 80% [Chughtai, 1999a]. Kinetic data for the interaction of water with different kinds of soot have been derived by non-equilibrium studies at relative humidities far below 1% [Seisel et al., 2004a], [Rogaski et al., 1997], [Chughtai, 1999a; 1999b; 2002], [Popovitcheva et al., 2001; 2003b], [Alcala-Jornod et al. 2000, 2002]. The uptake of water has found to be reversible [Seisel et al, 2004], [Rogaski et al., 1997] and initial uptake coefficients between $1 \cdot 10^{-4}$ and $4 \cdot 10^{-3}$ have been obtained [Seisel et al, 2004], [Alcala-Jornod et al. 2000, 2002], [Rogaski et al., 1997], [Popovitcheva et al., 2001].

However, studies of the interaction of water with soot particles at temperatures below 298 K as relevant for most parts of the troposphere are scarce. To our knowledge only two studies exists which, however, are in contradiction. [Popovicheva et al., 2001] measured adsorption isotherms and uptake coefficients of water on soot between 295 K and 250 K and observed a decrease of the amount of water adsorbed on the soot surface as well as a decrease of the uptake coefficient with decreasing temperature. In contrast, Alcala-Jornod et al [Alcala-Jornod et al. 2002] found that the initial uptake coefficient of water increased with decreasing temperature. In addition, the residence time of water on the surface increased by two to three orders of magnitude whilst lowering the soot surface temperature from 298 K to 193 K.

1.3.2 Reaction of NO₂ with soot surfaces

The reaction of NO₂ with soot has been extensively investigated in the laboratory with diverse laboratory methods, under different experimental conditions, with soot samples originating from gas as well as liquid fuels and produced under different combustion conditions.

The reaction between NO₂ and soot has been investigated with different laboratory techniques including: low pressure reactor – Knudsen cell [Stadler and Rossi, 2000], [Tabor et al., 1994], [Salgado and Rossi 2002], [Grassian, 2001], [Al-Abdaleh and Grassian, 2000] and molecular diffusion tube (MDT) – [Alcala Jornod et al., 2000]; flow tube reactor - [Longfellow et al.,

1. Introduction

1999], [Lelievre et al., 2004]; aerosol chamber studies – [Saathoff et al., 2001]; TPD - MS analysis - [Jeguirim et al., 2004], [Muckenhuber and Grothe, 2006]; FTIR Spectroscopy [Chughtai et al., 1990a, 1990b], [Al-Abdaleh and Grassian, 2000]; DRIFTS Spectroscopy [Muckenhuber and Grothe, 2006]; filter experiments [Kleffmann and Wiesen., 2005]; diode laser spectroscopy [Kleffmann et al., 1999]

Most of the references found describe the reaction of NO₂ with soot at ambient temperature [Saathoff et al., 2001], [Alcala Jornod et al., 2000], [Stadler and Rossi, 2000], [Tabor et al., 1994], [Salgado and Rossi 2002], [Grassian, 2001], [Al-Abdaleh and Grassian, 2000], [Kleffmann et al., 1999] but in some other studies the temperature dependence is investigated [Longfellow et al., 1999], [Chughtai et al., 1990a], [Jeguirim et al., 2004], [Lelievre et al., 2004], [Muckenhuber and Grothe, 2006].

A very good summary of the literature data for the uptake coefficients of NO₂ on soot for the period 1993 – 2004 is given by [Lelievre et al., 2004]. It is apparent that of great importance for the uptake coefficient values reported is the surface area of the sample. The values for γ referenced to the geometric surface area vary between $1.0 \cdot 10^{-1}$ and $1.2 \cdot 10^{-3}$ [Tabor et al., 1993, 1994], [Rogaski et al., 1997], [Gereke et al., 1998], [Longfellow et al., 1999], [Stadler and Rossi, 2000], [Salgado and Rossi, 2002] and these, calculated with the BET surface area of the sample vary from $1.2 \cdot 10^{-5}$ to $2.4 \cdot 10^{-8}$ [Kleffmann et al., 1999], [Kirchner et al., 2000], [Al-Abadleh and Grassian, 2000], [Stadler and Rossi, 2000], [Saathoff et al., 2001], [Lelievre et al., 2004]. This is due to the fact that the geometric surface area represents a lower limit for the surface involved in the heterogeneous reaction and the values of γ are upper limits, respectively. In terms of the temperature dependence of the uptake coefficients they are found to be temperature independent for the interval 240 – 350 K [Lelievre et al., 2004], and for the two temperatures investigated – 295 and 262 K [Longfellow et al., 1999].

In some earlier studies [Akhter et al., 1984], [Chughtai et al., 1994] NO, N₂O, CO as gas phase products from the reaction of soot with NO₂/N₂O₄, have been reported. For these studies the reaction was performed at 333K and with hexane soot, which was characterized as predominantly aromatic with oxygen containing functional surface groups [Smith and Chughtai, 1995]. [Tabor et al., 1994] found that the only major product resulting from the heterogeneous interaction with three different carbon samples at ambient temperature was NO, resulting from redox type chemistry on the surface of the amorphous carbon. They also

1. Introduction

found that the rate of conversion of NO₂ to NO differs greatly between the three carbon samples investigated. Similar 100% conversion of NO₂ to NO on commercial soot is reported by [Rogaski et al., 1997]. [Jeguirim et al., 2004] also found as main gas phase product NO, but they also report that the NO₂ adsorption leads to the formation of oxygen and nitrogen surface complexes such as $-C(O)$ and $-C(ONO_2)$, analysed by TPD measurements. From TPD-MS and DRIFTS investigations [Muckenhuber and Grothe, 2006] also suggest the formation of new acidic surface functional groups due to the reaction of NO₂ with soot surfaces, decomposing to CO₂ and NO upon heating. In another studies [Al-Abdalah and Grassian, 2000] and [Kirchner et al., 2000] the surface products formed due to the reaction of NO₂ with soot are investigated with FTIR spectroscopy. They observe formation of surface species like R-ONO, R-NO₂ and R-O-NO₂.

In some recent studies HONO is reported as an important gas phase product from the interaction of soot particles with NO₂ [Ammann et al., 1998a, 1998b], [Gerecke et al., 1998], [Longfellow et al., 1999], [Kleffmann et al., 1999], [Al-Abdalah and Grassian, 2000], [Alcala Jornod et al., 2000], [Stadler and Rossi, 2000], [Salgado and Rossi 2002], [Lelievre et al., 2004]. For example [Gerecke et al., 1998] have observed simultaneous formation of HONO and NO by the uptake experiments of NO₂ on ethylene, acetylene and toluene soot and the branching ratio for these two products have been found to be a function of the soot sampling position within the flame – with increasing distance of the flame base the HONO yield decreases. On the other hand in the study of [Lelievre et al., 2004], the HONO yield was found to be independent of the soot sampling position. Both [Lelievre et al., 2004] and [Longfellow et al., 1999] observed similar HONO yields for the different types of soot investigated, from 13±5 to 30±5 %. [Longfellow et al., 1999] investigated methane, propane, kerosene and hexane soot and [Lelievre et al., 2004] used toluene, kerosene and hexane soot for their studies. Both research groups, however, found that the HONO yield is temperature dependent – [Lelievre et al., 2004] investigated it for the interval 240 – 350 K, and [Longfellow et al., 1999] performed measurements at 323 and 373 K. Both groups found that HONO yield increases with increasing temperature, although the temperature interval investigated was relatively narrow. [Longfellow et al., 1999] also reported that water is involved in the conversion of NO₂ to HONO, and that relative humidity is a major factor determining the absolute amount of HONO produced. [Kleffmann et al., 1999] also observed the relative humidity influence on the HONO production rate. Working with commercial and freshly produced flame soot samples they observed a 15 – 80 % yield of HONO depending on

1. Introduction

the reaction time and relative humidity. Another research group pointed out that the air/fuel ratio by soots produced in diffusion flames is an important parameter influencing the NO₂ conversion to HONO or NO [Stadler and Rossi, 2000], [Salgado and Rossi 2002]. For soot samples originating from a rich flame HONO yield of up to 100% was observed and it decreased to a few percent for soot generated in a lean flame [Stadler and Rossi, 2000], and for soot generated in extremely lean flames as a main product was observed only NO [Salgado and Rossi 2002]. The reduced yield of HONO was explained with the possibility of HONO decomposition on the surface of samples generated under lean flame conditions. This is also confirmed from the investigations of [Alcala Jornod et al., 2000].

The number of active sites for reaction can be determined, for a first order process (one NO₂ molecule lost per active site), from the maximum number of NO₂ molecules which can be taken up per unit sample (per milligram or per cm²). [Lelievre et al., 2004] found from $3.1 \cdot 10^{13}$ to $4.8 \cdot 10^{13}$ active sites per cm² for the different types of soot measured (hexane, toluene, kerosene). [Kalberer et al., 1999] reported a lower limit of $\sim 1.0 \cdot 10^{14}$ molecules cm⁻² for a graphite spark generator soot. For the same type of soot [Kirchner et al., 2000] determined $2.2 \cdot 10^{14}$ molecules cm⁻². [Al-Abadleh und Grassian, 2000] reported $1.4 \cdot 10^{13}$ molecules cm⁻² for hexane soot. It is apparent that this parameter is very dependent upon the type of soot used in the investigation, the surface area used for the calculation and also the experimental conditions.

An important consideration for the atmosphere, besides the study of the primary products in the interaction of NO₂ with soot, is the role of the substrate in this reaction. Basically there are three possibilities. One is that the soot surfaces play a catalytic role in this interaction and remain unaltered. Second possibility is that soot is deactivated (saturated) due to the reaction to play further an important role in any other following interactions, and the third possibility is that soot is consumed in the course of reaction. The literature sources are rather split on this problem. For example [Tabor et al., 1994] suggested that the overall reaction reduced NO₂ while oxidizing carbon on the surface, and it would deactivate the soot over time. [Kleffmann et al., 1999] also proposed a complicated reaction mechanism in which soot is a reactant and the increase of the NO₂ consumption leads to deactivation of active sites on the soot surface. On the other hand [Longfellow et al., 1999] found that the reaction proceeds with no loss of soot, and rather soot is the catalytic site for the interaction with NO₂ and water to form HONO. [Lelievre et al., 2004] were able to observe deactivation of the soot samples towards

1. Introduction

NO₂ after ageing under outdoor conditions and for soot aged more than 20 hours complete deactivation and no uptake of NO₂ was observed.

Concerning the third possibility mentioned above, we have found several studies in which the consumption of soot due to the reaction with NO₂ is observed but for the higher temperatures interval – above 523 K [Kandylas and Koltsakis, 2002], [Setiabudi et al., 2004]. In these studies is investigated the possible application of the reaction in the soot particulate filter technology, for regenerating the filter part of the exhaust gas catalyst. They were mainly performed with diesel engine soot, and with the participation of different catalysts for better effectiveness of the reaction [Kureti et al., 2003a, 2003b, 2003c].

1.3.3 Reaction of SO₂ with soot surfaces

The reaction of SO₂ with soot is not so much studied like the already discussed interaction of NO₂ with soot.

In some earlier studies the interaction of SO₂ with black carbon and activated carbon was investigated. [Otake et al., 1971] measured the reaction kinetics of SO₂ on activated carbon at 323 and 373 K by exposing the substrate to streams of gases and then immersing it in water and measuring the pH. Fitting a Langmuir-Hinshelwood model, they obtained an enthalpy of adsorption of SO₂ of 27.6 kJ mol⁻¹. [Baldwin, 1982] investigated the interaction of SO₂ and charcoal and found a first order uptake process in both SO₂ concentrations (4·10⁻⁵ and 4·10⁻³ mbar) and in the amount of charcoal with a maximum of about 1 mg SO₂/ g carbon. Further [Rogaski et al., 1997] performed this reaction with black carbon (Degussa FW-2, virtually pure carbon) at room temperature and partial pressure of SO₂ from 6·10⁻⁴ to 1·10⁻² mbar in a Knudsen cell reactor. They obtained initial uptake coefficients for SO₂ adsorption of 3·10⁻³. However, all of these studies investigated only pure carbon soots, but it is known that for example the soot particles, collected in the exhaust plume of aircraft, show significant presence of oxygen and other organic components [Sheridan et al., 1985]. Therefore is also important the investigation of different flame soot types. [Akhter et al., 1991] and [Smith and Chughtai, 1995] measured the oxidation of SO₂ in the presence of n-hexane soot at room temperature with around 260 mbar SO₂, with and without oxygen and water. They found that SO₂ oxidizes to HSO₄⁻ but only in the presence of water and oxygen.

1.4 Aims of the work

As already discussed in the previous chapters gas phase chemistry of the atmosphere is much better studied than heterogeneous chemistry. For the latter there are some important questions which still remain uncertain. They concern the potential of the heterogeneous processes to change the aerosol particles in order to remove them or to modify their surface and activate them for further chemical processes in the atmosphere.

We have chosen mineral dust and soot surfaces as typical heterogeneous surfaces ubiquitous in the atmosphere, which role is still not very well understood. We have tried to characterize these surfaces in terms of two important issues. The first is their ability to serve as cloud/ice condensation nuclei, for which hydrophilicity is an important parameter. The second is the reactivity of these surfaces towards typical trace gases like NO_2 and SO_2 and their potential role in atmospheric chemistry. The results represented further in this work can be divided, regarding these two important issues:

i. Investigating the hydrophilicity of mineral dust and soot surfaces.

As already mentioned hydrophilicity is a critical but difficult to quantify parameter, characterizing the possibility of aerosol particles to act as surfaces for the nucleation of water vapour to form either liquid droplets or ice particles and hence influence the cloud formation. From the classical point of view hydrophilicity can be defined from the contact angle between the heterogeneous surface and a water droplet. The contact angle, however, is a macroscopic concept, and can not be applied for surface coverage of only a few monolayers. But in the atmosphere once a particle is completely covered with a monolayer of water, further water molecules can condense on that surface and activate it for further nucleation. Therefore the kinetic parameters for water adsorption at atmospheric conditions are very important to be studied. Adsorption and desorption rates together with the amount of water adsorbed, are important parameters in the assessment of the hydrophilicity of an atmospheric particle.

In the case of mineral dust there are no such kinetic studies for atmospheric relevant temperatures below 298 K. And in the case of soot the obtained results for this temperature region are controversial. Therefore, the adsorption and desorption kinetics of water on soot and mineral dust will be investigated in an extended temperature range from 203 K to 323 K for the first time. In the following chapters are represented the results from experiments

1. Introduction

performed at water vapour pressures below 1 Pa in a low pressure flow reactor (Knudsen cell). Obtained are kinetic data for the adsorption and desorption processes as well as thermochemical data in form of surface coverages and adsorption enthalpies. The results for the two surfaces are compared in order to assess whether hydrophilicity, a macroscopic property of a surface, can be characterized by fundamental quantities such as kinetic parameters.

ii. Investigating the reactivity of soot surfaces towards SO₂ and NO₂

The importance of SO₂ as typical atmospheric trace gas comes from the fact that it can be oxidized to form sulphuric acid which in turn contributes to acid precipitation. The two possibilities of SO₂ oxidation – via gas phase and aqueous mechanisms – are very well studied as discussed before. Not very well understood is the possibility of heterogeneous oxidation of SO₂ to sulphuric acid on soot surfaces. This process is very important because if SO₂ is oxidized to H₂SO₄ on soot, then the sulphuric acid can nucleate the formation of water droplets that may lead to visible aircraft contrails. Some studies of this interaction for lower temperatures relevant for the atmosphere exist, but all of them investigate only pure carbon soots, which are not representative for the soot particles collected in the exhaust plume of aircraft. And the studies investigating different flame soot types (which are believed to have similar structure to aircraft soot) are performed only at room temperature. Therefore another aim of our work was to investigate the interaction of SO₂ and two types of flame soot (ethylene and kerosene) at temperatures below 298 K and assess their relevance for the atmosphere.

NO₂ is part of the so called NO_x species in the atmosphere which play an important role in both polluted and unpolluted areas, because of their contribution to the distribution of the OH radical, which is responsible for the initiation of most of the daytime chemistry of the troposphere. The gas phase chemistry of the NO_x species is very well studied as discussed above, in contrast to their heterogeneous chemistry. It is possible that the NO_x species undergo heterogeneous reactions on soot surfaces, abundant in the atmosphere, and the latter could influence the NO/NO₂ balance in NO_x and indirectly have impact on the ozone formation, or could lead to some important products like HONO which could also have an impact on ozone formation at sunrise. Therefore, is important the investigation of the interaction of NO₂ and soot surfaces at lower temperatures, relevant for the atmosphere.

1. Introduction

Another very important implication for the interaction between soot surfaces and NO₂ at high temperatures, which is not very well studied but of great importance in the recent years, is its importance for the soot particulate filter technology. This reaction is used for regenerating the filter from the gathered particulate matter which is oxidized via NO₂ to NO and CO₂ at relatively low temperatures of about 250⁰C. Therefore one of the aims of our work was the investigation of this reaction at higher temperatures up to 670 K.

Summarized for the reactivity of atmospheric particles, in the following chapters are represented the results for the investigation of the behaviour of two different soot samples (ethylene and kerosene) towards NO₂ and SO₂ in a wide temperature interval (180 K < T < 670 K) for the first time, in order to assess the importance of these interactions, on one hand for the atmosphere in polluted urban areas (for the lower temperatures), and on the other hand for the possible application of the reaction of soot and NO₂ (at higher temperatures) for the soot particulate filter technologies.

2 EXPERIMENTAL PART

2.1 Knudsen cell reactor

All measurements for obtaining the kinetic results have been performed in a so called Knudsen cell. This kind of technique has been first described by [Golden et al., 1973], reviewed by [Caloz et al., 1997] and has been used in recent years to study the kinetics of chemical reactions of wide variety of systems [Caloz et al., 1998], [Aguzzi and Rossi, 1999], [Hanisch and Crowley, 2003], [Goodman et al., 2001], [Mochida et al., 2000].

2.1.1 Description of the apparatus

A detailed scheme of the Knudsen cell experimental setup can be seen in Figure 2.1-1:

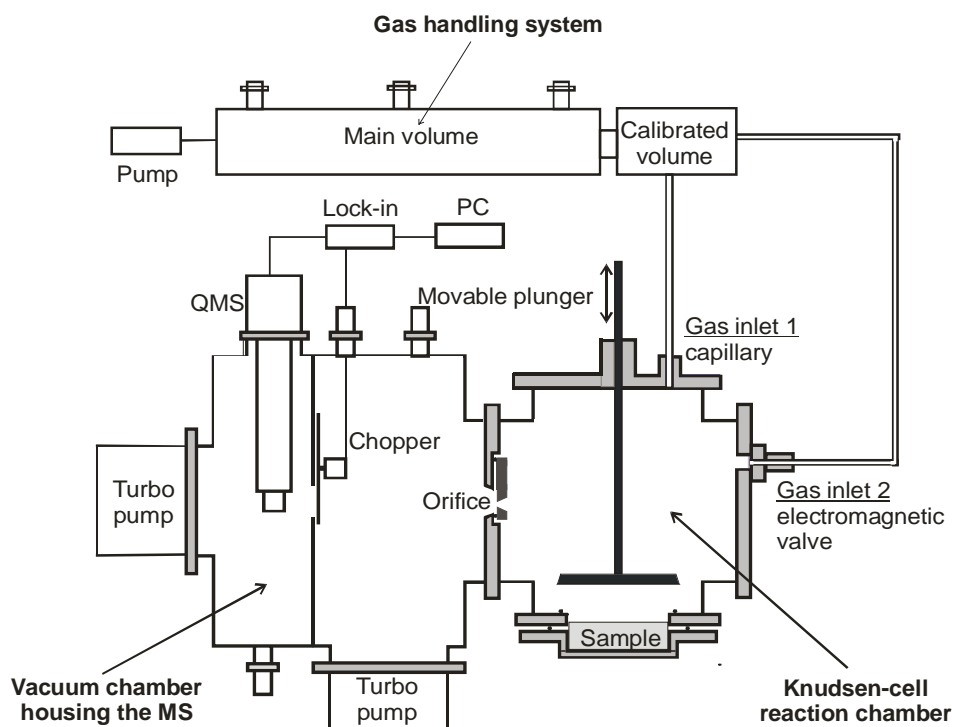


Figure 2.1-1: Schematic representation of the Knudsen cell experimental setup

2. Experimental part

It consists basically of a gas-handling system, Knudsen cell chamber and differentially pumped vacuum chamber, housing the quadruple mass spectrometer (QMS). The gas-handling system represents a glass tube with outlet for the pump (KF flange) and for the reactor (teflon tube), respectively, and three stop-cocks type Rotulex for the connection with the glass flasks with the reactive gases. The pressure inside it is regulated by a Rotary Vane Vacuum Pump, (Pfeiffer Vacuum, DUO 5) and measured by a Baratron® absolute pressure transducer (MKS Instruments, 522, range 0.01 to 10 Torr). Its volume is approximately 540 cm³ (including the specially measured calibrated volume of 65 cm³). For the long time steady state measurements an additional volume (2L) has been used in order to guarantee a constant flow of molecules entering the reactor during the whole time of the measurement.

The reactive gas species enter the Knudsen reactor either through a capillary (length = 50 mm; $d_{\text{inner}} = 0,2$ mm), for the steady state measurements, or through an electromagnetic valve (Parker Instrumentation), for the pulsed measurements, and leave the reaction compartment through a small orifice with adjustable diameter (2.2; 4; 8.2; 12 mm). This diameter determines the residence time and concentration of the gas molecules in the reaction chamber. The actual reaction chamber is represented by a stainless steel cross, the inner walls of which are coated with a fluoropolymer (Teflon, Dupont, FEP 120, dispersion) in order to eliminate adsorption or reaction of the gas species at the wall surfaces.

After escaping from the reaction chamber through the orifice, the effusive beam enters the differentially pumped vacuum chamber, housing the QMS, where it is modulated by a chopper operating at 70 to 80 Hz, and finally detected by a Quadruple Mass Spectrometer (Balzers Instruments, QMG 421). The pressure in the vacuum chamber is regulated by two turbo molecular vacuum pumps (Pfeiffer Vacuum, TMH 520; Leybold Vacuum, Turbovac 151) and is measured by two Compact FullRange™ Gauge (Balzers Instruments, PKR 251). The mass-spectrometer signals are lock-in amplified for better sensitivity and better signal-to-noise ratio and are processed by a PC. Depending on the gas under study detection limit of $5 \cdot 10^9$ to $5 \cdot 10^{10}$ molecules cm⁻³ is obtained with this experimental setup.

The condensed sample is placed at the bottom of the reaction chamber and can be isolated from the rest of the volume by a movable plunger. The sample compartment represents only about 2% to 4% (depending on the type of sample support used) of the total volume of the

2. Experimental part

reaction chamber which eliminates the effects of dilution of the reactant due to volume expansion as well as the systematic errors associated with the abrupt increase of the non-reactive surface area.

The sample is previously prepared either on a copper or a quartz disc sample holder (see Chapter 2.5), after which it is placed in the sample compartment. For the measurements performed four different sample supports have been used: for room temperature, for high temperature and for low temperature measurements. They are schematically represented respectively in Figure 2.1-2, Figure 2.1-3 and Figure 2.1-4.

The room temperature support represents just a quartz glass cover (1 cm thick), on which the sample is placed (gathered either on a copper or a quartz disc) and then mounted tight at the lower part of the reaction chamber.

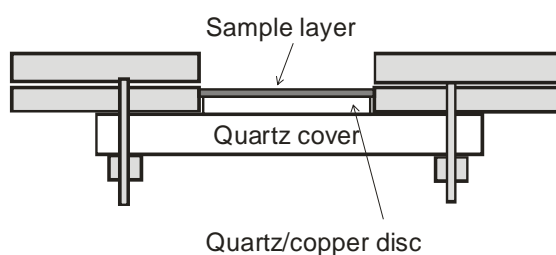


Figure 2.1-2: Room temperature sample support

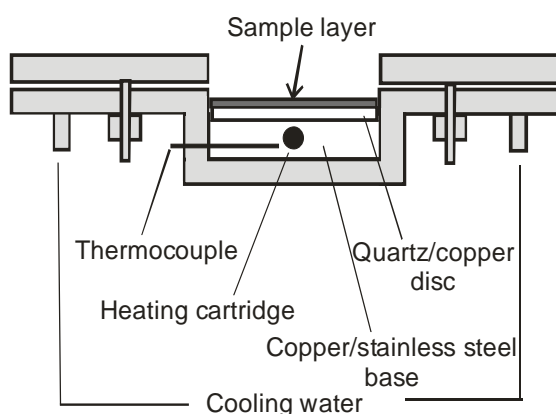


Figure 2.1-3: High temperature sample support

The high temperature support represents either a copper or a stainless steel block as a base, in which is embedded a heating cartridge (Metric Firerod Heating Cartridge, $d = 6\text{ mm}$, Watlow). It can be used for the temperature interval $300 - 700\text{ K}$ and the temperature of the block is

2. Experimental part

measured with a thermocouple type K (Omega[®]) and controlled with temperature controller (Eurotherm Controls Ltd, Model 2404). The whole system is cooled with water to prevent the heating of the O-rings and the rest of the reaction chamber.

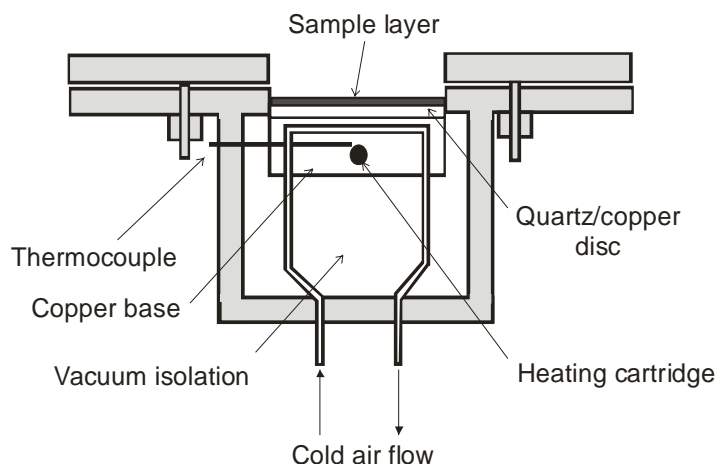


Figure 2.1-4: Low temperature sample support

The principle of the low temperature support is similar. In the copper block, besides the heating cartridge a cooling conduit is embedded through which dry air circulates, cooled with liquid nitrogen. The temperature is regulated with a temperature controller (Eurotherm Controls Ltd, model 2404) and measured with thermocouple type K (Omega[®]). With this support the samples can be cooled down to 140 K.

All important parameters of the Knudsen cell are summarized in Table 2.1-1:

Parameter	Symbol	Value
Operation pressure region	P_{in}	$10^{-3} - 10^{-5}$ mbar
Knudsen cell volume	V	$1.95 \cdot 10^{-3}$ m ³
Surface area of the inner walls	A_w	$1,25 \cdot 10^{-1}$ m ²
Geometric surface area of the sample	A_s	
Room temperature support		$1,89 \cdot 10^{-3}$ m ²
High temperature support		$1,66 \cdot 10^{-3}$ m ²
Low temperature support		$1,02 \cdot 10^{-3}$ m ²
Surface area of the escape orifice	A_o	
d = 2.2 mm		$3,80 \cdot 10^{-6}$ m ²
d = 4.0 mm		$1,26 \cdot 10^{-5}$ m ²
d = 8.2 mm		$5,02 \cdot 10^{-5}$ m ²
d = 12.0 mm		$1,17 \cdot 10^{-4}$ m ²

Table 2.1-1: Important parameters of the Knudsen Cell

2. Experimental part

2.1.2 Main calculations and measurement principle

The Knudsen cell reactor operates in the molecular flow regime. Because of the very low pressure inside (10^{-5} mbar $< p < 10^{-3}$ mbar) the mean free path of the molecules is larger than the dimensions of the reaction chamber itself. This means that gas – wall collisions are favored over the gas – gas collisions, making the Knudsen cell reactor very suitable for investigating heterogeneous processes.

Every Knudsen reactor of this type is characterized by a specific collision number Z_w with the walls:

$$\text{Equation 2.1-1} \quad Z_w = \frac{A_w}{A_0}$$

where A_w is the surface of the inner walls of the reactor chamber and A_0 the surface of the escape orifice.

Z_w is the average number of collisions of one molecule, which it undergoes during its residence time in the reactor. The gas phase residence time of the molecule in the Knudsen cell is given by the Knudsen equation:

$$\text{Equation 2.1-2} \quad \tau = \frac{4V}{A_0 \bar{v}}$$

where V is the reactor volume and \bar{v} the mean velocity of the molecule, defined by the kinetic theory of gases as:

$$\text{Equation 2.1-3} \quad \bar{v} = \sqrt{\frac{8RT}{\pi M}}$$

where R is the universal gas constant, M the molecular mass of the gas species and T the temperature.

When the molecule inside the Knudsen cell collides with the escape orifice it leaves the reactor, and the rate constant of this process (k_{esc}) is given by:

$$\text{Equation 2.1-4} \quad k_{esc} = \frac{1}{\tau} = \frac{A_0}{4V} \sqrt{\frac{8RT}{\pi M}}$$

Having in mind Equation 2.1-1 and Equation 2.1-2, we can define the collision frequency of the molecule with the inner walls of the reactor as the number of collisions per unit time, or:

2. Experimental part

$$\text{Equation 2.1-5} \quad \omega_w = \frac{Z_w}{\tau} = Z_w \cdot k_{esc} = \frac{A_w}{4V} \sqrt{\frac{8RT}{\pi M}}$$

Equation 2.1-5 shows that ω_w depends only on the geometry of the Knudsen cell reactor, but not on the size of the escape orifice.

In the presence of a sample the molecule inside the reactor can undergo collisions also with the sample surface and eventually adsorb or react. In both cases as a result it is removed from the gas phase. But not every collision with the sample leads to reaction or adsorption. The aim of the Knudsen cell measurements is to determine the uptake coefficient γ , which gives us the reaction probability. The uptake coefficient γ is defined as:

$$\text{Equation 2.1-6} \quad \gamma = \frac{\text{number of collisions leading to loss per unit time}}{\text{total number of collisions per unit time}} = \frac{k_r}{\omega_s}$$

where k_r is the rate constant of the uptake and can be measured with the Knudsen-reactor, and ω_s is the collision frequency of the molecule with the surface of the sample, and can be calculated with:

$$\text{Equation 2.1-7} \quad \omega_s = \frac{A_s}{4V} \sqrt{\frac{8RT}{\pi M}}$$

where A_s is the geometrical surface area of the sample.

For the measurements of k_r performed here, the Knudsen cell reactor has been used in two modes: steady state (SS) and pulsed (PU). They are both based on the idea of a differential observation of the out coming flow of the reactant gas in the absence and presence of a solid sample.

2.1.2.1 Steady state measurements

A typical steady state measurement is shown in Figure 2.1-5. In the beginning of each experiment a constant flow of molecules F_{in} is introduced into the cell, while the reactive surface is isolated (plunger down). At these conditions no reaction takes place and:

$$\text{Equation 2.1-8} \quad F_{in} = F_{out} = k_{esc} N_0 V$$

2. Experimental part

where N_0 is the number of molecules before reaction.

In case of reaction (plunger up, $t = 0$ s in Figure 2.1-5) F_{in} is the sum of the flow out of the reactor F_{out} and the flow to the reactive surface F_r :

$$\text{Equation 2.1-9} \quad F_{in} = F_{out} + F_r = k_{esc}N_tV + k_rN_tV$$

where N_t is the number of molecules of the reactant at time t and k_r is the first order reaction rate constant of the gas species with the surface.

From Equation 2.1-8 and Equation 2.1-9 follows:

$$\text{Equation 2.1-10} \quad k_{esc}N_0V = k_{esc}N_tV + k_rN_tV$$

$$\text{Equation 2.1-11} \quad k_r = \left(\frac{N_0}{N_t} - 1 \right) \cdot k_{esc}$$

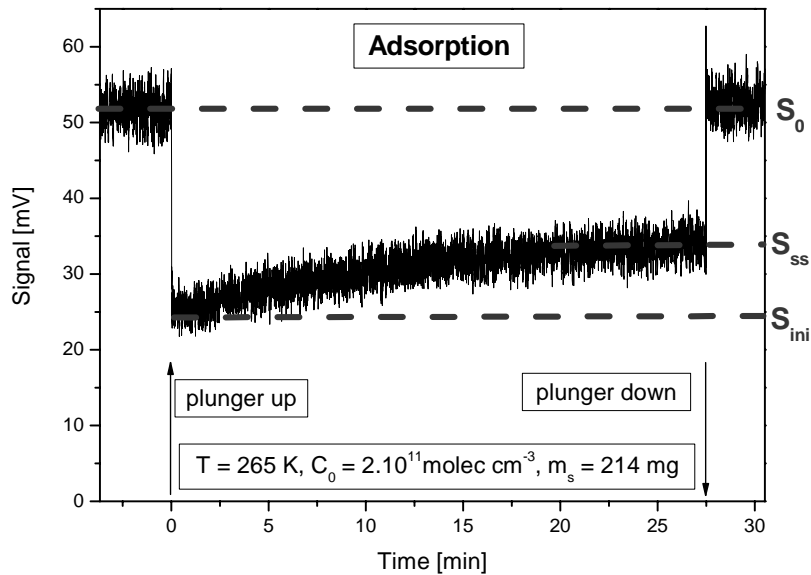


Figure 2.1-5: Typical temporal profile of a steady state measurement for the interaction of water vapour with a mineral dust surface

Having in mind Equation 2.1-6, Equation 2.1-11 and the fact that the number of molecules (N) is proportional to the mass-spectrometer signal (S), we can write:

$$\text{Equation 2.1-12} \quad \gamma = \left(\frac{S_0}{S_t} - 1 \right) \cdot \frac{k_{esc}}{\omega_s}$$

where S_0 is the signal at the beginning of the experiment (no reaction, plunger down), and S_t – the signal at time t during reaction. If we take the signal immediately after opening the plunger, or the initial signal (S_{ini}) – Figure 2.1-5, we can calculate the initial rate constant (k_{ini})

2. Experimental part

and respectively the initial uptake coefficient (γ_{ini}). If we consider the signal when steady state is reached (S_{ss}) we can calculate respectively $-k_{ss}$ and γ_{ss} .

The number of the adsorbed molecules (N_{ads}) during reaction can be determined from the integration of the reactive flow to the surface (F_r) in terms of the time t :

$$\text{Equation 2.1-13} \quad N_{ads} = \int_{t_0}^t F_r dt$$

Having in mind Equation 2.1-8 and Equation 2.1-9 for stationary conditions:

$$\text{Equation 2.1-14} \quad \frac{dN}{dt} = F_r = F_{out}(0) - F_{out}(t) = (S_0 - S_t)m$$

where $F_{out}(0)/S_0$ are out coming flow/signal, respectively, in the absence of sample (plunger down), $F_{out}(t)/S_t$ – out coming flow/signal in the presence of sample at time t and m is the calibration factor.

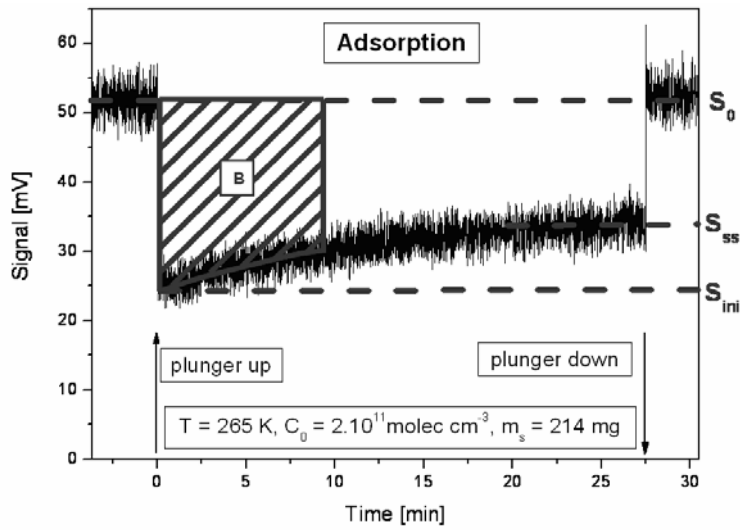


Figure 2.1-6: Calculating the number of adsorbed molecules from the integrated signal

Integration of Equation 2.1-14 yields the number of adsorbed molecules (N_{ads}):

$$\text{Equation 2.1-15} \quad N_{ads} = m \int_{t_0}^t (S_0 - S_t) dt$$

Graphically $\int_{t_0}^t (S_0 - S_t) dt$ is given by the hatched area (B), represented in Figure 2.1-6 and the

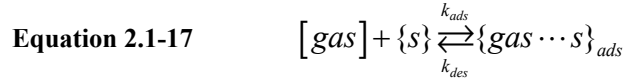
number of adsorbed molecules up to time t can be calculated with:

$$\text{Equation 2.1-16} \quad N_{ads} = m \cdot B$$

2. Experimental part

Because of the time dependence of the out coming signal, the integration for obtaining N_{ads} has been done numerically with the software Origin[®], version 6.0 (Microcal Corporation).

Having in mind the model of Langmuir adsorption for the interaction taking place into the Knudsen cell, we can calculate some more important coefficients describing the process. This model takes into consideration always the equilibrium process on the surface:



where $\{ \}$ indicates surface species, $[]$ – gas phase species and s – active surface sites for adsorption. This equilibrium is defined with the two rate constants of adsorption and desorption, respectively k_{ads} and k_{des} .

The rate of this reaction is defined with:

$$\text{Equation 2.1-18} \quad -\frac{d[gas]}{dt} = k_{ads} \cdot \{s\} \cdot [gas] - k_{des} \cdot \{gas \cdots s\} \cdot \frac{V}{A}$$

where $\{ \}$ indicates surface concentrations, $[]$ indicates gas phase concentrations, V is the volume of the gas and A is the area available for adsorption/desorption.

At the beginning of each experiment ($t = 0s$; immediately after opening the plunger) we have a fresh sample surface. This means that all the available surface sites for adsorption $\{s\}$ are free (surface coverage $\theta = 0$, surface concentration $\{gas \cdots s\} = 0$) and no desorption is taking place. In this case we can ignore the second term in Equation 2.1-18, which is responsible for desorption, and the rate of the reaction can be represented only with the *adsorption rate constant* (k_{ads}). The latter represents the initial rate constant (k_{ini}), measured with the Knudsen cell, directly after opening the plunger and exposing the fresh sample surface to the reactive gas species:

$$\text{Equation 2.1-19} \quad k_{ads} = k_{ini}$$

The *desorption rate constant* (k_{des}) can be also calculated based on the flow balance for the Knudsen cell during reaction. According to it:

$$\text{Equation 2.1-20} \quad 0 = F_{in}(0) - F_{out}(t) - F_r(t) + F_{des}(t)$$

where $F_{des}(t)$ is the desorption flow coming off the surface at time t during reaction. We can rearrange Equation 2.1-20 in terms of the desorption flow:

$$\text{Equation 2.1-21} \quad F_{des}(t) = F_{out}(t) + F_r(t) - F_{in}(0)$$

2. Experimental part

The reactive and the out-going flows for first order process can be given with:

$$\text{Equation 2.1-22} \quad F_{out}(t) = k_{esc} \cdot [gas(t)]$$

$$\text{Equation 2.1-23} \quad F_r(t) = k_{ads} \cdot [gas(t)]$$

After combining Equation 2.1-22 and Equation 2.1-23 we obtain:

$$\text{Equation 2.1-24} \quad \frac{F_{out}(t)}{k_{esc}} = \frac{F_r(t)}{k_{ads}}$$

and, having in mind Equation 2.1-19, we can calculate the reactive flow with:

$$\text{Equation 2.1-25} \quad F_r(t) = \frac{k_{ini}}{k_{esc}} \cdot F_{out}(t)$$

If we substitute in Equation 2.1-23 $F_r(t)$ with Equation 2.1-25 we obtain the final equation which has been used for calculating the desorption flow (desorption rate):

$$\text{Equation 2.1-26} \quad F_{des}(t) = F_{out}(t) \cdot \left[1 + \frac{k_{ini}}{k_{esc}} \right] - F_{in}(0)$$

On the other hand for a first order process the desorption rate is:

$$\text{Equation 2.1-27} \quad F_{des}(t) = -\frac{dN_{ads}}{dt} = k_{des} \cdot N_{ads}(t)$$

where $N_{ads}(t)$ is the number of adsorbed molecules during reaction at time t . It can be calculated from the integrated signal up to time t (as explained above).

Using Equation 2.1-27 we can obtain the desorption rate constant (k_{des}) as the slope of the line from the graphic representation $F_{des}(t)$ as a function of number of adsorbed molecules $N_{ads}(t)$.

The *reaction order* can also be determined with the help of the steady state measurements. For a heterogeneous reaction:



where G is referring to the gas species, S to the solid species and n , p are stoichiometric coefficients, the rate of the reaction can be given by the following equation:

$$\text{Equation 2.1-28} \quad F_r = -\frac{d[G]}{dt} = k \cdot [G]^n \cdot \{S\}^p$$

Under the assumption that the number of reactive surface sites on the solid surface is constant, we can write:

$$\text{Equation 2.1-29} \quad k_r = k \{Surface\}^p$$

where k_r is the rate constant for a pseudo-first order reaction. Then the rate law (Equation 2.1-28) changes to:

2. Experimental part

$$\text{Equation 2.1-30} \quad F_r = k_r [Gas]^n$$

Under this condition the rate constant of the reaction depends only on the concentration of the gas species. If we take the logarithm of Equation 2.1-30 we obtain:

$$\text{Equation 2.1-31} \quad \log F_r = n \cdot \log [Gas] + \log k_r$$

From Equation 2.1-31 follows that from the double logarithmic presentation of the loss rate to the surface versus gas concentration, we can obtain the reaction order n from the slope of the line.

The loss rate (F_r) to the surface can be calculated with:

$$\text{Equation 2.1-32} \quad F_r = F_0 - F_t = m(S_0 - S_t)$$

where F_0/S_0 is the flow/signal at the beginning of the experiment (plunger is closed), F_t/S_t is the flow/signal at time t during the experiment (plunger is opened) and m is the calibration factor.

2.1.2.2 Pulsed valve measurements

For the pulsed measurements the gas species are introduced into the chamber through an electromagnetic valve, which opens only for a few milliseconds (3 – 6 ms). Here, similar to steady state experiments, also is compared the outgoing flow in the absence (plunger down) and presence (plunger up) of the sample.

The advantage of the pulse technique compared to the steady state technique is that the net loss of the gas through effusion or reaction can be observed in “real time”. Because of the very small amount of substance which enters the Knudsen cell with one pulse, the effects of surface saturation can be avoided and the initial rate constant (k_{ini}) can be measured more accurately [Seisel et al., 2006].

A typical pulse measurement is shown in Figure 2.1-7. The upper curve represents the so called *control pulse* – when the sample is isolated (plunger down) and no reaction takes place. Then the decrease of the concentration inside the reactor is given by:

$$\text{Equation 2.1-33} \quad F_{out}(t) = -\frac{dN(t)}{dt} = k_{esc} N(t)$$

After rearranging the variables and integration:

2. Experimental part

$$\text{Equation 2.1-34} \quad \ln N_t = -k_{esc}t + \ln N_0 \Leftrightarrow \ln S_t = -k_{esc}t + \ln S_0$$

From the logarithmic presentation of the MS Signal as function of time, k_{esc} can be determined from the slope of the descending signal as shown in Figure 2.1-8.

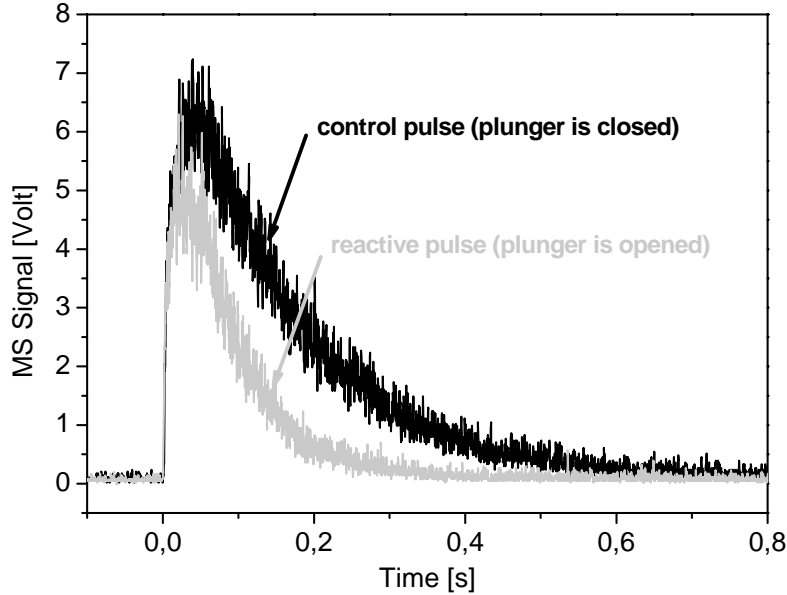


Figure 2.1-7: Typical pulsed measurement – uptake of D₂O on kerosene soot

The lower curve in Figure 2.1-7 represents the *reactive pulse*, in the presence of sample (plunger is opened). In this case:

$$\text{Equation 2.1-35} \quad F_{out}(t) = -\frac{dN(t)}{dt} = \underbrace{(k_{esc} + k_r)}_{k_{dec}} \cdot N(t)$$

After integration:

$$\text{Equation 2.1-36} \quad \ln N_t = -k_{dec}t + \ln N_0 \Leftrightarrow \ln S_t = -k_{dec}t + \ln S_0$$

From the logarithmic presentation of the MS Signal as function of time, k_{dec} can be determined from the slope of the descending signal (Figure 2.1-8).

In the presence of sample the signal of the reactive pulse has a steeper slope because of the additional loss process (the reaction). From the difference of the two slopes, the desired rate constant of the reaction (k_r) can be obtained:

$$\text{Equation 2.1-37} \quad k_r = k_{dec} - k_{esc}$$

2. Experimental part

And, respectively, from Equation 2.1-6 follows:

$$\text{Equation 2.1-38} \quad \gamma = \frac{k_r}{\omega_s} = \frac{k_{dec} - k_{esc}}{\omega_s}$$

If we know the corresponding calibration factor m we can calculate the total number of the gas molecules inside the Knudsen cell during the measurement.

For the *control pulse*:

$$\text{Equation 2.1-39} \quad F_{out}(t) = -\frac{dN(t)}{dt} = k_{esc} \cdot N(t) = m \cdot S(t)$$

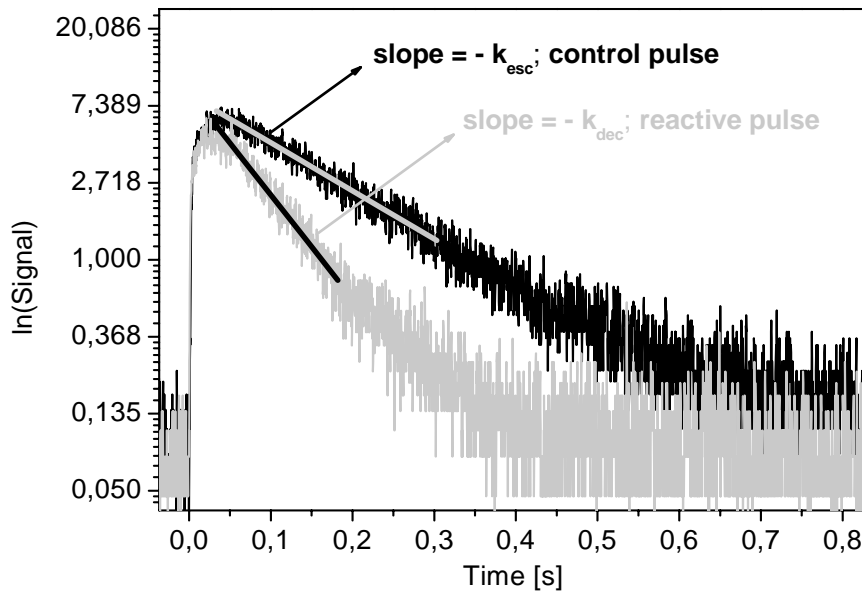


Figure 2.1-8: Logarithmic presentation of the pulse measurements signal (control and reactive pulse), shown in Figure 2.1-7, for obtaining the constants k_{esc} and k_{dec} .

From Equation 2.1-34 and the fact the MS Signal is proportional to the number of molecules in the cell, we can write:

$$\text{Equation 2.1-40} \quad S_t = S_0 \exp(-k_{esc}t)$$

After substituting Equation 2.1-40 in Equation 2.1-39 and following integration:

$$\text{Equation 2.1-41} \quad N_{total} = -\frac{mS_0}{k_{esc}} \exp(-k_{esc}t) \Big|_{t_0}^{t_{end}}$$

And if we have $t_0 = 0$ and $t_{end} = \infty$, the total number of molecules during the control experiment is given with:

$$\text{Equation 2.1-42} \quad N_{total} = \frac{m}{k_{esc}} S_0$$

2. Experimental part

From the same assumptions, for the total number of molecules during reaction can be written:

$$\text{Equation 2.1-43} \quad N'_{total} = \frac{m}{k_{dec}} S_0$$

And finally the number of adsorbed molecules, due to the uptake experiment is:

$$\text{Equation 2.1-44} \quad N_{ads} = N_{total} - N'_{total}$$

This pulse measurements regime has been used to determine the *rate constant of escaping from the cell* (k_{esc}) for the reactant molecules. For the gases used, all the escape constants, for the different orifices, are summarized in

Table 2.1-2.

	H₂O <i>m/e</i> 18	NO₂ <i>m/e</i> 46	NO <i>m/e</i> 30	HONO <i>m/e</i> 47	SO₂ <i>m/e</i> 64	HCl <i>m/e</i> 36
4 mm	0.60	0.47	0.53	0.47	0.45	0.60
8.2 mm	3.00	1.72	2.18	0.81	1.56	2.28
12 mm	5.92	3.74	4.22	2.05	3.30	3.98

Table 2.1-2: Escape constants for reactive gases for the different orifices

Having in mind Equation 2.1-4 for the theoretical calculation of k_{esc} , we should expect that k_{esc} is proportional to $1/\sqrt{M}$. In order to prove this dependence, the experimentally obtained values for all orifices are summarized as a function of $1/\sqrt{M}$, in Figure 2.1-9.

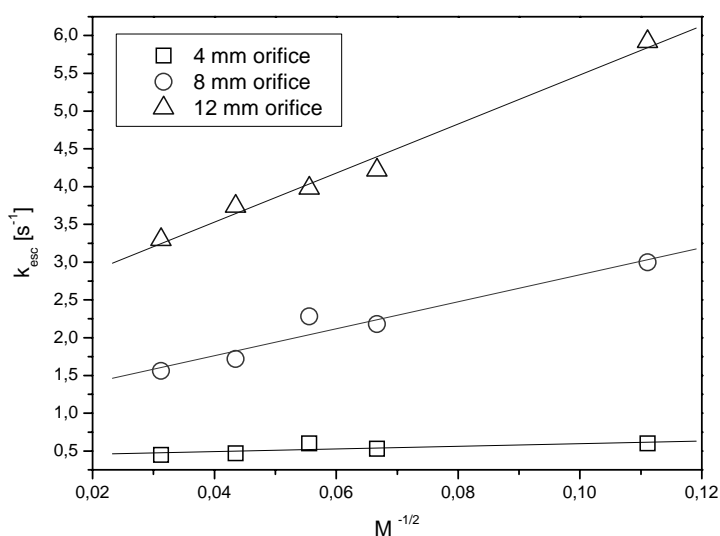


Figure 2.1-9: Graphic representation of the dependence of the escape constant (k_{esc}) on the molecular mass (M) of the reactant species

2.2 Diffuse Reflectance Infrared Fourier Transformation Spectroscopy (DRIFTS)

Vibrational spectroscopy is one of the few methods that can be easily adapted for *in-situ* characterization of solid sample surfaces. Especially DRIFTS (Diffuse Reflectance Infrared Fourier Transformation Spectroscopy) is very effective for investigating heterogeneous processes on numerous surfaces [Vogt and Finlayson-Pitts, 1994], [Börensén et al., 2000], [Börensén, 2000], [Ullerstam et al., 2003], [Reinhardt and Zellner, 2003]. The use of a diffuse reflectance set-up allows observations on powdered samples without any complicated previous sample preparation. Therefore, possible structural changes in the material, which may occur, *e. g.*, during the high-pressure fabrication of KBr-pellets required for transmission mode experiments, are avoided. Moreover, the possibility to pass reactant flows through the sample with precise control of temperature and flow rates predestines *in-situ* DRIFTS for measurements under conditions very close to those of many other technical applications.

Schematically the DRIFTS cell experimental setup, used for characterisation of our samples, is shown in Figure 2.2-1:

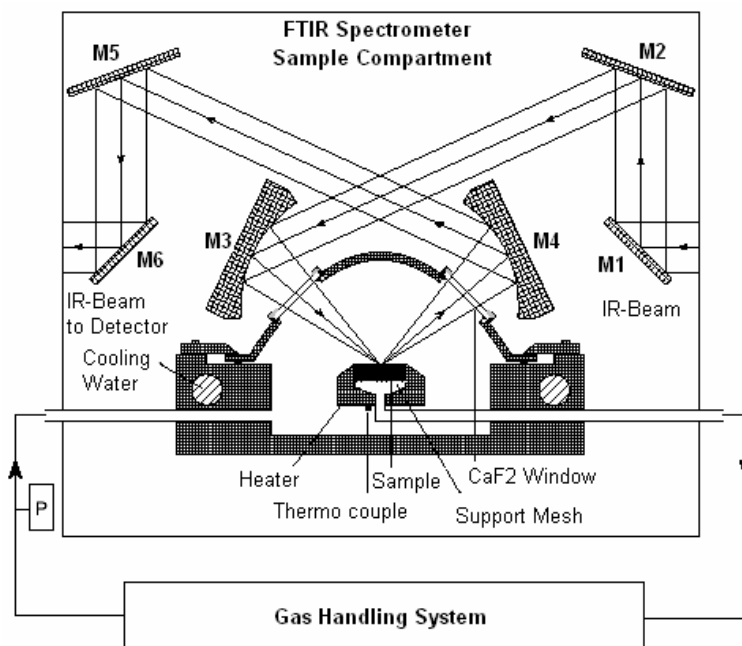


Figure 2.2-1: DRIFTS experimental setup

2. Experimental part

It consists of a gas handling system and the IR spectrometer Bruker IFS 66, where the Purged Praying Mantis™ Diffuse Reflectance Attachment (Harrick Instruments) is mounted in the path of the IR beam in the sample compartment. The gas handling system is similar to the one for the Knudsen cell experimental setup. The pressure inside is regulated by a Rotary Vane Vacuum Pump, (Pfeiffer Vacuum, DUO 5) and measured by a Baratron® Absolute Pressure Transducer (MKS Instruments, 522, range 1÷1000 Torr).

The sample is mounted in the Praying Mantis™ in a specially designed sample holder (for measurements at atmospheric pressure) or in a Low Temperature Reaction Chamber (for measurements under vacuum). Mirrors M1 and M2 transfer the spectrometer IR beam to the first of the ellipsoids, M3, which focuses the beam onto the sample (Figure 2.2-1). The second ellipsoid, M4, collects the radiation diffusely reflected from the sample. This radiation is then directed by mirrors M5 and M6 toward the detector. The design of the Praying Mantis allows for high throughput while discriminating against the collection of the specular component of the reflected beam which can interfere and worsen the obtained IR spectra.

The basic theory of the DRIFTS measurements and the fact that they can be used for qualitative as well as for quantitative analysis has been developed previously in the thirties [Kubelka and Munk, 1931] and later by Kubelka [Kubelka, 1948]. It relates the absorption and scattering of completely diffuse monochromatic radiation by a homogeneous isotropic substance (solid sample) to two parameters K and S accounting respectively, for absorption and scattering (Equation 2.2-1), which are proportional, under certain experimentally attainable conditions, to α and s (the true absorption and scattering coefficients) defined by exponential Bouguer laws [Delgas, 1979].

$$\text{Equation 2.2-1} \quad K / S = F(R_\infty) = \frac{(1 - R_\infty)^2}{2R_\infty}$$

The last expression (Equation 2.2-1) is the well known Kubelka–Munk function relating the experimentally obtained diffuse reflectance of an “infinitely” thick sample ($F(R_\infty)$) to the parameters K and S . For spectroscopic applications this expression is useful to the extent that for a system for which the scattering (S) is independent from the wavelength of the incident radiation (λ), K reflects the dependence of the absorption energy on the wavelength. This KM expression allows true absorption spectra to be obtained for strongly scattering samples [Kortüm, 1969]

2.3 Scanning Electron Microscopy (SEM)

Scanning electron microscopy (SEM) has long played a central role in structural characterisation of the samples. Its principle of operation can be summarized as follows. An energetically well-defined, highly focused beam of electrons, scanned across the surface of a sample, generates secondary electrons (SE), backscattered (or primary reflected) electrons (BSE), and characteristic X-rays. All these three types of emissions can be used to obtain topographical and elemental information of the sample. They are collected by different types of detectors to form images of the sample displayed on a cathode ray tube screen.

By the SEM technique, a detector close to the specimen surface collects SE, with kinetic energies much lower than the primary incident electrons, which are emitted from just below the specimen surface. Because of their low energies and low penetration depth, the detection of secondary electrons as a function of primary beam position makes it possible to attain high magnifications (as much as 100 000 times in some cases) and high resolutions (up to ~4 nm resolution) for imaging the areas of interest. Each captured secondary electron causes a flash of light in a scintillator, which passes down a light guide to a photomultiplier, and this converts it to an electrical signal. The final signal is proportional to the number of secondary electrons emitted from the specimen and is used to modulate the brightness of a display spot on the screen. Resolution is dependent on the size of the probe spot and modern microscopes can resolve detail to less than 1.0nm. Digital image capture is now a standard feature, allowing sophisticated image processing techniques to be applied, including colour enhancement [ICAL, 2005], [Reimer, 1998].

However, the requirements of SEM for the sample preparation, such as a high vacuum in the microscope sample compartment, and the need for a thin coating, if a non conducting sample is being analyzed, makes the investigation for some kinds of materials with this technique very difficult. A possibility for such samples is the Environmental Scanning Electron Microscopy (ESEM). The main difference between the two techniques is that whereas SEM requires a relatively high vacuum in the sample compartment to prevent atmospheric interference with primary or secondary electrons, an ESEM may be operated with high pressure (up to 10 mbar) in the specimen chamber. For such “wet mode” imaging, water is the most common gas used. When the electron beam (primary electrons) ejects secondary

2. Experimental part

electrons from the surface of the sample, the secondary electrons collide with water molecules, which in turn function as a cascade amplifier, delivering the secondary electron signal to the positively biased gaseous secondary electron detector (GSED). Because they have lost electrons in this exchange, the water molecules are positively ionized, and thus they are forced/attracted toward the sample (which may be nonconductive and uncoated, also a great advantage in favour of the ESEM technique), serving to neutralize the negative charge produced by the primary electron beam. The ESEM also retains the capabilities for conventional secondary and backscattered electron detection, and the field-emission source permits very high resolution imaging of coated or naturally conductive samples under normal high-vacuum and high-voltage conditions. [Prack, 1993], [Reimer, 1998]. In Table 2.3-1 the main differences between the two techniques are summarized once again [Prack, 1993].

	SEM	ESEM
Imaging	Secondary electrons Backscattered electrons	Secondary electrons, ESD detector Backscattered electrons
Detector	Everhart-Thornley (ET) – functions only in vacuum	Environmental Secondary Detector (ESD) – requires a gas background
Working distance	6 – 40 mm	6 – 15 mm Limited by scattering
Voltage	1 – 30 kV	1 – 30 kV
Vacuum	$10^{-3} - 10^{-7}$ torr	3 – 20 torr Atmosphere can be varied
Magnification	10 – 100 000 times	70 – 100 000 times
Resolution	1.8 to 6.0 nm usually 4.5 nm	5 – 7 nm
Sample	Vacuum compatible conductors only	Any sample type Dynamic reactions
Sample introduction	3 – 5 min	30 – 60 seconds
Advantages	Higher magnification possible Has good depth of field	Close to real world conditions Higher magnification possible Has good depth of field
Limitations	Requires conductive samples Fluids can not be analyzed	Limited field of view Requires subambient pressure

Table 2.3-1: Comparison of electron microscopy techniques (typical values)

The microscope used for our work was model Quanta 400F, FEI Company. For the SEM measurements regime we used the high vacuum mode (chamber vacuum $<6 \cdot 10^{-6}$ mbar) and for the ESEM mode we used the special Peltier stage in which the sample can be cooled down to 0°C and the chamber pressure was varied between 1 and 6 mbar.

2.4 Ion Chromatography

“Chromatography” is the general term for a variety of physico-chemical separation techniques, all of which have in common the distribution of a component between a mobile phase and a stationary phase. The various chromatographic techniques are subdivided according to the physical state of these two phases. Ion Chromatography (IC) was introduced in 1975 as a new analytical method. Within a short period of time, it evolved from a new detection scheme for a few selected inorganic anions and cations to a versatile analytical technique for ionic species in general. At the end of the 1970s, ion chromatographic techniques were used to analyze organic ions for the first time, based on the ion exclusion process. The 1980s witnessed the development of high efficiency separator columns with particle diameters between 5 μm and 8 μm , which resulted in a significant reduction of analysis time. In addition, separation methods based on the ion pair process were introduced as an alternative to ion-exchange chromatography, because they allow the separation and determination of both anions and cations. Since the beginning of the 1990s column development has aimed to provide stationary phases with special selectivities. The scope of ion chromatography was considerably enlarged by newly designed electrochemical and spectrophotometric detectors [Weiss, 2004].

The principle of IC is the following. For a sensitive detection of ions via their electrical conductance, the separator column effluent was passed through a “suppressor” column. This suppressor column chemically reduces the eluant background conductance, while at the same time increasing the electrical conductance of the analyte ions.

The Chromatograph used for our needs was model DIONEX, DX-120, with Analytical Column IonPac AS9-HC (4 x 250 mm) and guard column IonPac AG9-HC (4 x 50 mm).

The basic components of an ion chromatograph are shown schematically in Figure 2.4-1. A pump delivers the mobile phase through the chromatographic system. The sample is injected into the system via a loop injector. The sample loading is carried out at atmospheric pressure. After switching the injection valve, the sample is transported to the separator column by the mobile phase. Typical injection volumes are between 5 μL and 100 μL . The most important part of the chromatographic system is the separator column. The column tubes are

2. Experimental part

manufactured from inert material such as Tefzec, epoxy resins, or PEEK (polyether ether ketone). In general, separation is achieved at room temperature.

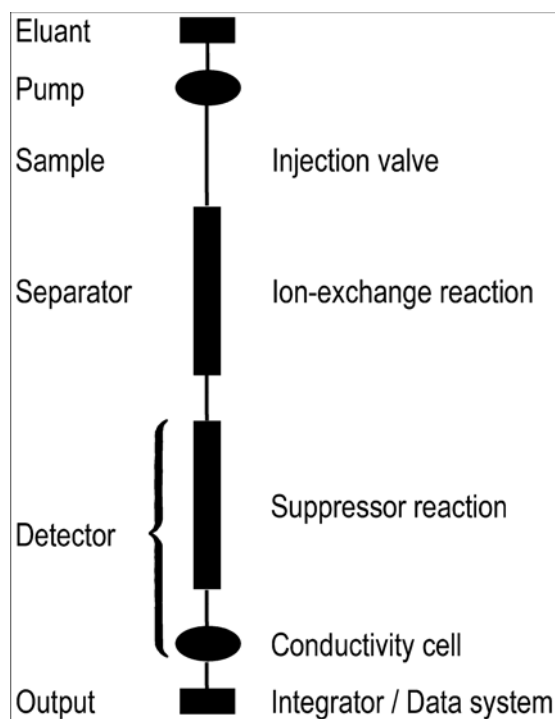


Figure 2.4-1: Basic components of a Ion Chromatographic System

The analytes are detected and quantified by a detection system. The most commonly employed detector in ion chromatography is the conductivity detector, which is used with or without a suppressor system. The main function of the suppressor system as part of the detection unit is to chemically reduce the high background conductivity of the electrolytes in the eluant, and to convert the sample ions into a more conductive form. The chromatographic signals can be processed further with suitable chromatography software.

2.5 Substances and sample preparations

For all the measurements performed in this work, the following substances have been used:

2.5.1 Gas phase species

Water (H₂O)

As a source of water vapour for the reaction with mineral dust and soot samples, deionized water has been used. The purification is accomplished with water purification system – Millipore Simplicity™, which produces ultra pure water Type I (18.2MΩ·cm resistivity at 25°C and < 10 ppb Total Organic Carbon). Around 10 ml of it was filled in a Rotulex cool finger condensation trap, and the air above was carefully evacuated. For further use the cool finger was connected directly with the gas-handling system and the needed amount of water vapour was let in. For the mass spectrometer measurements the detection of water was done at *m/e* 18 (its main peak).

Deuterium oxide (D₂O)

The so called heavy water (99,5% Aldrich) was used as a source for D₂O vapor, in order to explicitly investigate the interaction mechanism between water with mineral dust and soot. D₂O was filled under N₂ atmosphere in a cool finger and afterwards also carefully degassed. The purity of D₂O was checked mass spectrometrically. HDO was formed due to a fast H/D exchange on the walls of the gas-handling system and the reactor. The MS signal ratio of D₂O (*m/e* 20) and HDO (*m/e* 19) varied with the gas residence time in the cell from 5,5 ($\tau = 0,16$ s) to 1,2 ($\tau = 1,6$ s). In addition the measured escape rate constants of D₂O have been higher than for H₂O, indicating that HDO is mostly formed inside the reactor. The HDO concentration in the cell was estimated to vary between 15% and 50% of the D₂O concentration. The H₂O content in the D₂O/HDO mixture was estimated to be less than 5%.

Nitrogen dioxide (NO₂)

For our needs NO₂ was taken from a high pressure bottle (1.8, Messer) and filled in a 2L flask up to 500 – 600 mbar total pressure. In order to remove eventual gas phase contaminants it was cooled down with liquid nitrogen and the rest of the volume carefully degassed. Due to

2. Experimental part

the fragmentation of NO_2 in the mass spectrometer, two peaks have been simultaneously observed - m/e 30 (for fragment NO) and m/e 46 (for NO_2). The ratio $(m/e\ 30)/(m/e\ 46)$ was estimated to vary between 2,8 and 4,9 (separately calculated for each measurement).

Sulphur dioxide (SO_2)

Sulphur dioxide was also commercially available (4.5, Messer). For our needs it was filled in a 2L flask up to total pressure 600 mbar and directly connected to the gas handling system of the Knudsen cell reactor. Mass spectrometrically SO_2 is detected at its main peak at m/e 64 and also at peak m/e 48 (for the fragmentation SO). The last is estimated to be 76% of the main peak.

Nitrogen (N_2)

Nitrogen is commercially available and was taken directly from a high pressure bottle (5.0, Messer). It was used mainly for purging the system or for diluting the reactive gas species.

Hydrochloric acid (HCl)

HCl has been taken from a high pressure bottle (2.8, Air Liquide) and filled in a 6L flask up to 700 mbar. For our use the flask was directly connected to the gas handling system of the Knudsen cell.

Nitrous acid (HONO)

Gas phase HONO was needed only to calibrate the mass spectrometer for its signal, in order to estimate later its yield due to the reaction of NO_2 and soot. For our needs it was synthesized from the reaction of solid NaNO_2 and gas phase HCl, explained in detail in Chapter 2.5.4.

Ethene (C_2H_4)

Ethylene was used directly from high pressure bottle (3.5, Messer) as a gas fuel for the capillary burner to produce the ethylene soot investigated later.

Synthetic air

It was used for burning ethylene in the capillary burner in order to produce the ethylene soot samples used for the measurements. It consists of 80% N_2 and 20% O_2 .

2. Experimental part

2.5.2 Solid species

Sodium nitrite (NaNO_2)

Solid NaNO_2 ($\geq 99,0$ %, Fluka) was used for the reaction with HCl in order to be able to calibrate the signal of HONO (explained in detail in Chapter 2.5.4). For each measurement around 15g sodium nitrite was very good ground in a mortar and then mount in the Knudsen cell sample compartment and carefully evacuated at least for 4 hours, after which the measurement was performed.

Mineral dust

The mineral dust samples, used for the Knudsen cell measurements, were Sahara dust samples. This type of dust was chosen as an exemplary substance, because Sahara - the largest desert in the world – is the main source of mineral dust aerosol in the atmosphere [Schütz and Sebert, 1987]. The mineral dust used was gathered as a soil sample from the Sal Island, one of the Cape Verde Islands Group. This group of islands is situated on the west coast of Africa and is permanently subject to the air streams carrying particulate matter from Sahara desert [Rognon et al., 1996]. The samples were provided from LISA (Laboratoire Interuniversitaire des Systems Atmospheriques), University of Paris. In Figure 2.5-1 is given the elementary composition of the Sahara dust samples [Desboeufs et al, 1999].

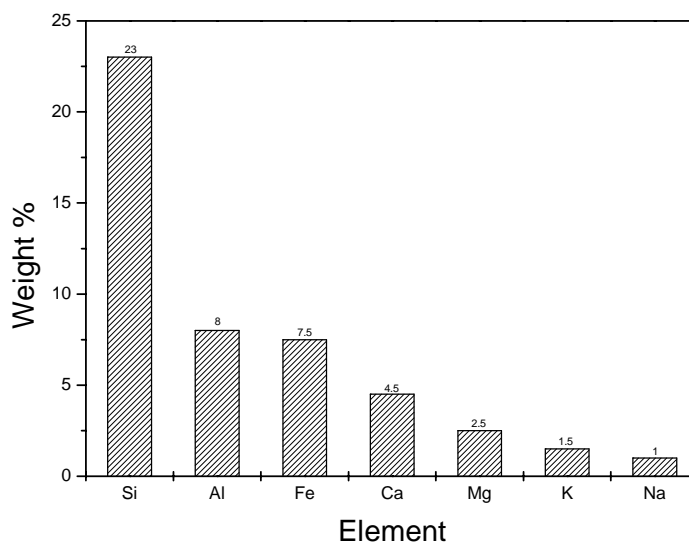


Figure 2.5-1: Elementary composition of mineral dust [Desboeufs et al., 1999]

For further analysis determination of the BET surface, particle size distribution and density analysis have been done. The results are summarized in Table 2.5-1:

2. Experimental part

BET surface area, [Seisel et al, 2004b]	50 m ² ·g ⁻¹
Range of grain size	1 – 500 μm
Mean diameter	15 μm
Bulk density	0.93 g·cm ⁻³
Density	2.86 g·cm ⁻³

Table 2.5-1: Properties of the mineral dust samples

Soot

Two different types of soot samples have been used for the measurements presented in this work: kerosene soot (KS), obtained by burning aviation kerosene in a simple oil lamp, and ethylene soot (ES), obtained using a special premixed flame capillary burner. Schematic presentation of this type of burner is given with Figure 2.5-2 [Hesse, 1988].

The capillary burner consists of an inner burner completely surrounded by an outer burner. The inner burner represents a stainless steel tube with diameter 57 mm and length 100 mm. It is divided into two parts – actual burner and mixing chamber. In the actual burner are placed around 1200 stainless steel capillaries with outer diameter 1,5mm, wall thickness 0,25 mm and length 60 mm. They are tightly packed on a sinter plate which holds them together and makes possible the regular and planar alignment of the capillaries which is very important for the stability of the flame. The inner burner is not water cooled and the flow passing through it was in the average 300 cm³/s with unburned gas velocity of 12 cm/s. The mixing chamber is the lower part of the inner burner and is filled with raschig rings.

The outer burner is concentrically situated towards the inner burner and their total diameter is 80 mm. It is filled also with stainless steel capillaries, but with dimensions 25 mm (length), 2 mm (diameter) and 0.25 mm (wall thickness). The gas flows passing through it were in the average 280 cm³/s with unburned gas velocity 14.2 cm/s. The outer burner is water cooled. It produces non sooting flames and its main function is to stabilize the flame formed above the inner burner. This type of burner, shown on Figure 2.5-2, is the so called premixed flame burner because the combustible mixture is prepared in advance. The gases used are ethylene (4.0, Messer) as burning substance and synthetic air as oxidant. The precise flow is regulated with four flow controllers type Rotameter (calibrated for flows measured in standard litre pro minute – SLM).

2. Experimental part

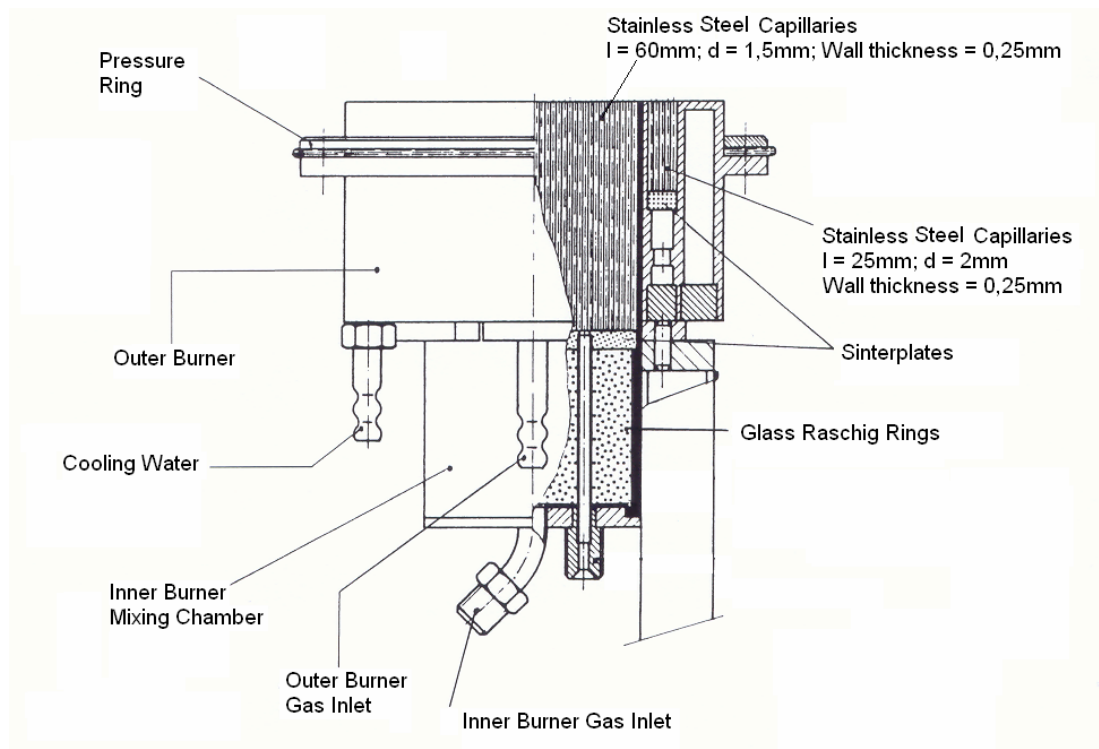


Figure 2.5-2: Capillary premixed flame burner

The advantage of the capillary burner over the usual oil lamp is that with it we can produce soot samples with very well defined Air/Fuel ratio (Table 2.5-2), and we can investigate how the different composition influences the properties of the different types of soot.

	Kerosene Soot	Ethylene Soot
Burner Type	Oil lamp	Capillary burner
Air/Fuel Ratio	-	8.4/1
Flame temperature [K]	1050 - 1100	1700 - 1750
BET surface [m² g⁻¹]	64.8	11.1
Pore volume [ml g⁻¹]	0.14	0.02
Mean particle diameter [μm]	15	25
Bulk density [g cm⁻³]	0.046	0.026
Density [g cm⁻³]	2	2
Elementary Analysis [wt %]		
Carbon	94.6	96.3
Hydrogen	0.5	1.0
Nitrogen	≤ 0.3	≤ 0.3
Sulphur	≤ 0.3	≤ 0.3

Table 2.5-2: Important properties of the two types of soot - comparison

2. Experimental part

For both types of soot determination of the BET surface and particle size distribution have been done, summarized in Table 2.5-2, which has also been expanded with some more important parameters. From Table 2.5-2 can be noticed the similarity in elementary composition of both types of soot, but at the same time the difference between the BET surface areas. This suggests a substantial difference in the structure of the two types of soot.

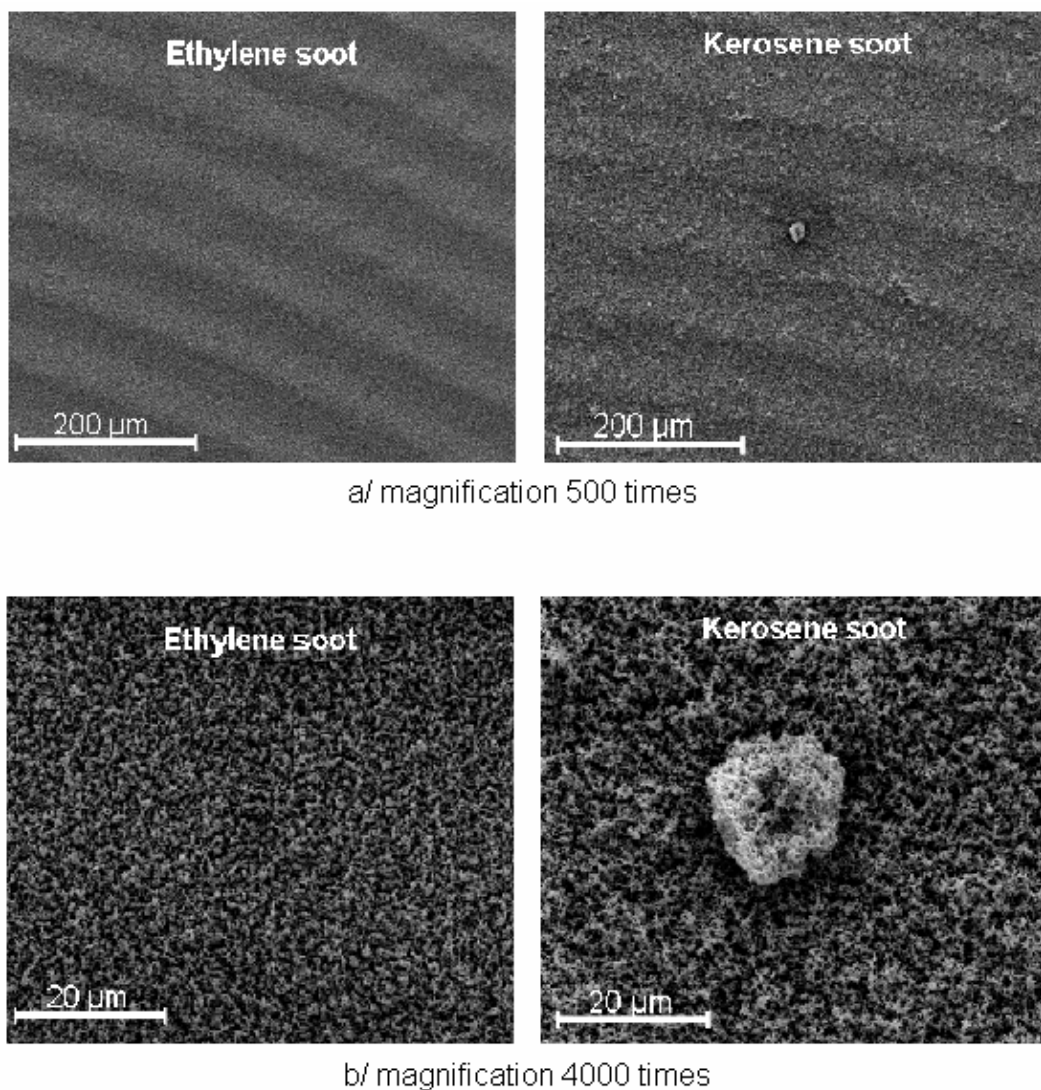


Figure 2.5-3: SEM picture of kerosene and ethylene soot at two different magnifications: a/ 500 times; b/ 4000 times

In order to gain some more information about the structure of our samples additional SEM measurements have been done. For them the samples were prepared in the same manner like for the measurements performed in the Knudsen cell – they were directly gathered from the flame on the sample holder of the microscope, forming a fine layer. In Figure 2.5-3 are represented the SEM pictures of ethylene and kerosene soot both magnified 500 times (a) and

2. Experimental part

4000 times (b). The waves, visible for the 500 times magnification, are due to the surface of the sample holder of the microscope and the fact that the sample is gathered as a very thin layer. But nevertheless for both magnifications it can be seen the finer structure of the ethylene soot surface, compared to that of the kerosene soot surface. In the case of ethylene soot the surface is smoother and with no irregularities in contrast to the case of kerosene soot where even small particles formed are observed (a – KS) and one of them is additionally magnified (b – KS).

For both types of soot is clearly observed the fine structure of the surface with the tightly packed soot agglomerates, visible first at the greater magnification (b/). It can be also said that the free space between these agglomerates in the case of ethylene soot is less than in the case of kerosene soot which is probably the reason for the smaller BET surface area of these samples. Quantitatively this free volume between the single agglomerates has been measured (dV/dD in $[\text{ml}\cdot\text{g}^{-1}\cdot\Delta\text{nm}^{-1}]$) for both of the samples, and represented as a function of the size range of the voids in $[\text{nm}]$ in Figure 2.5-4.

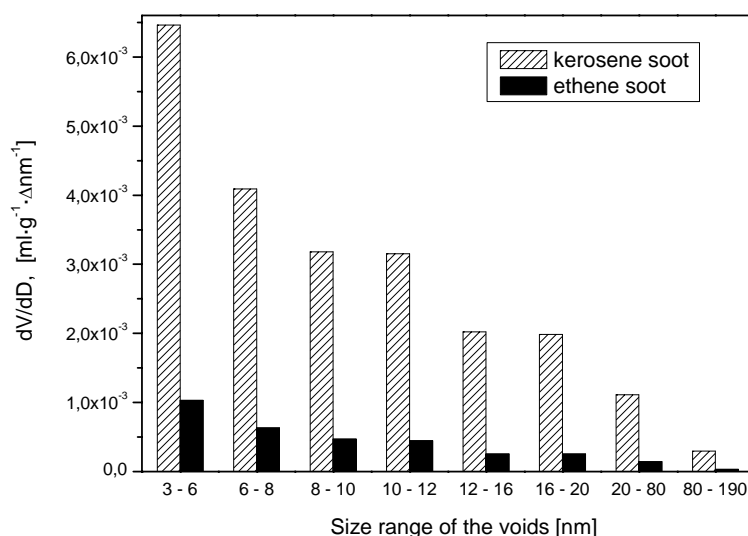


Figure 2.5-4: Free space distribution of the kerosene and ethene soot

Figure 2.5-4 shows that for both types of soot voids with small sizes are predominant than the big size voids and for each size range the voids in ethylene soot have definitely smaller volume (around 7 times smaller) than in kerosene soot.

2. Experimental part

For further analysis of the soot samples we have performed some DRIFTS measurements. A typical DRIFTS spectrum of fresh kerosene soot surfaces, taken in our laboratory, is represented in Figure 2.5-5. For the measurement the soot sample has been mixed in a mortar with CaF_2 as a reference material with ratio Soot/ $\text{CaF}_2 = 1/20$, in order to improve the reflectivity of the sample. The spectrum is obtained after subtraction of the spectrum of the reference material and following conversion into Kubelka-Munk units, with resolution of 4 cm^{-1} .

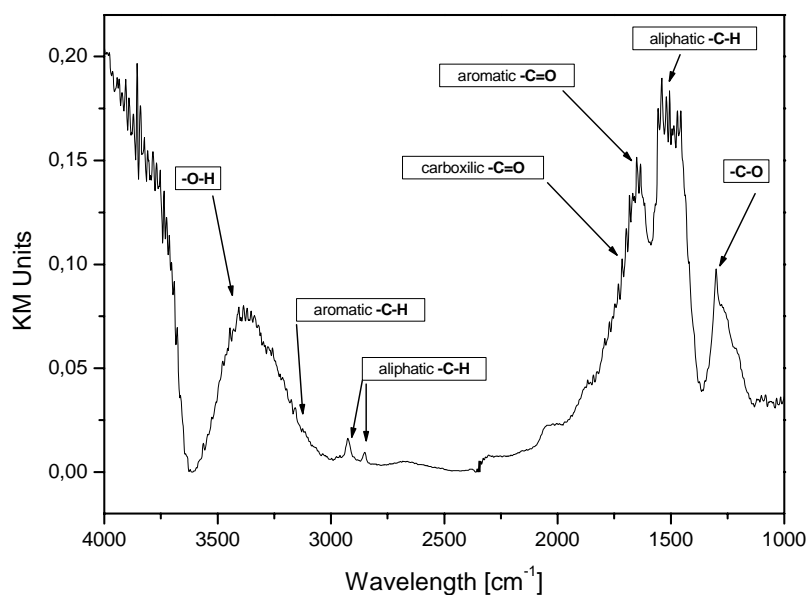


Figure 2.5-5: DRIFTS spectrum of fresh kerosene soot

One of the disadvantages of the DRIFTS method is its relative low sensitivity when used for highly absorbing materials like soot, due to the dilution with reference material. In DRIFTS we can observe relatively broad bands, compared to the pure IR spectra, but nevertheless several important regions in the spectrum can be very well distinguished. In Figure 2.5-5 is given the assignment of the bands, confirming the aromatic structure of the sample with surface oxygen containing groups, in good agreement with literature data [Akhter et al., 1985a], [Dandekar et al., 1998]. The DRIFTS spectra of kerosene and ethylene soot look very much alike. Unfortunately the method was not sensitive enough at our conditions in order to observe significant differences in the structure. However, as confirmed from our further results, the two types of soot show extremely different behaviour in their reactivity.

2.5.3 Sample preparations

Mineral dust samples:

For the Knudsen cell measurements the samples were prepared in the following manner: a quantity between 130 and 300 mg dry weight of mineral dust was suspended in approximately 0.5 ml de-ionised water and the suspension was subsequently spread on the sample holder (quartz glass/copper disc). The sample was then mount in either the room- or low-temperature support of the Knudsen cell and carefully dried under vacuum before each experiment.

For the SEM and ESEM measurements, the mineral dust samples were prepared in the same manner like for the Knudsen cell, but using much lower quantities (between 1 and 3 mg) and the sample holder of the electron microscope. The difference between the two techniques is that the samples analysed in the SEM mode should be made conductive. Therefore they were sputtered with gold for 10 minutes before the measurement.

Soot samples:

For the Knudsen cell measurements both kerosene and ethylene soot have been directly gathered from the flame on the sample holder surface (quartz or copper disc), after which it was mounted in the sample compartment of the Knudsen cell, and the samples carefully dried under vacuum for at least 10 hours. For the measurements of the reaction of NO₂ and soot, the samples were also additionally preheated to 573 K under vacuum for at least 1 hour. The reasons and effects from this preheating procedure are discussed further in detail.

For the SEM and ESEM measurements, both soot samples were prepared in the same manner like for the Knudsen cell – gathered directly from the flame of the burner on the sample holder of the electron microscope. Here again for the SEM mode, the samples were sputtered with gold for 10 minutes before the measurement.

For the DRIFTS measurements the soot samples were gathered again on quartz plate, but then mixed with CaF₂ in a mortar (for better reflectivity of the sample) and afterwards mount in the sample compartment of the DRIFTS cell.

2. Experimental part

For the ion chromatography measurements the soot samples from the Knudsen cell were diluted in slightly alkaline pure water and put in an ultra-sound bath for an hour before analysis.

2.5.4 Calibration of the mass spectrometer signals

In order to receive the absolute concentration of the gas species in the Knudsen cell reactor, the MS-signals should be previously calibrated.

For the calibration, a certain amount of gas is filled in the calibrated volume (V_c) and is introduced through the capillary into the Knudsen cell in the absence of sample (plunger down). The time is measured (Δt), for which the pressure in the calibrated volume decreases with 0,03 Torr ($\Delta p = 0,03$ Torr). The measurements are performed at least at four different pressures in the calibrated volume and for all four sizes of the escape orifice. The calculations are based on the ideal gas theory. For an ideal gas:

$$\text{Equation 2.5-1} \quad pV_c = nRT$$

$$\text{Equation 2.5-2} \quad pV_c = \frac{N}{N_A} RT \Leftrightarrow pV_c N_A = NRT \Leftrightarrow N = \frac{pV_c N_A}{RT}$$

$$\text{Equation 2.5-3} \quad F_{in} = \frac{dN}{dt} = \frac{dp}{dt} \frac{V_c}{RT} N_A$$

where V_c is the calibrated volume, p is the pressure in the calibrated volume, N is the number of molecules inside the cell, N_A is the Avogadro's constant, R is the universal gas constant and T the temperature in Kelvin. In the absence of a sample the flow entering the reactor (F_{in}) is equal to the flow escaping the reactor (F_{out}) and the calibration factor m can be calculated with the equation:

$$\text{Equation 2.5-4} \quad F_{in} = m \cdot S$$

where S is the output signal of the mass spectrometer. From the graphic representation of $F_{in}=f(S)$, the calibration factor m is defined as the slope of the calibration line. As an example in Figure 2.5-6 is represented calibration for NO_2 as a reactive gas. As already mentioned NO_2 is detected at m/e 46 and m/e 30 at the mass spectrometer. The calibration factors for these two signals are respectively: $m_{30} = 5.11 \cdot 10^{13} [\text{mV}^{-1} \text{ s}^{-1}]$ and $m_{46} = 2.24 \cdot 10^{13} [\text{mV}^{-1} \text{ s}^{-1}]$.

2. Experimental part

Knowing the calibration factor m for a given gas, its concentration can be calculated with:

$$\text{Equation 2.5-5} \quad C = \frac{F_{in}}{k_{esc}V} = \frac{m \cdot S}{k_{esc}V}$$

where V is the volume of the Knudsen cell, k_{esc} is the escape rate constant and S the output signal of the mass spectrometer.

All the gas species used for this work, except HONO, are commercially available and can be directly used for calibration of the mass spectrometer signal. The difficulty with HONO calibration comes from the fact that there is no available commercial source for it.

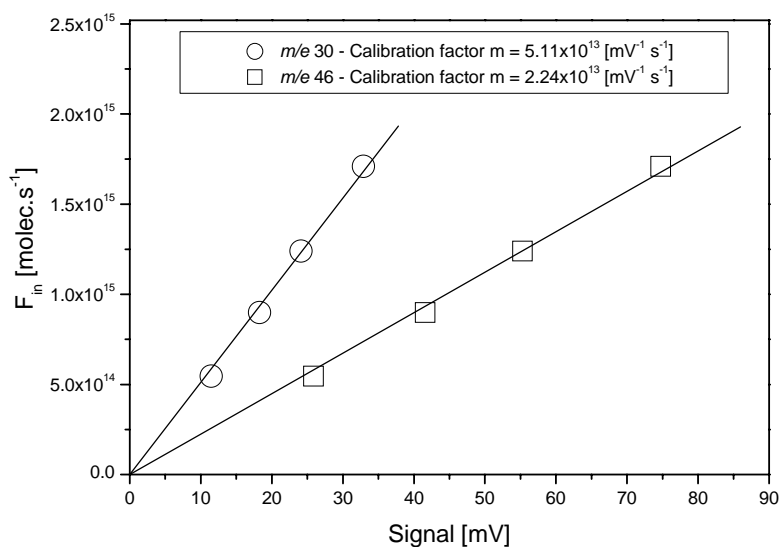
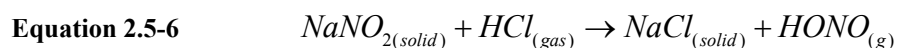


Figure 2.5-6: Calibration factors for NO₂

To calibrate the HONO signal (which is detected at peaks m/e 47 and m/e 30) the following chemical reaction has been used:



It has been performed in the Knudsen cell reactor. Solid NaNO₂ was mounted in the sample compartment, and gas phase HCl was used as a reactant. A typical temporal profile of the signal for this reaction is shown in Figure 2.5-7.

2. Experimental part

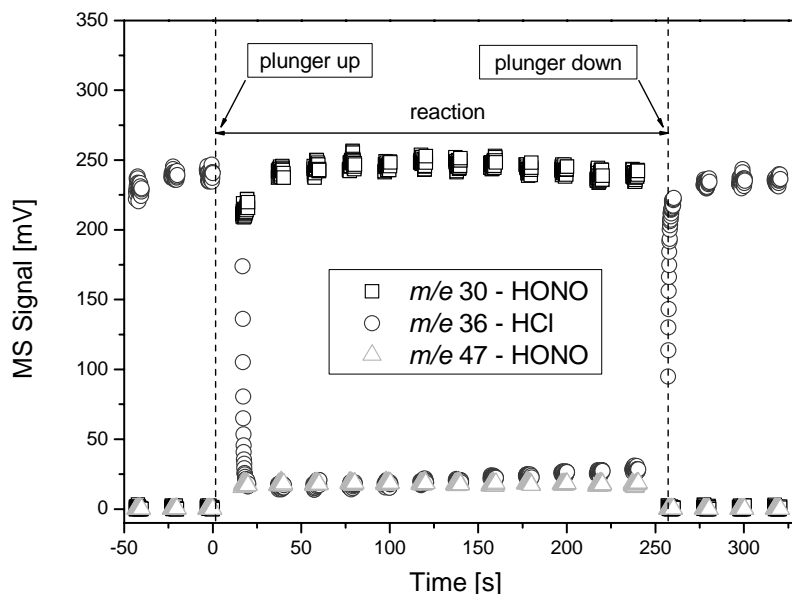


Figure 2.5-7: Typical temporal profile for the reaction of NaNO_2 and HCl , used for the calibration of HONO

It can be seen that before reaction when the plunger is closed (times from -50 to 0s) we observe only the signal for HCl (m/e 36). At time $t = 0\text{s}$ the plunger is opened and the fresh NaNO_2 surface is exposed to the gas phase HCl . In the time interval from 0 to 250s we can observe the rapid decrease of the signal for HCl and the immediate appearance of signals for the product HONO (m/e 30 and m/e 47). At time $t = 250\text{s}$ the plunger is closed again and the reaction is stopped.

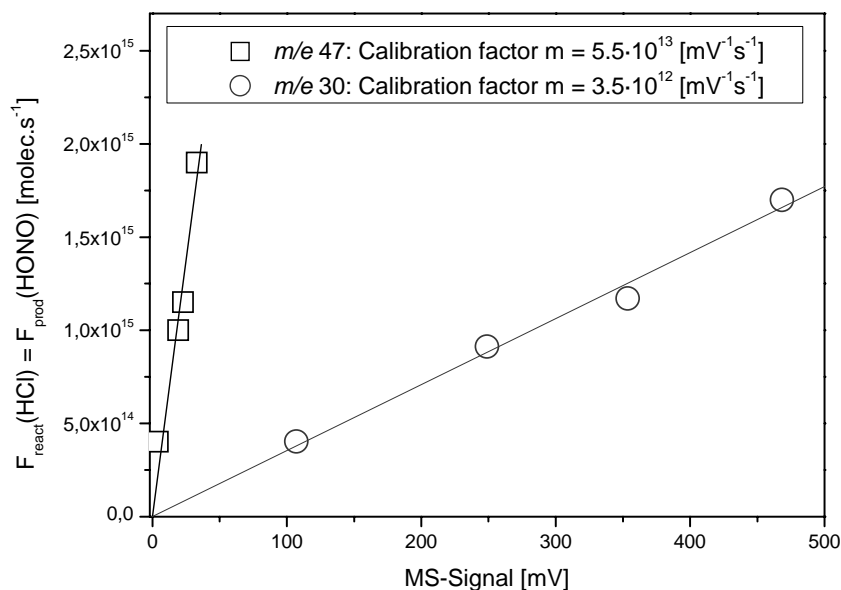


Figure 2.5-8: Calibration factors for HONO

2. Experimental part

From the measurement shown in Figure 2.5-7 the reactive flow of HCl to the surface ($F_{react}HCl$) can be calculated, and under the assumption that for each molecule HCl, due to this reaction, one molecule of HONO is produced, we can estimate the produced flow of HONO as:

$$\text{Equation 2.5-7} \quad F_{prod}(HONO) = F_{react}(HCl)$$

After investigating the reaction at different initial concentrations of HCl we obtain different $F_{prod}HONO$ which we can plot against the signal for HONO in mV (obtained directly from the measurement) for m/e 30 and m/e 47, As a result the calibration factor m can be calculated from the slope of the fitted line, as shown in Figure 2.5-8.

3 RESULTS AND DISCUSSION

3.1 Adsorption of H₂O on mineral dust and soot surfaces

In this work results for the uptake of water on mineral dust (MD) at temperatures below 298 K are presented for the first time. In addition, the interaction of water (and deuterated water) with kerosene soot (KS) at temperatures below 298 K has been studied. The experiments have been performed at water vapour pressures below 1 Pa in a low pressure flow reactor (Knudsen cell). Kinetic data for the adsorption and desorption processes as well as thermo-chemical data in form of surface coverages and adsorption enthalpies have been obtained. The results for the two surfaces are compared in order to assess whether hydrophilicity, a macroscopic property of a surface, can be characterized by fundamental quantities such as kinetic parameters.

Both mineral dust [Ginoux et al., 2001], [Husar et al., 2001], [Tabazadeh et al., 1998] and soot surfaces [Israel et al., 1996], [Blake and Kato, 1995], [Petzold et al., 1998] are ubiquitous in the atmosphere and are believed to have a direct effect on its radiation budget and on the climate, due to their possibility to act as cloud or ice condensation nuclei (CCN/ICN) and form cirrus clouds [DeMott et al., 2003b], [Hung, et al., 2003], [Pruppacher and Klett, 1980]. In order to estimate this possibility the ability of the particle to act as a surface for nucleation of water vapour to form either liquid droplets or ice particles should be known. This last parameter, however, is very difficult to quantify.

From the point of view of the classical nucleation theory the efficiency of a particle to act as condensation nuclei is given by the contact angle between a water droplet and the particle's surface and is referred to as wettability or hygroscopicity [Pruppacher and Klett, 1980]. The contact angle, however, is a macroscopic concept, and can not be applied for surface coverage of only a few monolayers. But once a particle is completely covered with a water layer, further water molecules can condense on that surface. The activation of such particle for water condensation then only depends on the size of the particle which has to be large enough to overcome the Kelvin effect at a given relative humidity. Therefore, the microscopic approach

3. Results and discussion

to the subject of hygroscopicity is also very important. From its point of view a water molecule colliding with a surface, not completely covered with water, may adsorb at a reactive surface site and/or desorb back into the gas phase. If the reactive surface sites are numerous a monolayer of water is readily formed, the particle is completely covered with water and is consequently activated for water condensation and may be regarded as hydrophilic. Therefore the adsorption and desorption rates together with the amount of water adsorbed, are important parameters in the assessment of the hydrophilicity of an atmospheric particle which will be discussed in this chapter in detail for the two different types of surfaces (mineral dust and kerosene soot).

The results obtained for the interaction between water and mineral dust/soot can be regarded basically from two points of view: kinetics and thermodynamics. The kinetic parameters (rate coefficients, uptake coefficients, reaction order) can be directly calculated from the measurements with the Knudsen cell reactor. More important is that, based on the kinetic measurements, we have tried to describe the system thermodynamically in terms of standard enthalpies and entropies of adsorption, as presented later in this work.

3.1.1 Adsorption of water on kerosene soot surfaces

The investigation of the interaction between soot and water was performed with the two different types of soot – ethylene and kerosene. For ethylene soot we could observe uptake only below 140 K, which was interpreted as condensation of water on the cold sample surface because the vapour pressure of water under our experimental conditions at 140 K and below, was always higher than the saturation vapour pressure of water. Further in this chapter, only the results of the interaction of water with kerosene soot are presented.

3.1.1.1 Kinetic approach

For the investigation of the uptake of water vapour on kerosene soot, the samples were produced in the oil lamp as described before (Chapter 2.5.2). The measurements have been performed with gas phase concentrations in the range of $5 \cdot 10^{11}$ to $8 \cdot 10^{12}$ molecules \cdot cm $^{-3}$, surface temperatures between 203 and 298 K and sample masses between 10 and 23 mg.

3. Results and discussion

Before the start of each experiment all kerosene soot samples have been carefully dried under vacuum until by opening or closing the plunger the background signal for water did not change.

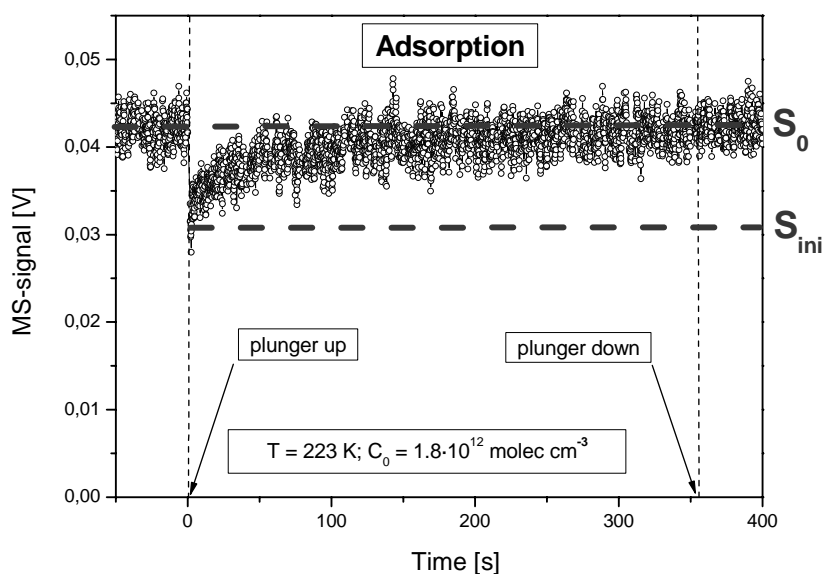


Figure 3.1-1: Typical temporal profile for the uptake of water on kerosene soot surfaces at 223K, $c_0 = 1.8 \cdot 10^{12}$ molecules cm^{-3} , $m(\text{soot}) = 15.5$ mg.

A typical signal profile for the measurement is shown in Figure 3.1-1. The measurement has been done at $T = 223$ K, and gas phase concentration of water $c_0 = 1,8 \cdot 10^{12}$ molecules $\cdot \text{cm}^{-3}$. At the beginning of each experiment a constant flow of water vapour is introduced into the Knudsen cell until receiving a steady MS signal S_0 . At time $t = 0$ s the plunger is opened, the reactive surface is exposed to the water vapour, and due to the uptake, the signal steeply decreases to the value S_{ini} followed by an increase and fast complete saturation with approximately 200s and reaching the initial value (S_0). At time $t = 350$ s the plunger is closed and the interaction is stopped.

It is obvious from Figure 3.1-1 that the uptake of water on kerosene soot is strongly time dependent and it would be interesting to interpret this signal behaviour in terms of reversibility of the process and effects of surface saturation.

We assume two basic possibilities for the uptake mechanism which can lead to such a signal shape: *reversible* and *irreversible* uptake. The schematic signal profile for these two cases is represented in Figure 3.1-2. In the reversible case (a) water is taken up with constant time

3. Results and discussion

independent rate but with advancing exposure time, the desorption rate also increases which results in a reduced steady state signal and, respectively, reduced net uptake.

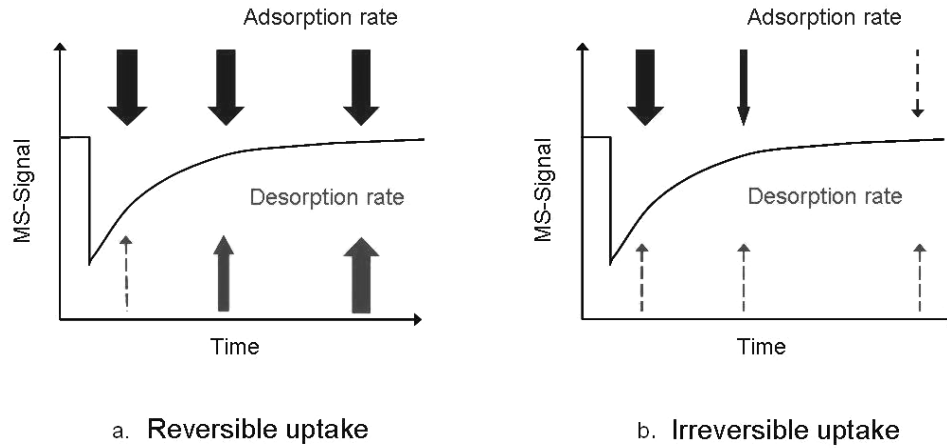


Figure 3.1-2: Schematic representation of the temporal profile of the MS-signal. The thickness of the arrows is proportional to the adsorption (desorption) rate.

The second possibility (Figure 3.1-2, b) for explaining such a temporal profile is the irreversible case where with advancing exposure time the adsorption rate decreases due to the occupation of active surface sites whilst no significant desorption can be observed. In each case, however, the uptake of water should cease after a certain time either because desorption rate equals adsorption rate (equilibrium) or because of the complete occupation of the active surface sites for water adsorption.

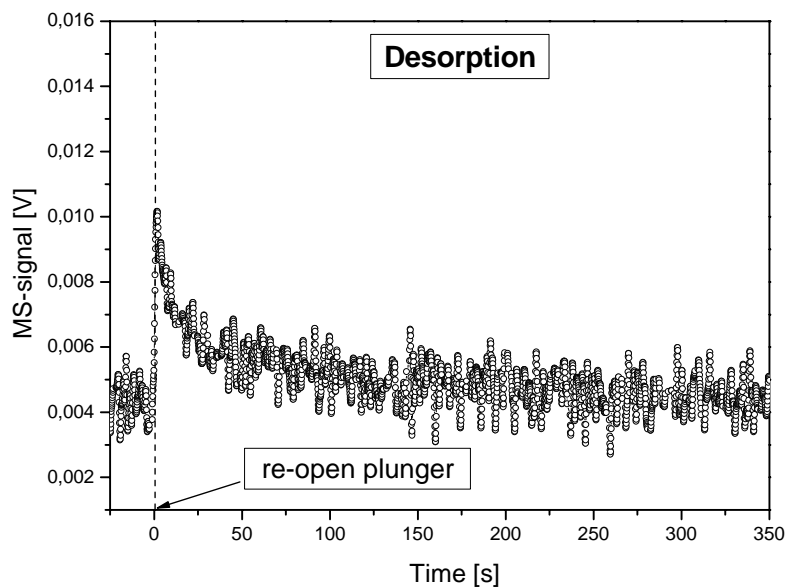


Figure 3.1-3: Observed desorption of water from the soot surface, after the end of the experiment, represented in Figure 3.1-1, and re-opening the sample compartment

3. Results and discussion

In order to investigate the possible desorption of water from the surface back into the gas phase, after the end of the experiment the flow of water into the cell has been stopped, and after reaching the background signal, the plunger has been re-opened (0 s, in Figure 3.1-3). Desorption of water from the surface has been observed. This finding indicates that the uptake of water on soot is reversible even at lower temperatures, as the number of desorbed molecules can be deduced from the integration of the signal (see Chapter 2.1.2.1).

In Figure 3.1-4 the dependence of the number of desorbed H_2O molecules ($N_{des}^{H_2O}$) as a function of the number of adsorbed H_2O molecules ($N_{ads}^{H_2O}$) is represented. It can be seen that 72% of the water molecules adsorbed are released back into the gas phase and only 28% remain on the surface even at lower temperatures of 223K.

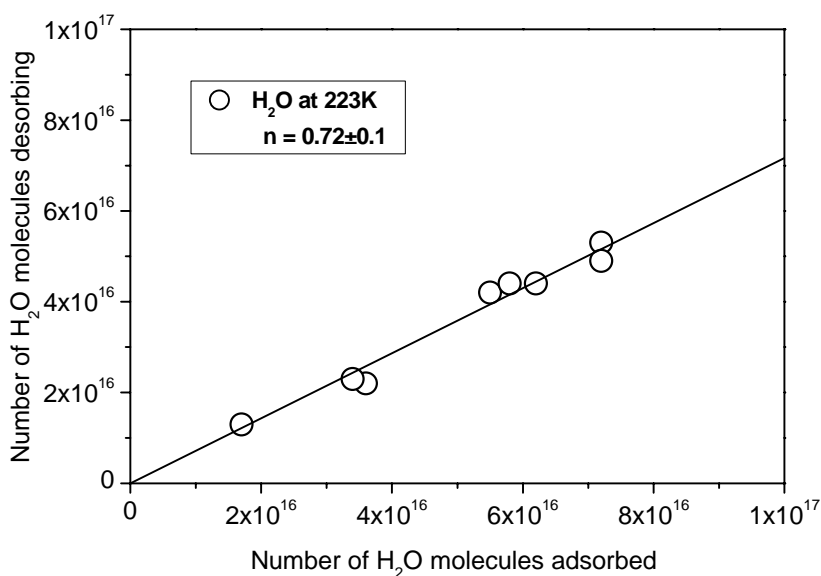


Figure 3.1-4: Number of desorbed H_2O molecules as a function of the number of the H_2O molecules adsorbed (T = 223 K)

A determination of the rate constants and uptake coefficients from the MS signals according to the calculations previously described (Chapter 2.1.2.1) is only valid for a first order uptake process. Therefore it should be proved if this condition is fulfilled. As already described in detail in Chapter 2.1.2.1, the order n of the uptake process is obtained from a linear regression of a double logarithmic plot of the loss rate versus the gas phase concentration. For the interaction between H_2O and kerosene soot, the uptake has been shown to follow a first order

3. Results and discussion

rate law for the whole temperature interval investigated, as can be seen in Figure 3.1-5, where it is represented for 223K.

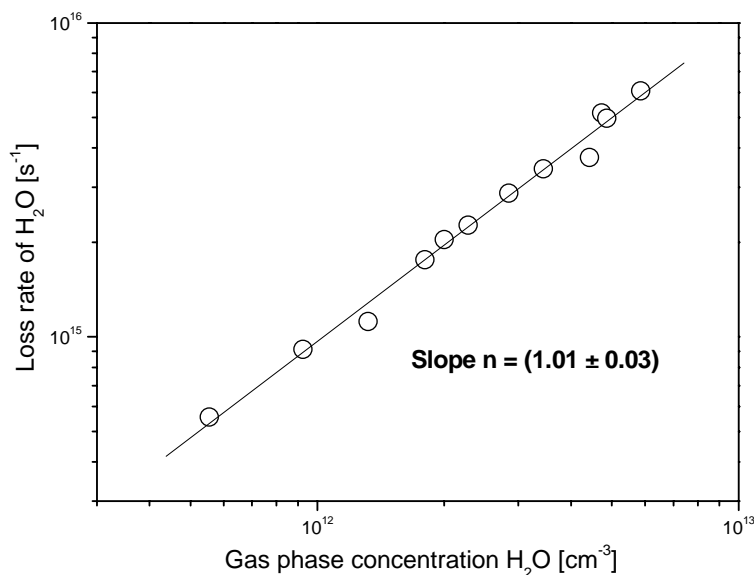


Figure 3.1-5: Double logarithmic plot of the loss rate of H₂O versus the gas phase H₂O concentration. The solid line has a slope of 1 indicating a first order uptake process

Knowing the order of the process, initial rate constants and, respectively, initial uptake coefficients have been calculated, again using the values for S_0 and S_{ini} , Equation 2.1-11 and Equation 2.1-12.

The calculated initial uptake coefficients have been found to be strongly dependent on the sample temperature as it is represented in Figure 3.1-6. No uptake has been observed at 298 K in contrast to the lower temperatures ($T < 243$ K). As can be seen in Figure 3.1-6 between 243K and 203K the initial uptake coefficient is increasing by nearly one order of magnitude from $\gamma_{ini} = 7 \cdot 10^{-4}$ to $\gamma_{ini} = 5 \cdot 10^{-3}$. This is in agreement with [Alcala-Jornod and Rossi, 2004].

The uptake of water on kerosene soot as a function of sample mass is represented in Figure 3.1-7 for $T = 223$ K. Each point is a mean value from at least 3 different measurements. It can be seen that γ_{ini} increases slightly with increasing sample mass, indicating a possible diffusion of the gas phase molecules into the bulk of the sample at this temperature, confirmed later from the mass dependence of K_p (Figure 3.1-16).

3. Results and discussion

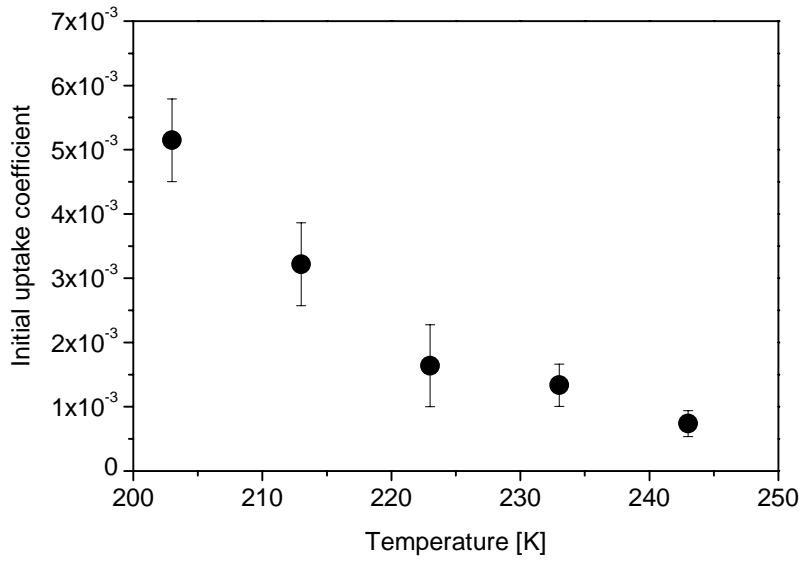


Figure 3.1-6: Temperature dependence of the initial uptake coefficients of water on kerosene soot.

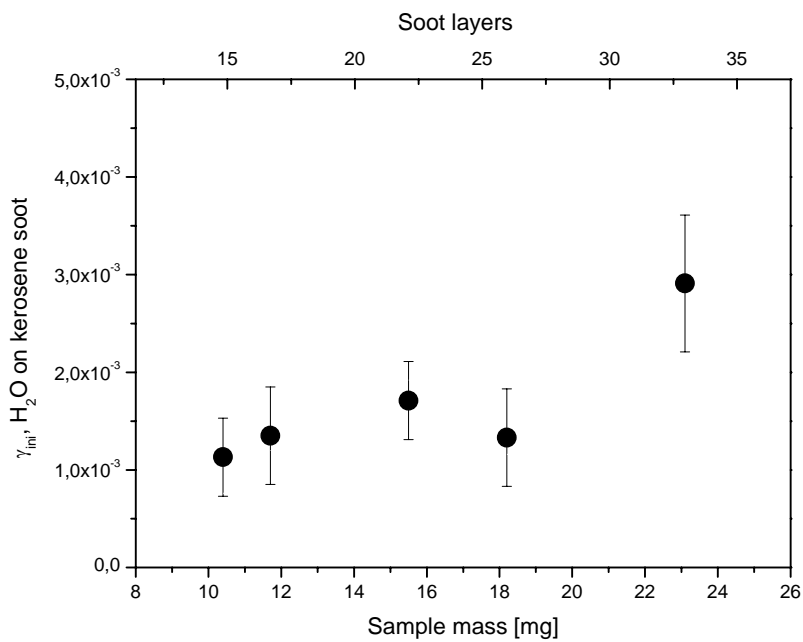


Figure 3.1-7: Initial uptake coefficients of H_2O on kerosene soot, as a function of the sample mass at 223 K

D₂O measurements:

Having in mind that the uptake coefficient describes the net loss of the gas species on the surface and the fact that after stopping the experiment we could observe desorption of water from the surface, we assume that adsorption as well as desorption processes can contribute to the net uptake. In order to distinguish whether the negative temperature dependence of γ_{ini} is

3. Results and discussion

due to an increasing adsorption rate constant or decreasing desorption rate constant, additional measurements with D₂O have been performed.

It is known that isolated –OH groups, which are responsible for water adsorption, are present on the surface of the sample [Zettlemoyer and Narayan, 1966]. The advantage of using D₂O is that it could undergo a H/D exchange with such acidic surface H-atoms, in order to form HDO, hence with the behaviour of D₂O as a reactant we can assess the availability of such active surface sites and their occupation during the experiment. And also from the detection of HDO as gas phase product we can distinguish both processes of adsorption and desorption.

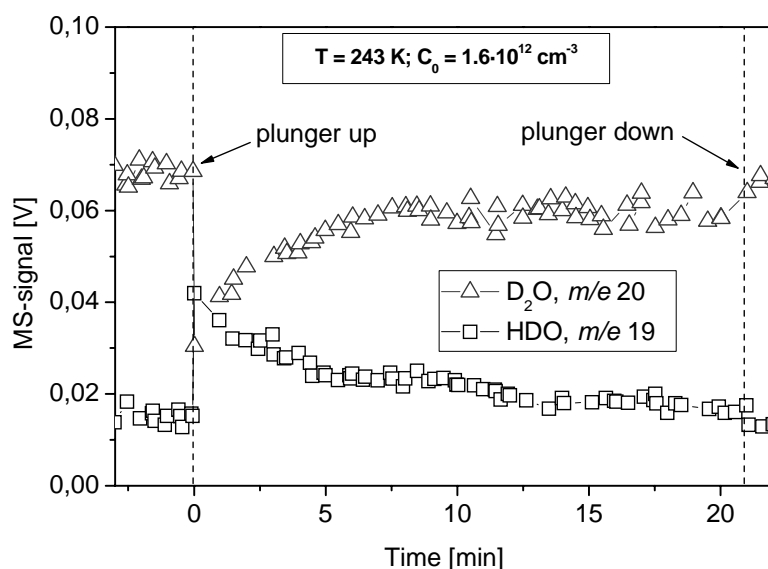


Figure 3.1-8: Typical temporal profile for the measurement of D₂O vapour on kerosene soot at 243K, ($c_0 = 1,6 \cdot 10^{12}$ molecules cm^{-3} ; $m(\text{soot}) = 30.7$ mg)

A typical D₂O measurement performed at 243K is shown in Figure 3.1-8. Here the signals for m/e 20 (D₂O) and m/e 19 (HDO) are represented. At time $t = 0$ min the plunger is lifted and the sample is exposed to the reactive flow. We observe an immediate initial uptake, followed by a time dependent uptake for at least 10 min, which results finally into a steady state uptake. At time $t = 21$ min the plunger is closed and the interaction stopped.

In Figure 3.1-8 the signal for D₂O is represented together with the signal for HDO. As already discussed above, a HDO signal always accompanies the D₂O signal because of the very fast H/D exchange on the walls of the Knudsen cell. From Figure 3.1-8, however, it is clearly

3. Results and discussion

visible that HDO forms instantly as a product from the interaction of soot and D₂O, indicating that D₂O undergoes H/D exchange at the sample surface on groups, containing acidic H-atom. Such surface groups are also responsible for the adsorption of H₂O on the soot surface so that D₂O and H₂O uptake measurements should show the same pattern.

Another proof of the instantaneous formation and release of HDO in the gas phase is the pulse measurement for the uptake of D₂O, represented in Figure 3.1-9. In Chapter 2.1.2.2, the measuring principle and the main calculations for the pulse measurements have been explained in detail. Apparently HDO is instantaneously formed and released into the gas phase due to the reaction. The control pulse for HDO is due to the H/D exchange with the walls of the reactor, but the reactive pulse of HDO is much higher than the control pulse, indicating additional HDO production.

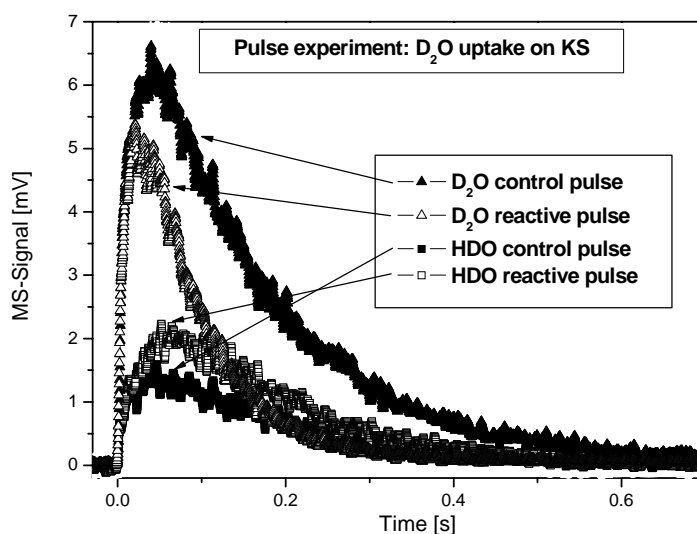


Figure 3.1-9: Pulse experiment of D₂O on kerosene soot at 297 K – formation of HDO

In contrast to the initial uptake coefficients for H₂O on soot, the calculated initial uptake coefficients for D₂O on soot show no mass dependence, as it is represented in Figure 3.1-10 for a temperature of T = 300 K. This indicates once again that in the case for D₂O we measure the actual initial uptake coefficient. This is also confirmed from the value of γ_{ini} obtained for the pulse measurements of D₂O, which is in good agreement with the obtained steady state values (Figure 3.1-11).

3. Results and discussion

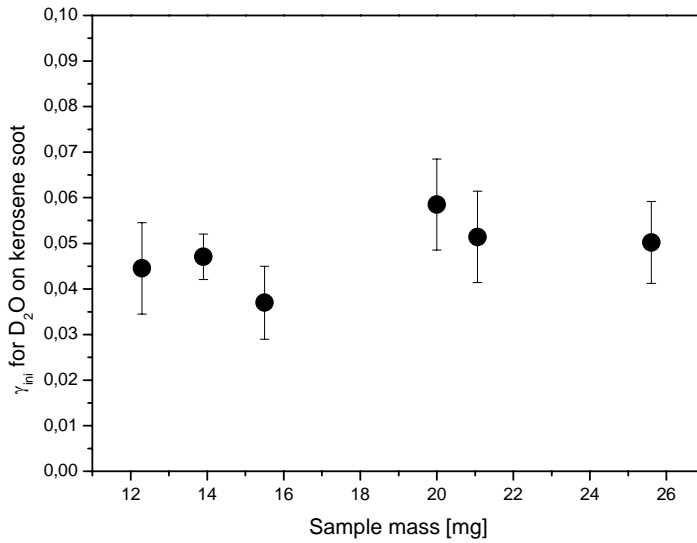


Figure 3.1-10: Initial uptake coefficients for D₂O on kerosene soot as a function of the sample mass

Further for comparison the initial uptake coefficients calculated for the D₂O measurements are represented together with the uptake coefficients for H₂O on kerosene soot in Figure 3.1-11. Two important conclusions can be made:

➤ The uptake of D₂O is apparently much larger than that of H₂O on soot. It results in a mean value of $\gamma_{ini} = (4.7 \pm 0.2) \cdot 10^{-2}$ which is more than one order of magnitude larger than the value for the uptake of H₂O on soot.

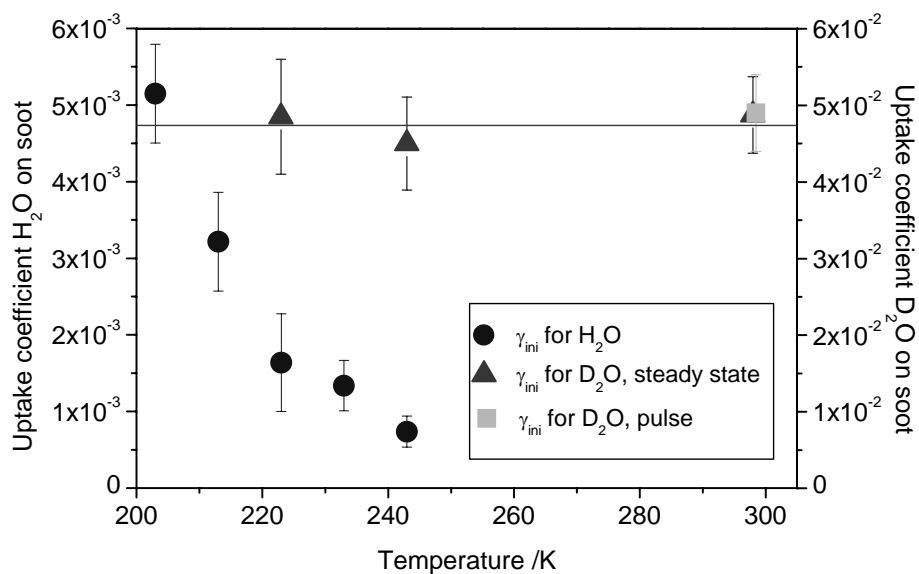


Figure 3.1-11: Comparison of the initial uptake coefficients for H₂O and D₂O on kerosene soot as a function of the surface temperature

3. Results and discussion

This fact is due to the formation of HDO and its observed desorption from the surface. Unlike for the case of H₂O, where the net uptake is zero after a few minutes (Figure 3.1-1) and at 223K 72% of the H₂O molecules desorbed back into the gas phase (Figure 3.1-4). D₂O is desorbing from the surface in the form of HDO and consequently the adsorption and desorption processes could be distinguished. If we take the sum of the adsorbed D₂O and desorbed HDO signals, Figure 3.1-8 would result in a similar uptake behaviour as observed for H₂O (Figure 3.1-1). This is also confirmed by the mass balance of D₂O and HDO shown in Figure 3.1-12. It indicates that at 298K 82% of the D₂O molecules taken up are consequently released back into the gas phase as HDO upon reaching steady state. This value is slightly higher than the one for H₂O at 223K (Figure 3.1-4) in agreement with a slower desorption rate at lower temperatures.

➤ Unlike the uptake of H₂O, the uptake of D₂O is independent of temperature. For the temperature interval measured, as already shown in Figure 3.1-11, it results in the mean value of $\gamma_{ini} = (4.7 \pm 0.2) \cdot 10^{-2}$ which corresponds to the value of $k_{ini} = 3.7 \text{ s}^{-1}$.

To exclude the fact that the initial uptake coefficients for D₂O are also affected by desorption, some pulse valve D₂O experiments on soot have been done at the highest temperature (298K), where the process of desorption should be most effective. The advantage of the pulse valve technique is that the process can be followed in a millisecond interval, and we can be sure that with it we can observe only the initial adsorption process on a fresh sample surface. The value for the initial uptake at room temperature from the pulsed valve measurements is in a very good agreement with the value obtained from the steady state experiments as shown in Figure 3.1-11, indicating that the initial uptake coefficients received from the D₂O measurements on soot are not affected by desorption.

These findings about the interaction of D₂O with kerosene soot surfaces helped us to make two major conclusions about the interaction of H₂O on kerosene soot:

- i. The fact that the initial uptake of D₂O on soot has proved to be temperature independent (the adsorption rate remains constant) indicates that the observed negative temperature dependence of the uptake of H₂O is due to the decreased desorption rate upon lowering the temperature of the surface.

3. Results and discussion

ii. The initial uptake coefficients determined for H₂O on soot are affected by desorption and are therefore underestimated. Their more realistic value should be taken from the D₂O measurement results ($\gamma_{ini} = (4.7 \pm 0.2) \cdot 10^{-2}$, $k_{ini} = 3.7 \text{ s}^{-1}$).

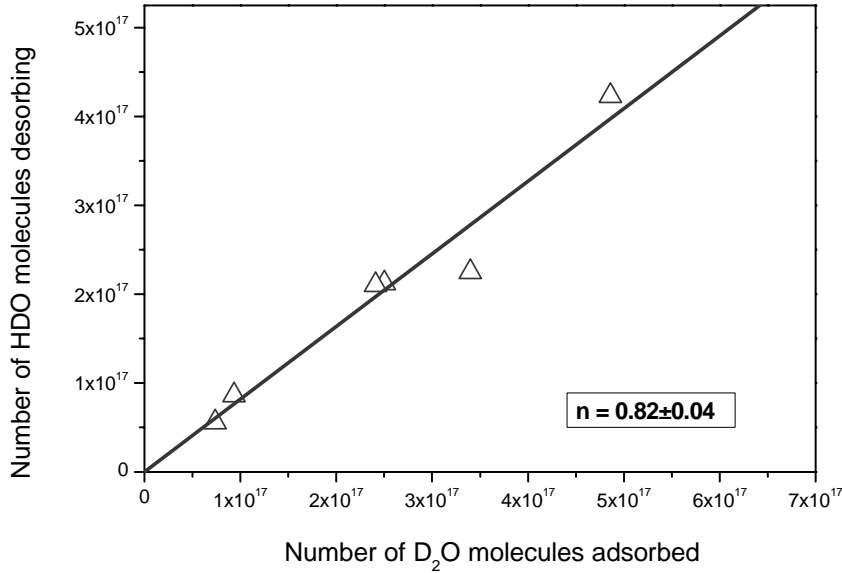


Figure 3.1-12: Number of HDO molecules desorbed as a function of the number of adsorbed D₂O molecules; T = 298 K

Not only the adsorption but also the desorption process for the interaction of water with soot can be estimated with respect to its kinetics. For sub-monolayer coverage at equilibrium, the adsorption ↔ desorption process can be described with:

$$\text{Equation 3.1-1: } k_{ads} N(gas)_{eq} = k_{des} N(ads)_{eq}$$

where k_{ads} and k_{des} are the adsorption and desorption rate constants, respectively, $N(gas)_{eq}$ is the number of gas phase molecules at equilibrium, and $N(ads)_{eq}$ is the number of the adsorbed molecules at equilibrium. $N(gas)_{eq}$ can be determined from the gas phase concentration of water at saturation ($\gamma = 0$) and $N(ads)_{eq}$ is given from the total amount of water taken up during the experiment. For the adsorption rate constant k_{ads} the temperature independent value of $k_{ini} = 3.7 \text{ s}^{-1}$ is taken, in accordance with the D₂O measurements.

The desorption rate constants calculated with Equation 3.1-1 vary from 1.3 s^{-1} for the highest temperature to $9.7 \cdot 10^{-2} \text{ s}^{-1}$ for the lowest temperature. They are represented in the form of Arrhenius expression in Figure 3.1-13. From a linear regression, an activation energy of $27.5 \pm 0.4 \text{ kJ mol}^{-1}$ has been derived in good agreement with the standard adsorption enthalpy derived below.

3. Results and discussion

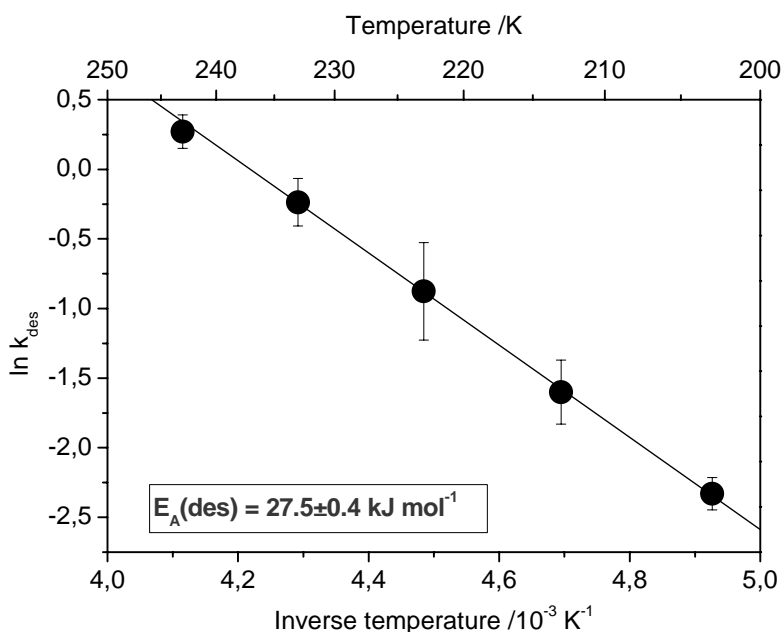


Figure 3.1-13: Arrhenius representation of the k_{des} of water for kerosene soot

This value is significantly smaller than the enthalpy of evaporation of 44 kJ mol^{-1} [Chase, 1985] and indicates that the interaction between water and soot is weaker than that between H_2O molecules themselves. To our knowledge, there is only one study to which our results could be compared. In agreement with the results obtained in this work [Alcala-Jornod et al., 2002] also found relatively low activation energies between 29.3 kJ mol^{-1} and 37.7 kJ mol^{-1} for the desorption of water from different types of soot. In addition, in that work desorption rate constants have been determined which are, however, roughly one order of magnitude higher than the one derived here. These differences might be due to the use of soot samples produced from different fuels as well as by different preparation procedures. These samples will certainly exhibit a different degree of surface oxidation which is known to strongly influence water adsorption [Chughtai et al., 1999a]. [Chughtai et al., 2002].

3.1.1.2 Thermodynamic approach

In order to determine the thermochemistry of the process, adsorption isotherms based on the experimental data, have been constructed. In Figure 3.1-14 the total number of molecules adsorbed is represented as a function of gas phase concentration of water for three different temperatures. It can be seen that this number is increasing with decreasing temperature and increasing gas phase concentration, as it is expected for adsorption-desorption mechanism

3. Results and discussion

with non-activated adsorption. This result is in contrast to the adsorption isotherms measured by [Popovitcheva et al., 2001] where it was found that the amount of water adsorbed at a given relative humidity decreased with decreasing temperature. However, this work has been performed at more than four orders of magnitude higher vapour pressures and at temperatures above 253 K.

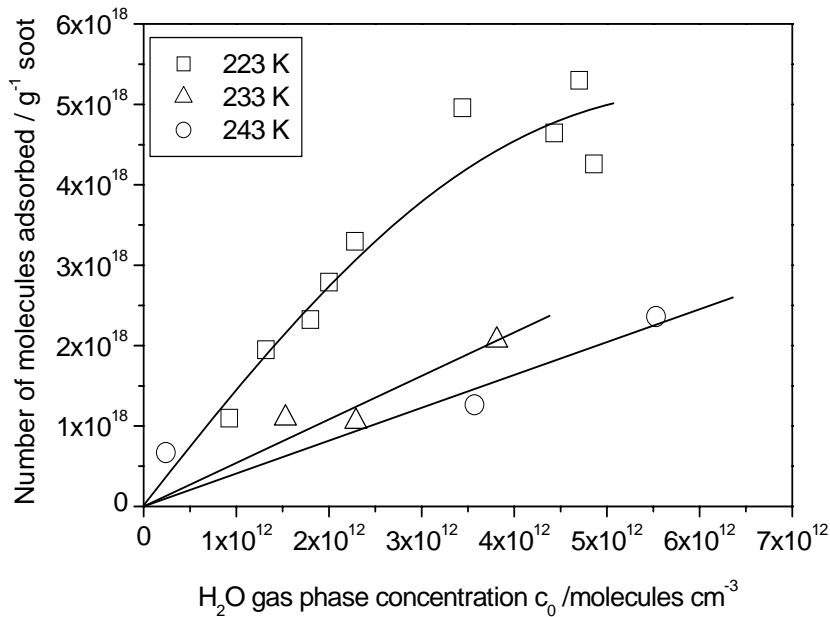


Figure 3.1-14: Total number of molecules adsorbed as a function of gas phase concentration for the uptake of water on kerosene soot.

As can be seen from Figure 3.1-14, at 223 K the number of adsorbed molecules is increasing to the limiting value of $5 \cdot 10^{18}$ molecules·g⁻¹. Taking into account the BET surface area of soot ($6.4 \cdot 10^5$ cm²·g⁻¹) this value corresponds to $8 \cdot 10^{-3}$ monolayers of water. This result is in agreement with the conclusion drawn by [Alcala-Jornod et al., 2002].

To determine the exact reactive surface area available for adsorption, however, is one of the difficulties of the experiment. But still we can assume two reasonable existing limiting cases, schematically represented in Figure 3.1-15 where the grey circles stand for water molecules and with black are represented the soot agglomerates. The upper limit of available surface area is to take the BET surface of the soot sample ($6.4 \cdot 10^5$ cm²·g⁻¹), because it assumes that the whole sample is available for adsorption (Figure 3.1-15, b) which is not always the case. The lower limit of available surface area (Figure 3.1-15, a) is to take for the calculations the

3. Results and discussion

surface area of the uppermost layer (450 cm^2). The latter can be calculated having in mind the particle size, bulk density and BET surface area of the sample (Table 2.5-2).

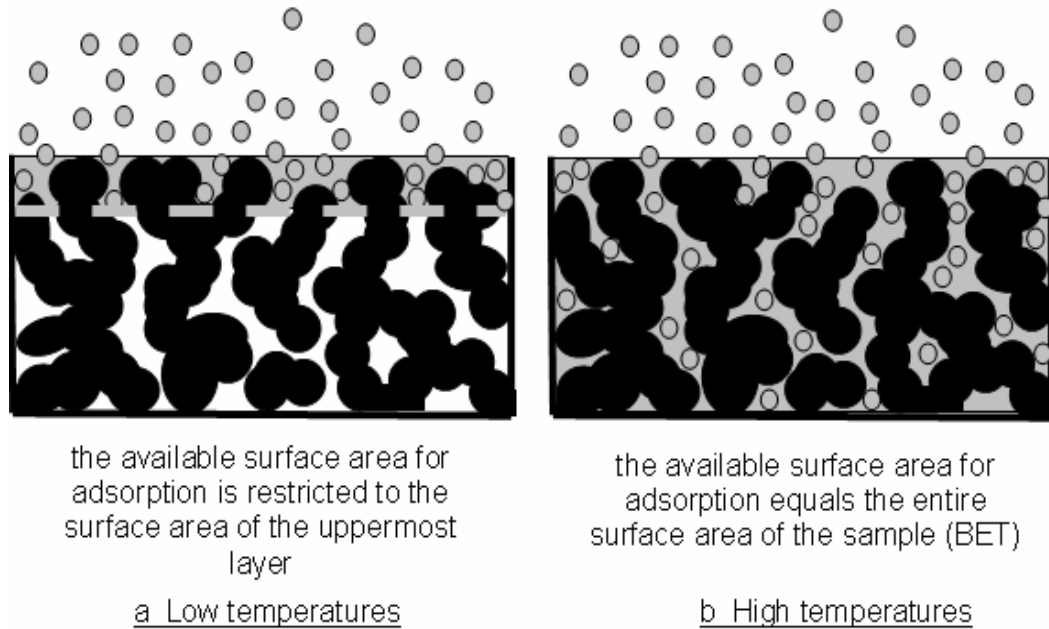


Figure 3.1-15: Limiting cases of available surface area during the measurement. With black are represented the chain formed soot agglomerates and the grey circles represent water molecules

Both values for available surface area, however, depend very much on possibility for diffusion of H_2O molecules into the bulk of the sample. Diffusion is a temperature dependent process and its rate is higher at higher temperatures due to the higher thermal motion of the molecules. Having in mind the relatively wide temperature interval in which our measurements have been performed, we can assume that the case in Figure 3.1-15 (a) is likely to happen at low temperatures where diffusion is slower and is restricted only to the uppermost layer of the sample, and the second case (b) is correct for higher temperatures, where the diffusion rate is higher and it is more likely that the whole surface area of the sample is available for adsorption.

Having in mind the reversibility of the uptake of water on kerosene soot (previously discussed) we can define the adsorption equilibrium constant K_C , which gives us the ratio between the gas phase and adsorbed water molecules at equilibrium:

Equation 3.1-2
$$K_C = \frac{\{H_2O\}}{[H_2O]}, \left[\frac{\text{cm}^3}{\text{cm}^2} \right]$$

3. Results and discussion

where $\{H_2O\}$ is the surface concentration of water (molecules cm^{-2}) and $[H_2O]$ is the gas phase concentration of water (molecules cm^{-3}). K_C can be transferred into the dimensionless equilibrium constant K_P via:

$$\text{Equation 3.1-3} \quad K_P = K_C \frac{A}{V} = \frac{\{H_2O\} A}{[H_2O] V}$$

where A is the standard surface area of $6.7 \cdot 10^{10} \text{ cm}^2 \text{ mol}^{-1}$ and V is the standard volume of the gas $2.24 \cdot 10^4 \text{ cm}^3 \text{ mol}^{-1}$ [De Boer, 1968]. The advantage of K_P is that it is connected to the standard enthalpy of adsorption ΔH_{ads}^0 , and the standard entropy of adsorption ΔS_{ads}^0 :

$$\text{Equation 3.1-4} \quad -RT \ln K_P = \Delta H_{ads}^0 - T \cdot \Delta S_{ads}^0$$

From Equation 3.1-3 two sets of equilibrium constants K_P can be calculated, based on the two limiting cases for the available surface area for adsorption (Figure 3.1-15):

- i. with surface water concentration, relevant to the surface area of the uppermost layer (450 cm^2),
- ii. with surface water concentration, relevant to the entire BET area of the sample (6.4 $cm^2 \text{ g}^{-1}$)

In Figure 3.1-16 these two sets of K_P are represented as a function of sample mass for a given temperature. It can be seen that the equilibrium constants, calculated according to i., are increasing with increasing sample mass, indicating diffusion of water into the bulk of the soot sample. With increasing sample mass the available surface area is increasing and consequently the surface concentration of water is overestimated by taking only into account the uppermost layer.

Another indication for diffusion of water into the bulk of the sample comes from the mass dependence of the D_2O measurements on soot. In Figure 3.1-17 the number of molecules D_2O adsorbed (respectively HDO desorbed) as a function of the sample mass at room temperature are represented. It can be seen that with increasing sample mass both numbers increase indicating diffusion. So taking only into account the surface area of the uppermost layer is not the realistic case for the interaction of water and soot and it would underestimate to great extent the calculated equilibrium constants.

In contrast, the equilibrium constant calculated according to ii. are independent of sample mass (Figure 3.1-16). If only a part of the soot sample were accessible, especially at higher sample masses, the surface concentration would be underestimated and consequently the

3. Results and discussion

derived equilibrium constants would decrease with increasing sample mass, which is not the case.

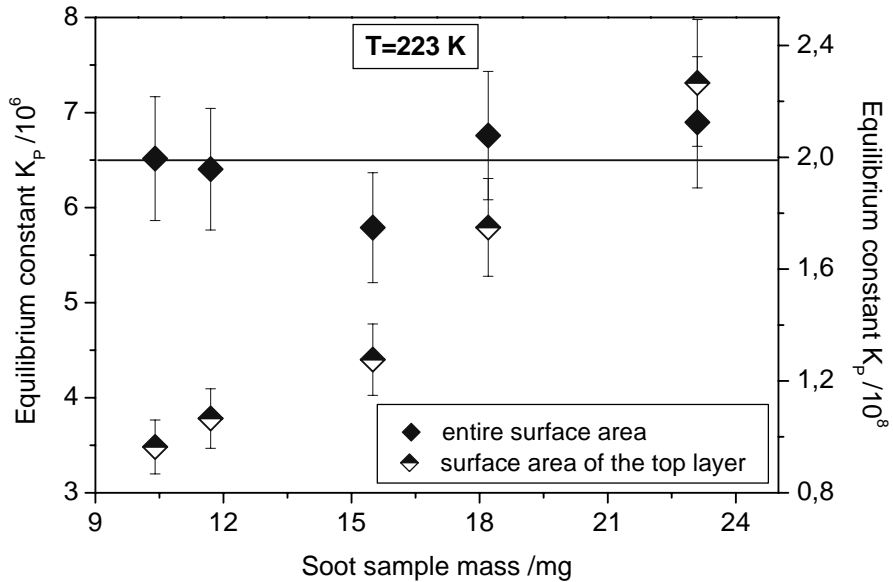


Figure 3.1-16: Dependence of the two sets of equilibrium constants on the sample mass

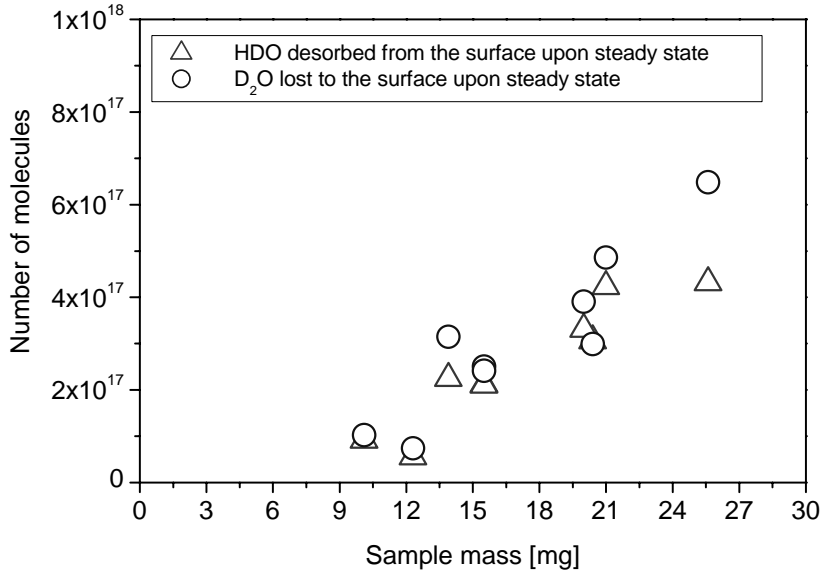


Figure 3.1-17: Mass dependence of the D₂O uptake and HDO production on kerosene soot

The obtained equilibrium constants according to ii. are represented in Figure 3.1-18 as a function of temperature in the form of a Van't Hoff expression. A linear regression of the data yields a standard adsorption enthalpy of $\Delta H_{ads}^0 = -27 \pm 3 \text{ kJ.mol}^{-1}$. This value agrees with results from a theoretical study by [Picaud et al., 2004] obtained by low surface coverages,

3. Results and discussion

which is in good agreement with our findings for submonolayer coverage found above. They have performed molecular dynamic simulations based on quantum chemical results to characterize the adsorption of water molecules on activated graphite surfaces at 250 K.

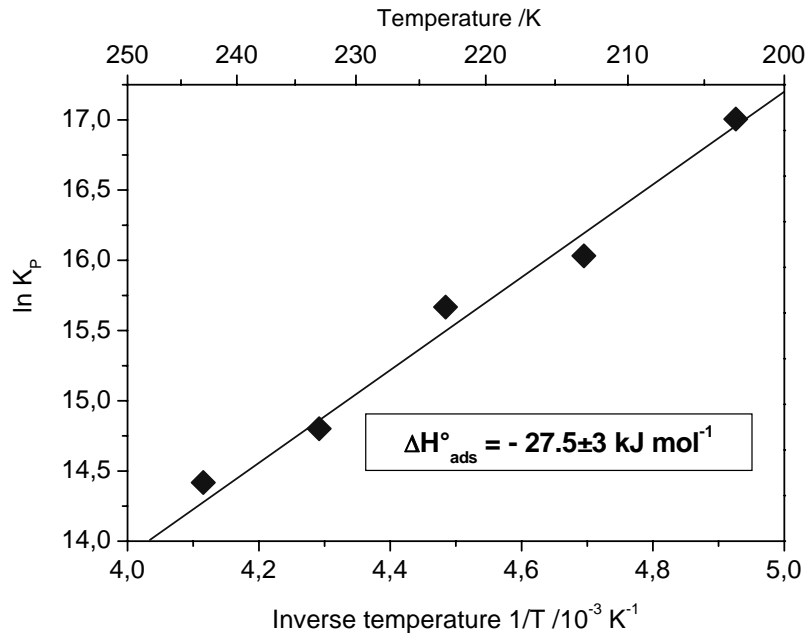


Figure 3.1-18: Van't Hoff representation of the equilibrium constants for the adsorption of water on soot

The study of [Picaud et al., 2004] suggests that at low active-group concentrations on the surface, these sites act as a strong trap for adsorbing water molecules due to hydrogen bonding. These hydrogen bonded molecules act further as nucleation centres for other water molecules forming aggregates tied to the active-site. And for the higher active group concentrations and higher water coverage, this theoretical study demonstrates that water adsorption on activated graphite surfaces is dependent not only on the type of sites but also on their number and their relative position.

3.1.2 Adsorption of water on mineral dust surfaces

3.1.2.1 Kinetic approach

The adsorption of water on mineral dust has been investigated for a gas phase water concentrations from $6 \cdot 10^{10}$ to $2 \cdot 10^{12}$ molecules cm^{-3} , surface temperature range from 203 to 323 K and sample masses between 130 and 300 mg. The samples have been prepared as previously described in Chapter 2.5.2.

At the beginning of each experiment a constant flow of water vapour is introduced into the Knudsen cell until receiving a steady MS-signal S_0 (as shown in Figure 3.1-19). At time $t = 0$ min the plunger is opened, the reactive surface is exposed to the water vapour, and due to the uptake, the signal immediately steeply decreases to the value S_{ini} followed by a constant increase until reaching a steady state value S_{ss} . At time $t = 27$ min the plunger is closed, the sample is isolated again and we can observe again an increase of the signal to the initial value S_0 .

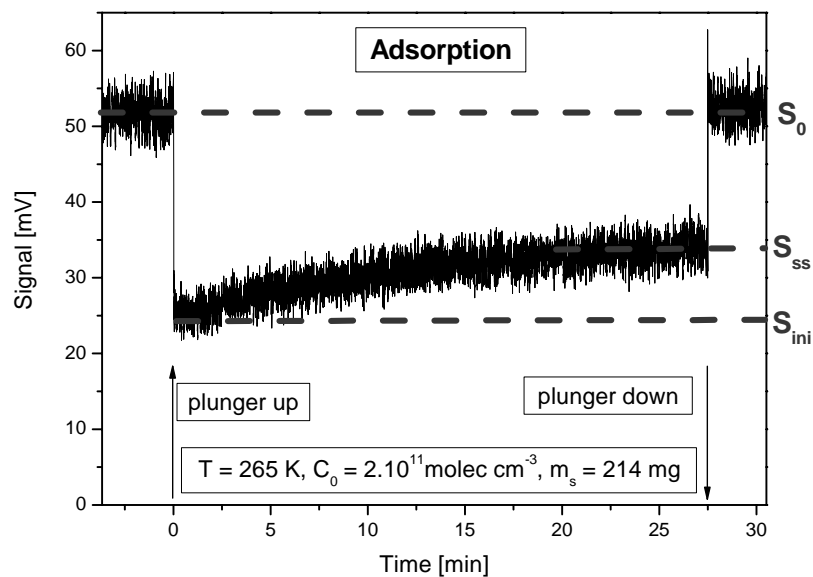


Figure 3.1-19: Typical signal for the uptake of water on mineral dust at $T = 265 \text{ K}$

A determination of the rate constants and uptake coefficients from the MS signals according to the calculations previously described (Chapter 2.1.2.1) is only valid for a first order uptake process. Therefore it should be tested if this condition is fulfilled. As already described in detail in Chapter 2.1.2.1, the order n of the uptake process is obtained from a linear regression of a double logarithmic plot of the loss rate versus the gas phase concentration.

3. Results and discussion

For the interaction between H₂O and mineral dust, the uptake has been shown to follow a first order rate law for the whole temperature interval investigated (consistent with the measurements of [Seisel et al., 2004a] for room temperature), as can be seen in Figure 3.1-20, where it is represented for 265K.

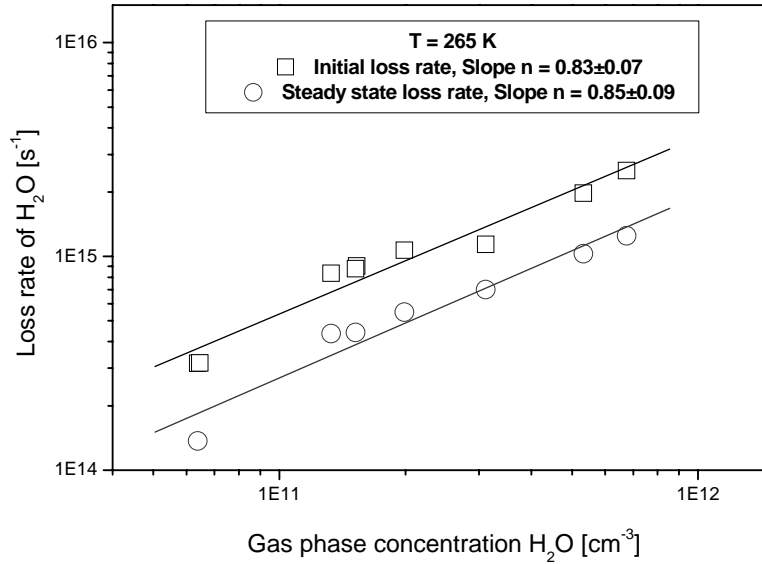


Figure 3.1-20: Double logarithmic plot of the initial and steady state loss rate of H₂O on mineral dust, T = 265 K

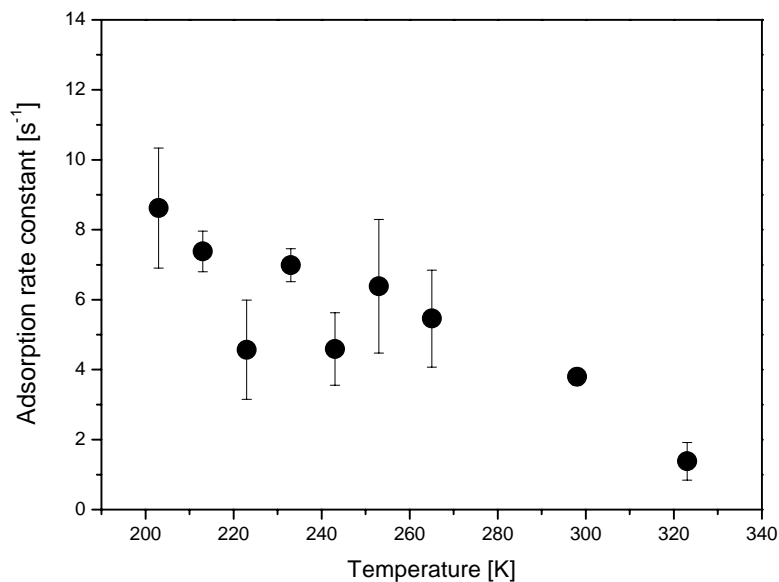


Figure 3.1-21: Initial rate constants as a function of temperature for the uptake of water on mineral dust

With the knowledge of the order of the uptake process, the adsorption rate constant (k_{ads}), which is given with the initial rate constant (k_{ini}) of the process, can be determined from the

3. Results and discussion

signals in absence and presence of sample, S_0 and S_{ini} , respectively. It has been found to be temperature dependent for the interval measured – decreasing with increasing temperature as represented in Figure 3.1-21. Each point in Figure 3.1-21 is a mean value of at least five independent experiments at a given temperature.

In addition to the temperature dependence we have also investigated the dependence of the initial rate constant on the sample mass. The results are summarized in Figure 3.1-22 where each point represents a mean value of at least ten independent experiments. This study is important in order to estimate the possible effect of the available surface area on the rate coefficient due to the diffusion of the gas phase molecules into the voids between the individual dust particles (discussed later in detail in Chapter 3.1.2.2). As it can be seen in Figure 3.1-22, in our case the initial rate constants do not show a significant mass dependence in the mass range investigated.

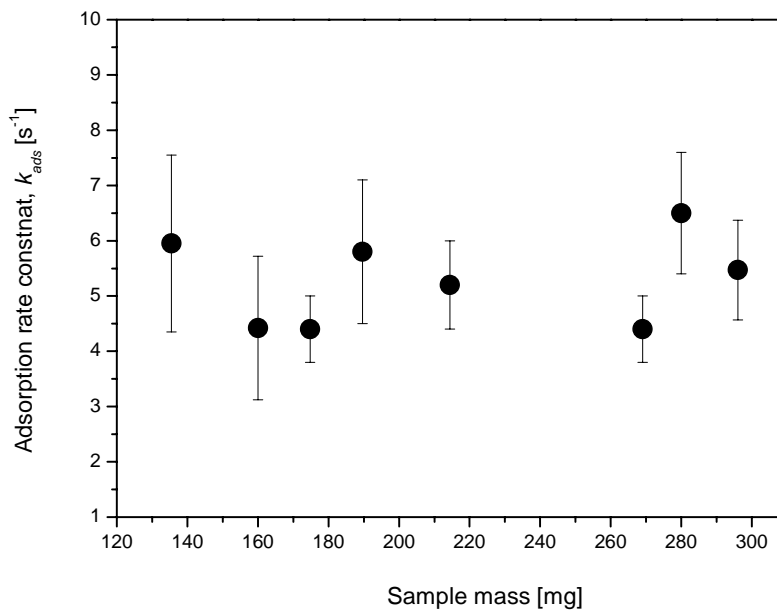


Figure 3.1-22: Initial rate constants k_{ini} for the uptake of water on mineral dust as a function of the dust sample mass

Another important aspect is the interpretation of the temporal profile of the signal shown in Figure 3.1-19 in terms of the reversibility of the process. We have in mind the two basic possibilities assumed before (Figure 3.1-2) for *reversible* and *irreversible* uptake process.

To determine if we have the reversible or the irreversible type of uptake, and to distinguish between adsorption and desorption processes in the case of water on mineral dust, of great

3. Results and discussion

importance is also to investigate the interaction of D₂O and mineral dust. The considerations explained before for the case of soot are valid also for the D₂O experiments on mineral dust.

In the work of [Seisel et al., 2004a] D₂O experiments on mineral dust at room temperature are represented. Their typical measurement is shown also in Figure 3.1-23, where are represented the temporal profiles of the signals for *m/e* 19 (HDO) and *m/e* 20 (D₂O).

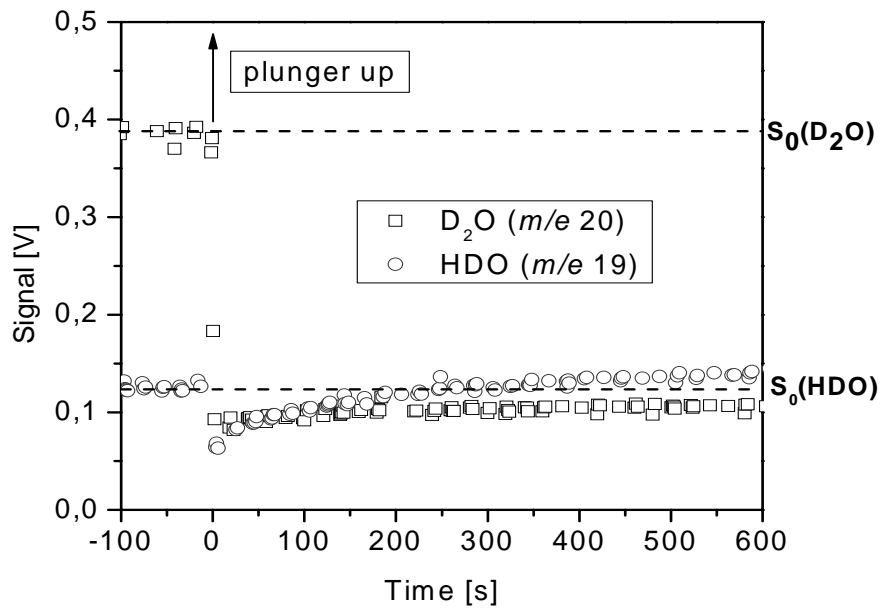


Figure 3.1-23: Uptake of D₂O and HDO on mineral dust at room temperature [Seisel et al., 2004a]

In the beginning of each experiment a constant flow of D₂O (*m/e* 20) is introduced into the cell. As already explained in Chapter 2.5.1 the signal of D₂O is always accompanied with this of HDO (*m/e* 19) because of the very fast H/D exchange on the walls of the Knudsen cell. At time $t = 0$ s the plunger is opened and it can be observed the immediate decrease of the D₂O signal, which is taken up with a high and non-saturating rate for the timescale of the experiment. Whereas the initial uptake of HDO is followed by an instantaneous increase of the signal, which finally exceeds its initial value S_0 and indicates that HDO is produced during the experiment.

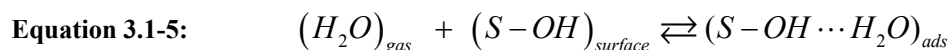
The main conclusions from the D₂O measurements by [Seisel et al., 2004a], applicable to the measurements reported in this work, can be summarized with the following three points:

- The constant uptake rate of D₂O during the experiments shows that blocking of reactive surface sites is negligible on the time scale of the experiment;

3. Results and discussion

- Formation of gas phase HDO during the experiment implies that the uptake of water is reversible;
- The observed uptake of D₂O together with formation of HDO confirms the fact that surface sites which contain acidic H – atoms are responsible for water adsorption.

For our measurements we assume the following, proposed by [Seisel et al., 2004a], reversible mechanism of the adsorption of water on mineral dust surfaces:



where $(H_2O)_{gas}$ represents a gas phase water molecule which adsorbs on an active surface site $(S-OH)_{surface}$ and can desorb back into the gas phase, because it stays in equilibrium with its adsorbed state $(S-OH \cdots H_2O)_{ads}$.

In order to investigate, in our case, the possible desorption of water from the mineral dust surface, after the end of the experiment, the flow into the cell has been stopped, and after waiting for some minutes until we obtain the background signal in the cell, the plunger has been reopened. In contrast to the measurements of 298K, where desorption from the surface has been observed [Seisel et al., 2004a], for temperatures below 265K no desorption of water has been observed. However, it should be noted that the background of water in the Knudsen cell can be estimated as $5 \cdot 10^{10}$ molecules cm^{-3} which corresponds to the flow of 3 to $5 \cdot 10^{14}$ molecules s^{-1} and therefore desorption flows below this value can not be measured.

However such desorption flows can be calculated knowing the reversible mechanism of the process and using the flow balance given with Equation 2.1-26. Using Equation 2.1-27 we can obtain the desorption rate constant (k_{des}) as the slope of the line from the graphic representation: desorption rate ($F_{des}(t)$) as a function of number of adsorbed molecules ($N_{ads}(t)$). Desorption rates have been calculated using Equation 2.1-26 and the number of adsorbed molecules is obtained from integrating the signal to the desired time t and Equation 2.1-16. This dependence is shown in Figure 3.1-24 for two different surface temperatures.

From Figure 3.1-24 it can be seen that for the lower temperature ($T = 223\text{K}$) the desorption rate increases linearly with increasing number of adsorbed molecules showing a first order kinetic throughout the range of coverage. For the higher temperature ($T = 265\text{K}$), however, the desorption rate is strongly non-linear.

3. Results and discussion

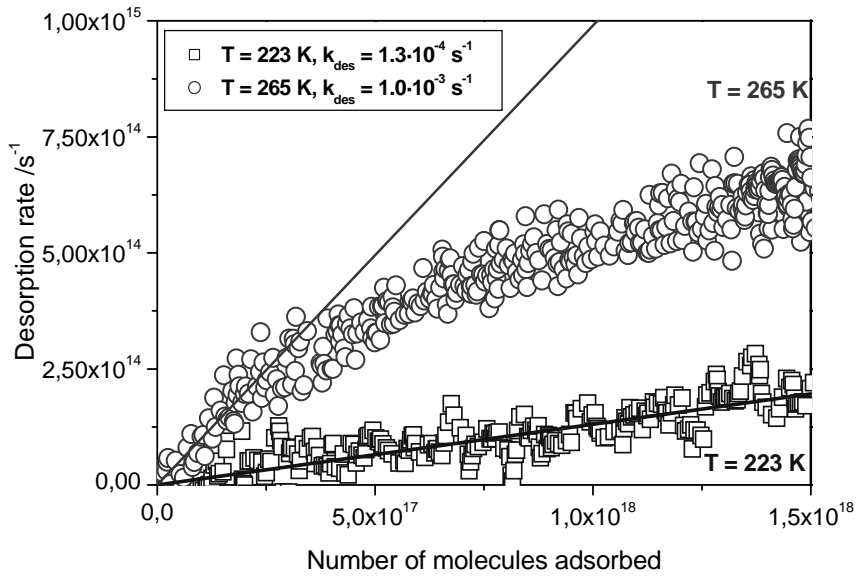


Figure 3.1-24: Desorption rate of water on mineral dust as a function of the number of molecules adsorbed for two different temperatures $T = 223\text{K}$ and $T = 265\text{K}$

This means that at these temperatures only for extremely low surface coverage the desorption rate can be represented with a first order process as expected for monolayer desorption. Consequently, the desorption rate constant for higher temperatures have been obtained from the linear extrapolation of the data at low coverage.

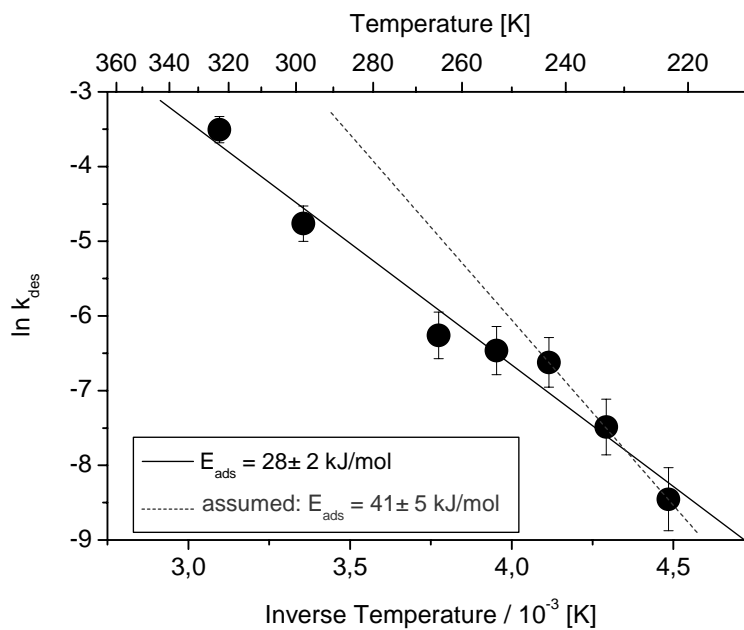


Figure 3.1-25: Arrhenius presentation of the desorption rate constants of water for mineral dust

3. Results and discussion

The desorption rate constants thus obtained can be plotted in form of an Arrhenius expression as represented in Figure 3.1-25. From the linear regression of the points we can obtain the activation energy of desorption $E_A = 28 \pm 2 \text{ kJ.mol}^{-1}$. However, taking only the three lowest temperatures into account higher activation energy for desorption ($41 \pm 5 \text{ kJ.mol}^{-1}$) is obtained. The reason for this assumption will be discussed later.

3.1.2.2 Thermodynamic approach

In order to determine the thermochemistry of the process, adsorption isotherms have been measured. For calculation of the theoretical total number of adsorbed molecules on the surface (N_{ads}^{total}) during the whole timescale of the experiment (for $t \rightarrow \infty$) at a given temperature, the temporal profiles of the reactive flow to the surface ($F_R = F_0 - F(t)$, shown in Figure 3.1-19) have been fitted with a double exponential expression (Equation 3.1-6) and integrated afterwards from time $t = 0$ (the beginning of the experiment) to time $t = \infty$.

The exponential function fitted is of the type:

$$\text{Equation 3.1-6} \quad y = A_1 \cdot \exp\left(-\frac{t}{A_2}\right) + A_3 \cdot \exp\left(-\frac{t}{A_4}\right)$$

Where y is the MS-Signal [mV] and t is the measurement time [s] and A_1, A_2, A_3, A_4 are constants. The integration of this equation yields:

$$\text{Equation 3.1-7} \quad \int_0^{\infty} y = A_1 \cdot \int_0^{\infty} \exp\left(-\frac{t}{A_2}\right) dt + A_3 \cdot \int_0^{\infty} \exp\left(-\frac{t}{A_4}\right) dt$$

$$\text{Equation 3.1-8} \quad N_{ads}^{total} = A_1 \cdot (-A_2) \exp\left(-\frac{t}{A_2}\right) \Big|_0^{\infty} + A_3 \cdot (-A_4) \cdot \exp\left(-\frac{t}{A_4}\right) \Big|_0^{\infty}$$

$$\text{Equation 3.1-9} \quad N_{ads}^{total} = A_1 \cdot A_2 + A_3 \cdot A_4$$

For each measurement the integration has been done numerically with the software Origin® (Figure 3.1-26). First the obtained signal (Figure 3.1-26 a/) is normalized in a suitable form for fitting (Figure 3.1-26 b/). The grey curve is the obtained fit with exact values for the coefficients A_1, A_2, A_3 and A_4 .

3. Results and discussion

The total number of adsorbed molecules, calculated using Equation 3.1-9, can be plotted as a function of the total gas phase concentration of water to obtain the adsorption isotherms. In Figure 3.1-27 this dependence is shown for five different temperatures.

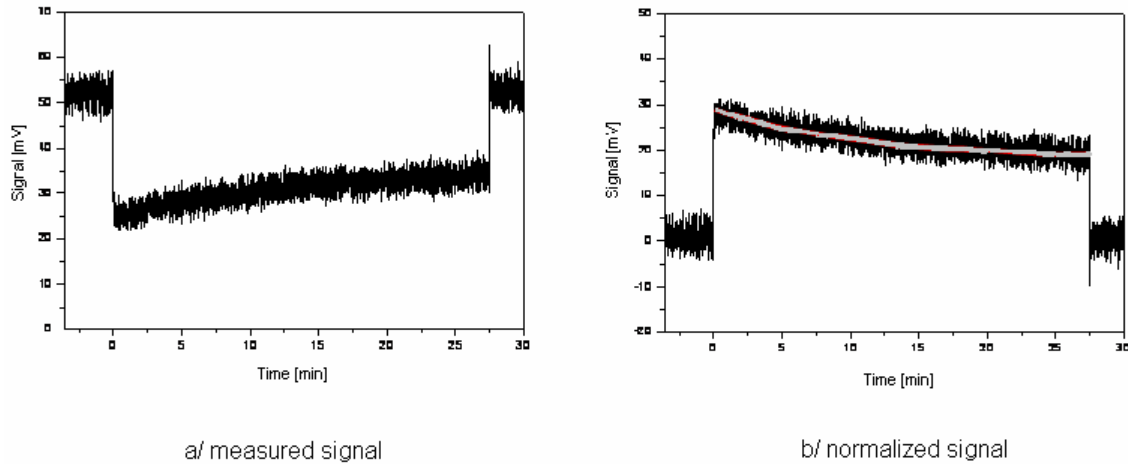


Figure 3.1-26: Numerical fit with Origin in order to obtain $N_{\text{ads,total}}$: a/ measured signal; b/ normalized signal. The grey curve is the obtained numerical fit

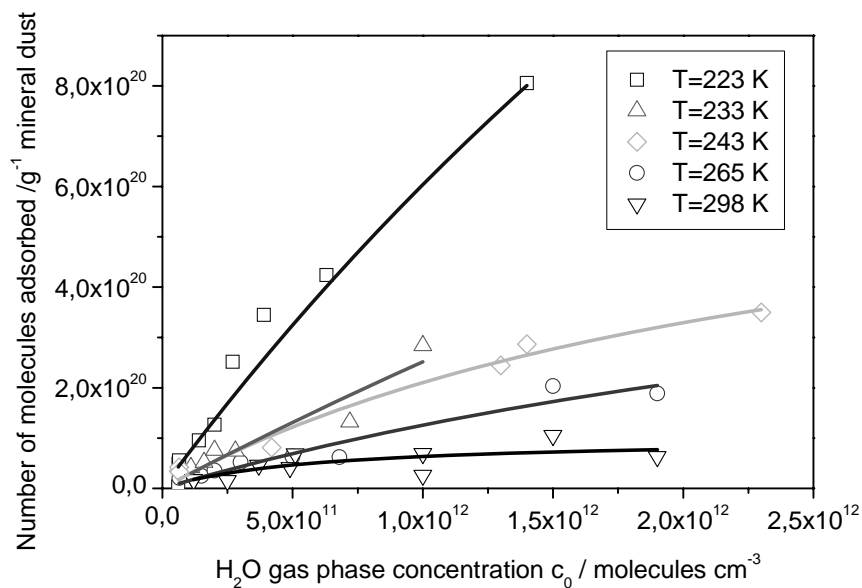


Figure 3.1-27: Adsorption isotherms for the uptake of water on mineral dust for five different temperatures

Here, as expected, the total number of adsorbed molecules per gram of the sample increases with increasing gas phase concentration and decreasing temperature.

3. Results and discussion

From Figure 3.1-27 it can be seen that for the lowest temperature (223 K) the number of adsorbed molecules is estimated to be up to $1.3 \cdot 10^{20}$ molecules, corresponding to $8 \cdot 10^{20}$ molecules g^{-1} of mineral dust. If we assume that our reactive surface area equals the BET surface area of the dust of $5 \cdot 10^5 \text{ cm}^2 \text{ g}^{-1}$ and knowing the size of an adsorbed water molecule of $1 \cdot 10^{-15} \text{ cm}^2$ [Newman, 1983], we can calculate that the surface coverage correspond to 0.6 monolayer.

As already discussed in the case of soot, to determine the exact reactive surface area available for adsorption is one of the difficulties of the experiment. For the case of mineral dust we also assume the two limiting cases, represented in Figure 3.1-15:

- i) with surface water concentration, relevant to the surface area of the uppermost layer
- ii) with surface water concentration, relevant to the entire BET area of the sample

If we take into consideration the surface area of the uppermost layer ($3.3 \cdot 10^3 \text{ cm}^2$), then the $1.3 \cdot 10^{20}$ molecules correspond to a coverage of roughly 40 formal monolayers. This argument clearly indicates that more than one formal monolayer is effectively adsorbed on the mineral dust surface.

For the two limiting cases the two sets of equilibrium constants K_p have been calculated and plotted in Figure 3.1-28 as a function of temperature. As expected K_p increases with decreasing temperature, for both cases. A linear fit of the data for each case (solid lines in Figure 3.1-28) yields slopes and hence unrealistic standard enthalpies of adsorption of around -12 kJ mol^{-1} .

We tried to explain these findings assuming that the surface area for adsorption changes (respectively the equilibrium constant K_p changes) due to the diffusion of water molecules into the bulk of the mineral dust sample, although no significant mass dependence for the uptake kinetics has been observed, and this change is a function of temperature. For higher temperatures the process of diffusion is faster. Therefore the available surface area is largest and in the limit of complete diffusion can be equated to the BET area of the sample. On the opposite, for low temperatures the diffusion is much slower and is restricted to the uppermost layer of the sample. As a consequence, we assume that there is a switch in surface coverage between the two extreme temperatures and the corresponding equilibrium constants. Having in mind the data points for the extreme temperatures (223 K, 233 K, 298K and 323K) we

3. Results and discussion

obtain a standard enthalpy of adsorption ΔH_{ads}^0 of around -45 kJ mol^{-1} (broken line in Figure 3.1-28) which is close to the condensation enthalpy of water [Chase et al., 1985] and also in agreement with results of Cantrell [Cantrell and Ewing, 2001].

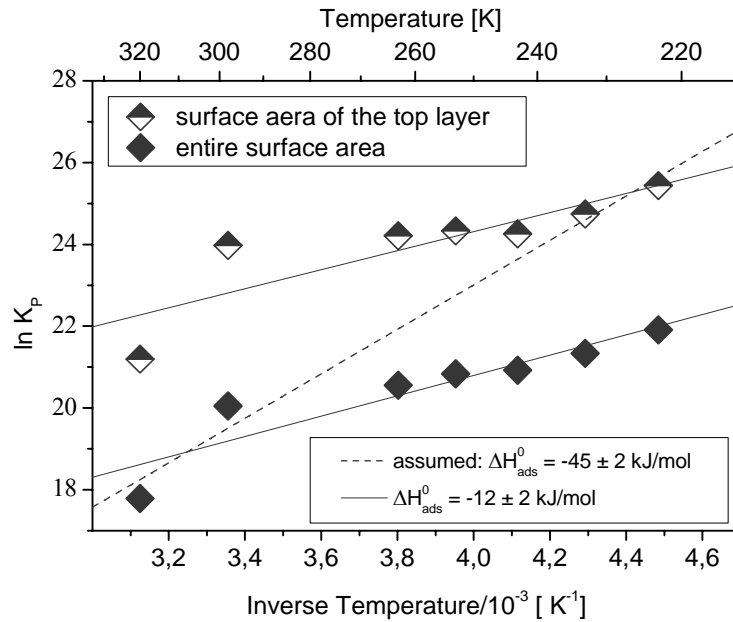


Figure 3.1-28: Two sets of equilibrium constants (K_p) for the adsorption of water on mineral dust as a function of the surface temperature. The broken line yields an adsorption enthalpy of $-45 \pm 2 \text{ kJ mol}^{-1}$

The low activation energy for desorption (obtained from the Arrhenius plot, Figure 3.1-25, solid line), is also assumed to be affected by the temperature dependence of the diffusion into the bulk in the same way like the equilibrium constants. At higher temperatures, especially, the desorption rate constants obtained are underestimated and consequently the activation energy obtained is overestimated. According to our assumption the values for the desorption constants (not affected from diffusion) are the values for the lowest three temperatures (243K, 233K and 223K). From the linear regression of these low temperature values (broken line in Figure 3.1-25) more realistic activation energy of desorption of $41 \pm 5 \text{ kJ mol}^{-1}$ is obtained, closed to the value estimated above for the standard enthalpy of adsorption.

3.1.3 ESEM measurements

ESEM has been used as an additional tool for investigating the behaviour of mineral dust and kerosene soot samples towards water under environmental conditions (RH up to 100%), in contrast to the Knudsen cell where the RH is far below 1%. The measurements have been

3. Results and discussion

performed using the cooling unit of the microscope. It is a special Peltier stage with which the sample can be cooled to -4°C . For our purposes we have cooled it always to 2°C and with verifying the water vapour pressure inside the microscope we could obtain different RH up to 100%.

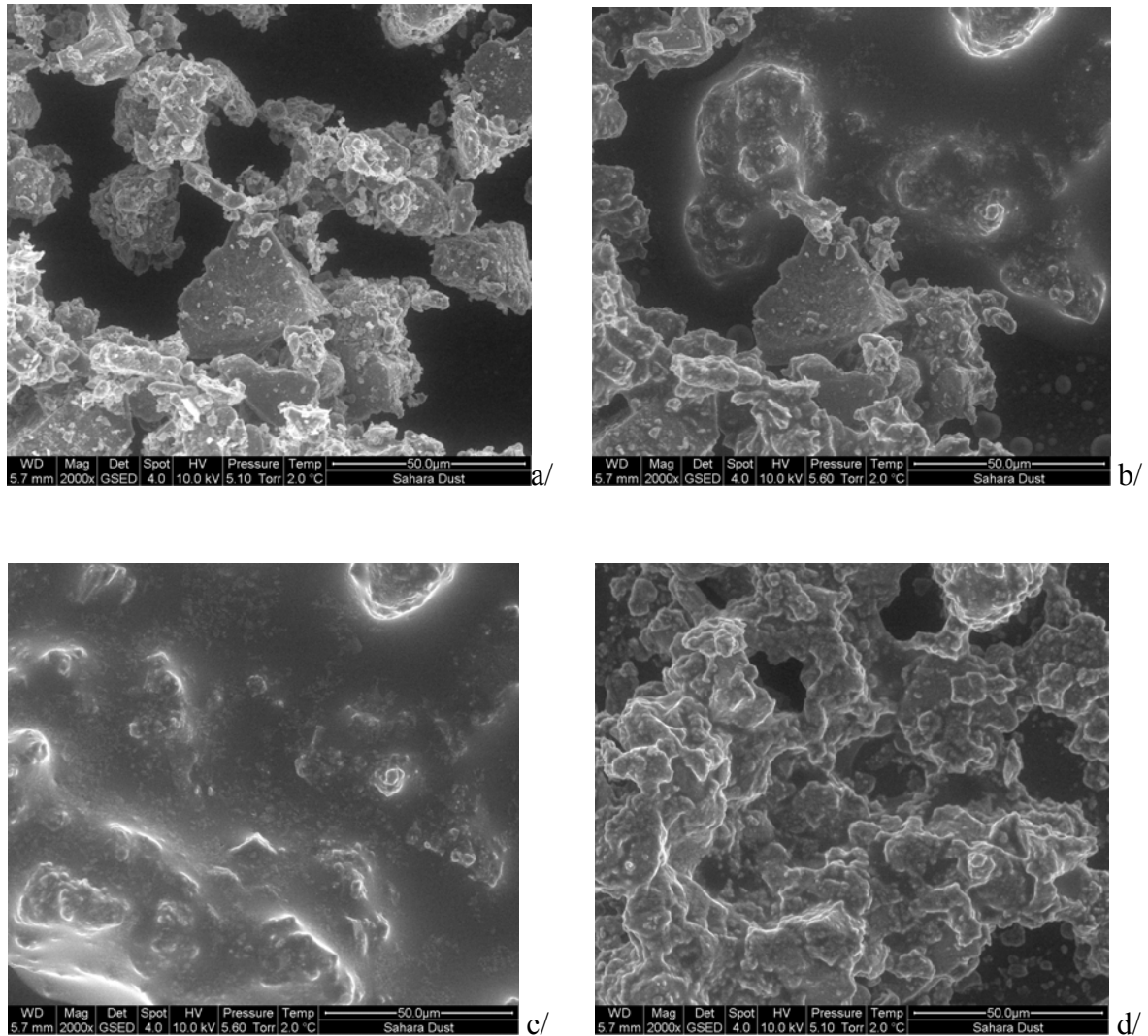


Figure 3.1-29: ESEM pictures of mineral dust samples for different relative humidities: a/ 85%; b/ 100% after 180s; c/ 100% after 360 s; d/ 96%

In Figure 3.1-29 the measurement for mineral dust [Czarnetzki, 2005] is represented. We have started the measurement at 55% RH and gradually increased it up to 100% with a rate about 15% RH for 30s. In Figure 3.1-29 a/ is represented a picture for 85% RH where, although different in shape and size, the single particles of the mineral dust sample can be very well distinguished. With further increase of RH, we could observe water uptake only for 100% RH and after a certain time (180 s), as it is represented in Figure 3.1-29 b/, where can be clearly

3. Results and discussion

seen that some of the mineral dust particles have lost their morphology due to the water uptake. After 360 s at 100% RH (Figure 3.1-29 c/) the whole sample is completely covered with water. With further decrease of RH back to 95% (Figure 3.1-29 d/) it is visible that even a small change in RH (5%) is enough to observe the desorption of water, and the renewed formation of the particles with the similar contours like before the uptake experiment.

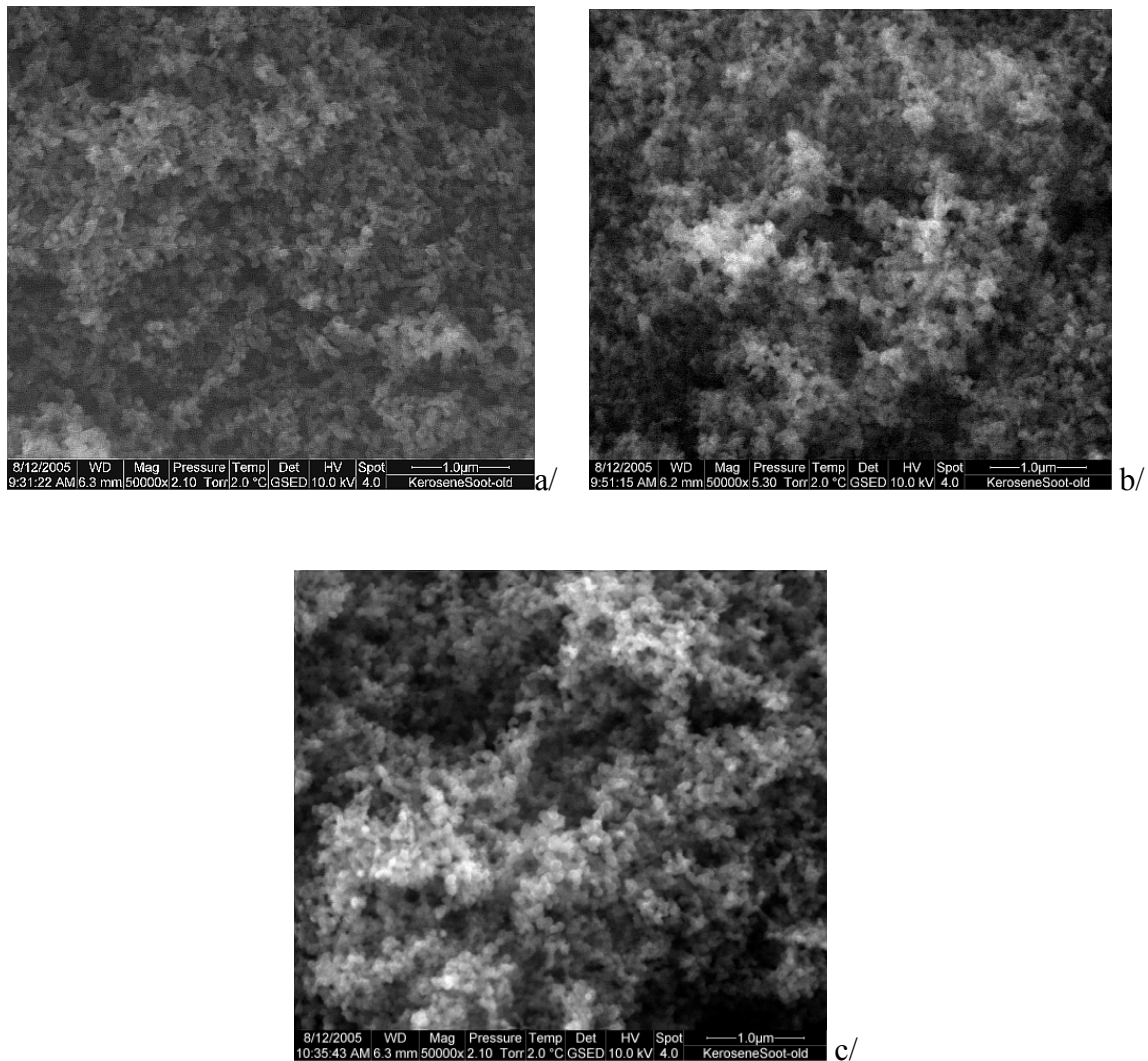


Figure 3.1-30: ESEM pictures of kerosene soot (Spot 1) at different RH: a/ 40 %, b/100% for 12 min, c/ 40%

The investigation of kerosene soot at different RH is represented in Figure 3.1-30 for 40% RH (a/), sharp increase to 100% RH for 12 min (b/) and again sharp decrease to 40% (c/). The pictures have been taken at very high magnification (50000 times) so that the separate agglomerates can be very well distinguished, but no visible change of the surface with changing RH could be observed. In order to obtain some more information, we have decreased the magnification from 50000 times to 7000 times and looked at a spot near to the

3. Results and discussion

one shown in Figure 3.1-30. The ESEM pictures for this second spot are represented in Figure 3.1-31.

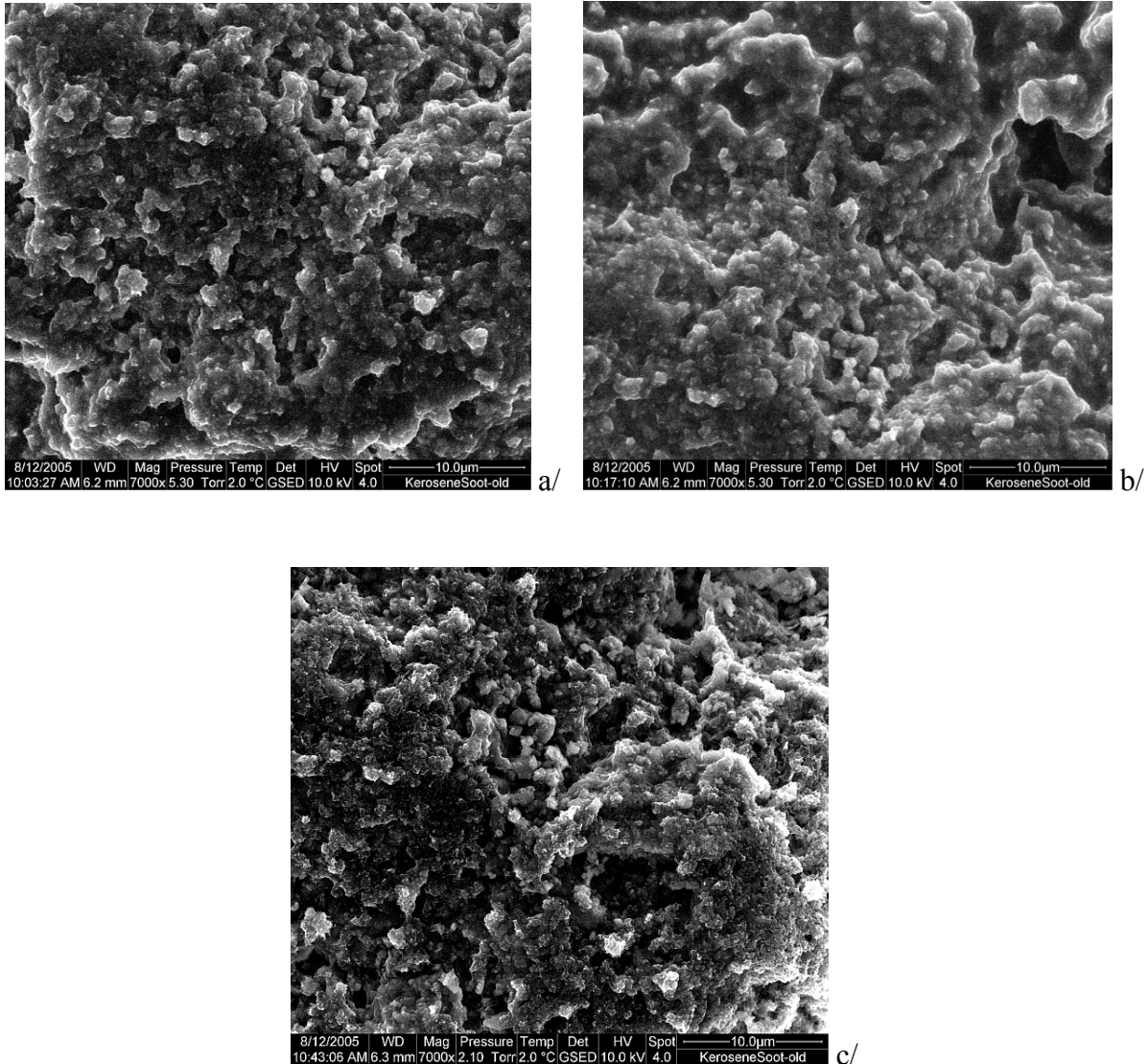


Figure 3.1-31: ESEM picture of kerosene soot (Spot 2) at different RH: a/ 100% for 23 min; b/ 100 % for 30 min; c/ 40 %

It can be clearly seen that after 23 min at RH 100% (Figure 3.1-31 a/) the separate agglomerates can not be so well distinguished like in Figure 3.1-30 a/, due to the water uptake. With advancing time this effect is enhanced and after 30 min at RH 100% (Figure 3.1-31 b/) the fine structure of the sample is smoothed, which we interpret with the formation of water film on the surface. However, in the case of kerosene soot we do not observe an extreme lost of the particles morphology like in the case of mineral dust (Figure 3.1-29.c). After sharp decrease of RH back to 40% (Figure 3.1-31 c/) the water has desorbed from the surface and the contours of the separate agglomerates can be again clearly distinguished.

3. Results and discussion

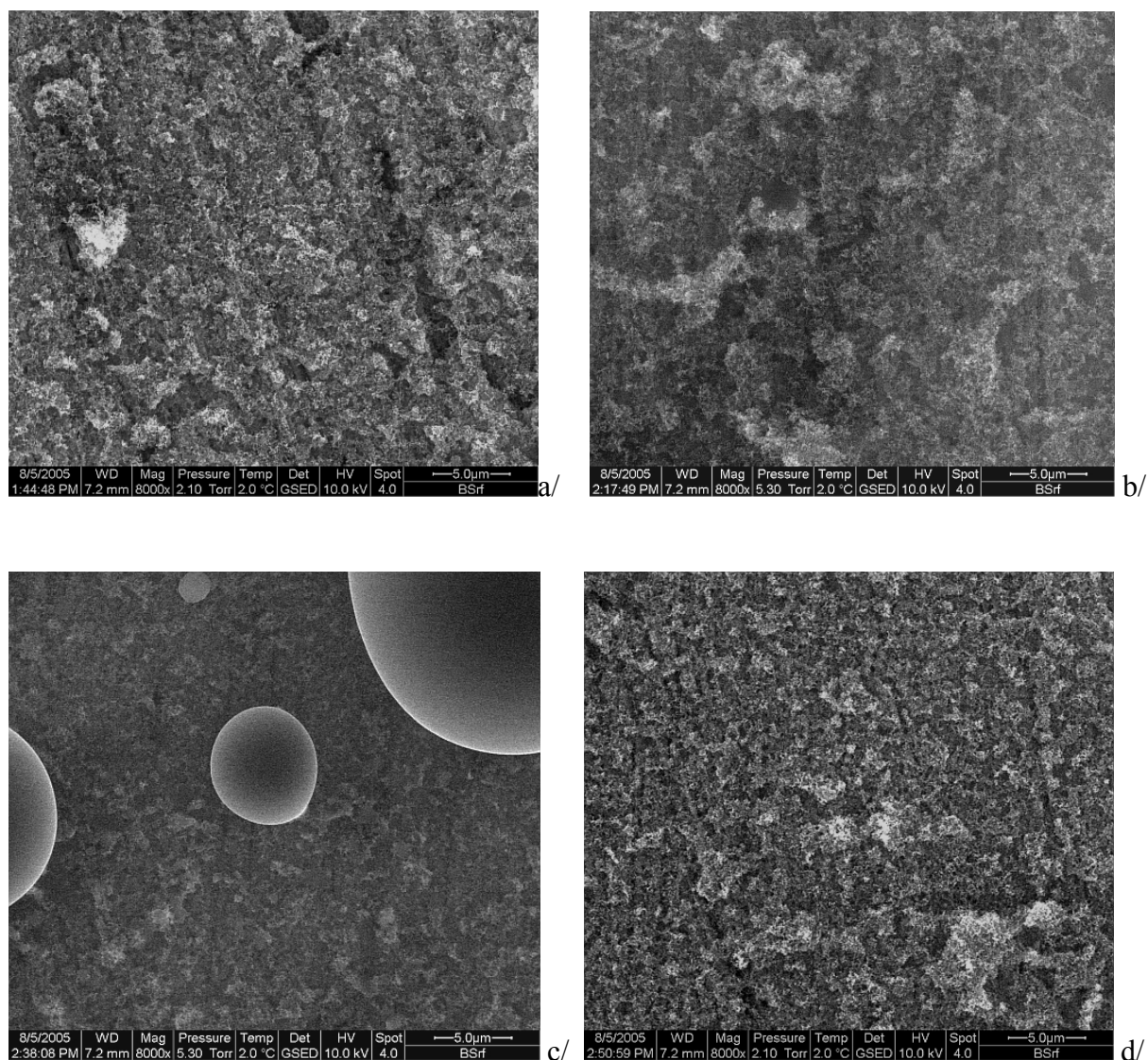


Figure 3.1-32: ESEM pictures of ethene soot samples for different RH: a/ 40%; b/ 100% for 17 min; c/ 100% for 40 min; d/ 40%

In Figure 3.1-32 is represented the behaviour of ethylene soot at different RH. We have started the measurement at 40% RH (Figure 3.1-32 a/) where for 8000 times magnification can be distinguished the fine structure of the sample surface. Then we sharply increased RH directly to 100% but even after 17 minutes we could not observe a change in the sample surface (Figure 3.1-32 b/). However, after 40 minutes at RH 100%, water droplets on the surface of the sample are clearly formed (Figure 3.1-32 c/) which disappear, leaving the surface of the sample unchanged, after the renewed drop of RH back to 40% (Figure 3.1-32 d/).

3. Results and discussion

3.1.4 Discussion

In order to assess the hydrophilicity of the soot and mineral dust particles, their behaviour towards water has been investigated at temperatures between 298 K and 203 K. In both cases the amount of water adsorbed is increasing with decreasing temperature with initial adsorption rate constants of 5 s^{-1} and 3.7 s^{-1} on mineral dust and kerosene soot respectively.

However, significant differences in the derived desorption rate constants and surface coverages have been observed. Whereas on a soot surface approximately only $5 \cdot 10^{18}$ molecules g^{-1} are adsorbed, leading to sub-monolayer coverage, multilayer coverage has been observed for mineral dust. Although the desorption rate constants determined for water from soot as well as from mineral dust have to be regarded as lower limits, the difference of three orders of magnitude indicates that water is much stronger bonded on mineral dust than on soot. This conclusion is further reflected by the estimated adsorption enthalpies of -45 kJ mol^{-1} and -27 kJ mol^{-1} for water on mineral dust and soot, respectively.

As pointed out in the introduction, the term hydrophilicity of a surface on a macroscopic scale refers to its contact angle with a water droplet. With the assumption that the contact angle between a surface completely covered with water and a water droplet is zero, hydrophilicity on a microscopic scale may be defined by the adsorption rate with which a complete water monolayer is formed. Consequently, a particle surface may be regarded as hydrophilic if the density of surface sites for water adsorption is high and a complete monolayer is readily formed. In this context our results suggest that mineral dust may be regarded as hydrophilic and soot as hydrophobic. Although this conclusion is also expected intuitively, it clearly demonstrates that adsorption and desorption rates can be used to assess the hydrophilicity of such particles.

This conclusion about the hydrophilicity of the two types of surfaces is also supported qualitatively from the ESEM measurements performed. As already shown, mineral dust particles readily adsorb water at RH 100% and after 3 min, the smaller particles lose their morphology due to the uptake, and after 6 min the whole sample is covered with water. In the case of kerosene soot, on the other hand, we could not observe a sharp change in the sample structure. Even after 20 minutes at RH 100% the shapes of the separate agglomerates can be very well distinguished, after 30 min at RH 100% we can observe the formation of a water film, which disappears with decrease of RH back to 40%. And in the case of ethylene soot, we

3. Results and discussion

could not observe water uptake and after 40 min at RH 100% the formation of water droplets on the surface could be clearly observed, indicating that this surface is hydrophobic, in good agreement with our Knudsen cell observations.

The experiments with the Knudsen cell presented here have been performed at relative humidities far below 1%, whereas in the atmospheric environment the particles will act as potential cloud/ice condensation nuclei (CCN/IN) at relative humidities above 100%. Nevertheless, some conclusion concerning the atmospheric implications can be drawn. As suggested above, the hydrophilicity of a particle may be defined on a microscopic scale by the rate of reaching a monolayer coverage. Once a particle is completely covered by a water layer it may be regarded as hydrophilic in the sense that the contact angle between that surface and a water droplet becomes zero. Consequently, the activation of an insoluble particle for water condensation then only depends on the particle size which has to be large enough to overcome the Kelvin barrier at a given relative humidity. By comparing the results obtained for water adsorption on soot and on mineral dust one may conclude that:

- (i) A mineral dust particle will reach a monolayer coverage much faster than a soot particle and therefore will be activated faster at a given RH.
- (ii) In case the particles are exposed to relatively dry air, water will desorb from a mineral dust particle much slower than from a soot particle and hence the mineral dust particle will readily be activated again if the RH rises.

The importance of our results to the ability of soot and mineral dust particles to act as ice nuclei (IN) is more difficult to assess, since heterogeneous ice nucleation proceeds via different modes which have different dependences on the hydrophilicity of the particle [Pruppacher and Klett, 1980]. In the deposition mode a surface which exhibits only few hydrophilic sites surrounded by an hydrophobic environment is thought to be the most effective type of nuclei. In contrast, nucleation processes which occur via the immersion or contact mode seem to be more effective with hydrophilic particles. With respect to these arguments our results suggest that ice nucleation on soot and mineral dust particles should proceed via different nucleation modes. Consequently the results of this study on the adsorption of water on mineral dust and soot can help to interpret recent field observations [DeMott et al., 2003b], [Hung et al., 2003] and nucleation experiments [Project PAZI, Cologne 2003] with respect to the nucleation mechanism occurring.

3.2 Reactions of SO₂ and NO₂ with soot surfaces

3.2.1 Reactions of SO₂ with soot surfaces

SO₂ is an important gas phase species in the atmosphere because it can be a precursor for the formation of sulphuric acid which in turn contributes to acid precipitation and atmospheric particulates. Therefore it is important to understand the ways for the oxidation of SO₂ in the atmosphere. For the free troposphere there are two well studied possibilities of SO₂ oxidation: via gas phase and aqueous mechanisms described in detail in Chapter 1.1.1.2. However, recent measurements of exhaust gas plumes particulates of aircrafts indicate that these two known mechanisms are not rapid enough to explain sulphuric acid aerosol formation in combustion exhaust [Fahey et al., 1995], [Toon and Miake-Lye, 1998]. One possible explanation for these facts is that ions formed during combustion [Yu and Turco, 1997] or ions from ambient air [Arnold et al., 1998] may be involved and enhance the particle formation.

What is more important from our point of view, and one reason for investigating the interaction of SO₂ with soot particles is, that soot particles may catalyze the oxidation of SO₂ to sulphuric acid, resulting in much higher conversion rates than the gas phase oxidation of SO₂ [Schumann et al., 1996], [Fahey et al., 1995], [Novakov, 1982]. If SO₂ is oxidized to H₂SO₄ on soot, then the sulphuric acid can nucleate the formation of water droplets that may lead to visible aircraft contrails [Gleitsmann and Zellner, 1999].

For the investigation of the interaction of soot samples with SO₂, we used both kerosene and ethylene soot. The samples have been gathered directly from the flame of the burner on a quartz plate and mounted in the sample compartment of the Knudsen cell. Before each experiment the sample has been dried under vacuum at 300K for at least 10 hours. The measurements have been performed with gas phase concentrations of SO₂ from $3 \cdot 10^{11}$ up to $8 \cdot 10^{12}$ molecules cm⁻³, sample masses from 2.4 to 14.6 mg and in the temperature interval $180 \text{ K} < T < 550 \text{ K}$. Both types of soot have shown a significant discrepancy in their behaviour towards SO₂ which is discussed further.

Kerosene soot has shown no reactivity towards SO₂, under our experimental conditions, for the whole temperature interval, as can be seen from Figure 3.2-1, where a measurement for

3. Results and discussion

330 K is represented. Mass spectrometrically the signals for m/e 64 (SO_2), m/e 98 (H_2SO_4) and m/e 82 (H_2SO_3) have been followed.

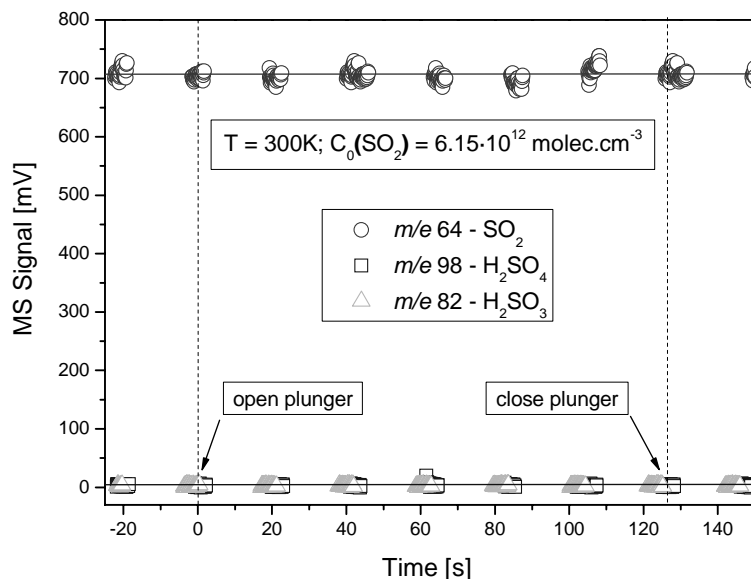


Figure 3.2-1: Typical temporal profile of the MS signals for the interaction of SO_2 with kerosene soot

At the beginning of the experiment a constant flow of SO_2 is introduced into the Knudsen cell, resulting in a steady signal (empty circles in Figure 3.2-1). At time $t = 0$ s the plunger has been lifted and the sample exposed to the reactive gas. As can be seen, no change of the signals for SO_2 , as well as for the eventual products, could be observed, indicating that kerosene soot is not reactive towards SO_2 under our experimental conditions. An upper limiting value for the initial uptake coefficient of $\gamma \leq 2 \cdot 10^{-4}$ has been assigned due to the detection limit of the Knudsen cell.

Ethylene soot has shown a reactivity towards SO_2 only below 225 K. Therefore for the temperatures higher than 225 K we have also assigned the limiting value of $\gamma \leq 2 \cdot 10^{-4}$. In Figure 3.2-2 an uptake experiment at the lowest temperature (180 K) with its typical signal profile is represented where with the mass spectrometer m/e 64 for SO_2 has been followed. At the beginning of the experiment a constant flow of SO_2 is introduced into the Knudsen cell corresponding to a steady state signal. After lifting the plunger at time $t = 0$ s and exposing the fresh sample surface to the reactive gas, we were able to observe uptake but also very fast saturation of the sample surface and for about 50 s the signal rises up to its initial value. After stopping the flow of SO_2 into the cell, and re-opening the plunger ($t = 340$ s) we were able to observe SO_2 desorbing from the surface back into the gas phase with the number of desorbed

3. Results and discussion

SO₂ molecules with respect to the SO₂ adsorbed, of 50% for the lowest temperature. No gas phase products due to the interaction have been observed either.

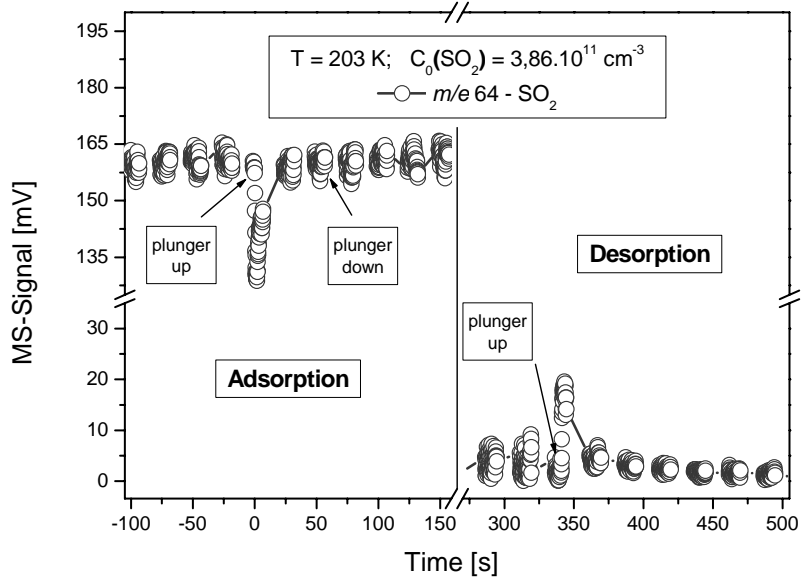


Figure 3.2-2: Temporal signal profile for the interaction of SO₂ and ethylene soot

The initial uptake coefficients calculated are summarised in Figure 3.2-3. Here the values for steady state (open circles) and pulsed (filled circles) measurements are represented.

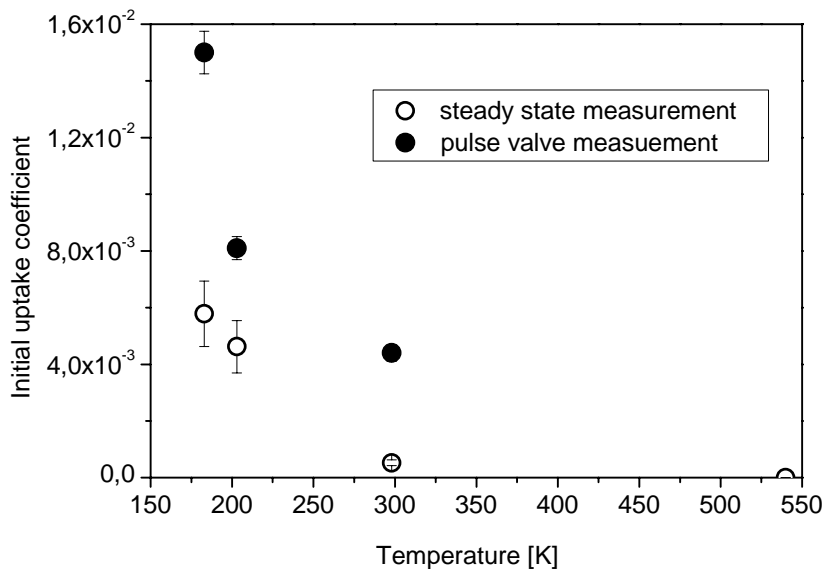


Figure 3.2-3: Initial uptake coefficients for the interaction of SO₂ with ethylene soot as a function of the sample temperature

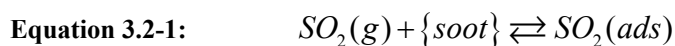
A negative temperature dependence of γ_{ini} can be observed for both steady state and pulsed values, indicating the fast establishment of the adsorption/desorption equilibrium. With

3. Results and discussion

decreasing temperature desorption is slower which leads to an increase of the uptake coefficient.

Our findings for the reversible nature of the uptake of SO₂ on soot and the calculated values for the uptake coefficients are in good agreement with literature. [Rogaski et al., 1997] performed the reaction with SO₂ with black carbon (Degussa FW-2, virtually pure carbon) at room temperature and partial pressure of SO₂ from 6·10⁻⁴ to 1·10⁻² mbar in a Knudsen cell reactor. They obtained initial uptake coefficients for SO₂ adsorption of 3·10⁻³ in good agreement with our values. [Köhler et al., 1999] investigated the reaction of SO₂ and n-hexane soot in the temperature interval 143 to 233 K with transmission FTIR spectroscopy. They also found a very rapid reversible SO₂ initial adsorption on soot with initial uptake coefficients of 2·10⁻³, comparable to our values. Similar to our results, they also found that the amount of SO₂ rapidly adsorbing on soot increases with decreasing temperature and increasing partial pressure of SO₂.

We can summarize that in the case of the interaction of ethylene soot and SO₂ we observed a reversible uptake mechanism (Equation 3.2-1 and Figure 3.2-2), with the number of desorbed molecules increasing up to 50% with decreasing temperature:



Because of the fact that no gas phase products could be observed from the interaction, and also because of the very fast saturation of the sample surface (for about 50s even at the lowest temperature, Figure 3.2-2), we considered this interaction not to be interesting from atmospheric point of view and concentrated further our efforts on the investigation of the interaction of NO₂ with soot surfaces, presented in the following sections.

3.2.2 Reactions of NO₂ with soot surfaces

Among all nitrogen containing compounds, NO_x plays probably the most important role in both polluted and unpolluted areas, because of their contribution to the distribution of the OH radical, which is responsible for the initiation of most of the daytime chemistry of the troposphere [Hernandez, 1996]. The idea is that possible heterogeneous reactions on soot surfaces, abundant in the atmosphere, could influence the NO/NO₂ balance in NO_x and indirectly impact on the ozone formation, or could lead to some important products like

3. Results and discussion

HONO [Lelievre et al., 2004], [Stadler and Rossi, 2000] which could also have an impact on ozone formation at sunrise.

On the other hand the investigation of the interaction between soot particles and NO₂ at high temperatures is of great importance for soot particulate filters. This reaction is used for regenerating the filter from the gathered particulate matter which is oxidized via NO₂ to NO and CO₂, and the advantage is that this happens at relatively low temperatures of about 250⁰C, compared to the oxidation with oxygen, for which much higher temperatures above 500⁰C are needed [Jacquot et al., 2002], [Kandylas et al., 2002].

The reaction of NO₂ with soot has also been performed with the two types of soot samples – kerosene and ethylene soot – in the Knudsen cell. The samples have been gathered directly from the flame of the burner on a quartz plate and mounted in the sample compartment of the Knudsen cell. Before each experiment the sample has been dried under vacuum at 300K for at least 10 hours and then preheated to 573 K for 60 min. The reaction was performed with gas phase concentrations of NO₂ from $2 \cdot 10^{11}$ up to $2 \cdot 10^{12}$ molecules cm⁻³, sample masses from 7.2 to 16.8 mg and in the temperature interval $300 \text{ K} < T < 670 \text{ K}$. After the end of the experiment the samples have been diluted in slightly alkaline water and put for 30 minutes in an ultrasound bath, before further ion chromatographic analysis. Kerosene and ethylene soot have also shown discrepancies in their behaviour towards NO₂ which is discussed further in detail.

Kerosene soot has shown also no reactivity towards NO₂, in the temperature interval measured, as can be seen from Figure 3.2-4, where is represented a measurement for room temperature. The MS signals for m/e 46 (NO₂), m/e 30 (fragmentation of NO₂, or fragmentation of HONO in the mass spectrometer) and m/e 47 (HONO) have been followed.

At the beginning of the experiment a constant flow of NO₂ is introduced into the Knudsen cell, resulting in a steady signal (empty circles in Figure 3.2-4). At time $t = 0$ s the plunger has been lifted and the sample exposed to the reactive gas. As can be seen, no change of the signals for all three masses could be observed, indicating that kerosene soot is not reactive towards NO₂ under our experimental conditions and the limiting value of $\gamma \leq 2 \cdot 10^{-4}$ for the uptake coefficient can be assigned.

3. Results and discussion

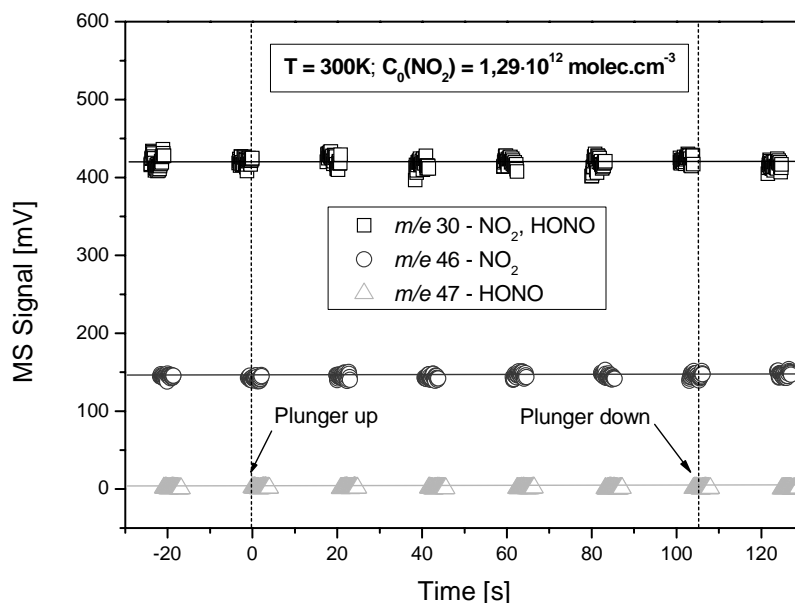


Figure 3.2-4: Typical temporal profile of the signal for experiment of NO₂ and kerosene soot. No interaction can be observed.

In contrast ethylene soot has shown reactivity towards NO₂ for the whole temperature interval measured. Therefore further in detail the results from this interaction are presented:

3.2.2.1 Sample pre-treatment

As already mentioned the sample has been heated under vacuum to 573K for at least 30 min, up to 1 hour, before the beginning of each measurement. This preheating procedure was applied in order to remove eventually adsorbed contaminants, or water on the surface of the sample, and to be assured to have a reproducible sample surface and identical measurement conditions at the beginning of each experiment.

However, this heating procedure has also an influence on the structure and reactivity of the soot surface. It is known that the reactivity and structure of soot depends on fuel type and burning conditions [Chughtai et al., 2002], but generally soot has predominantly aromatic layered structure with oxygen-containing surface groups such as aldehydes, ketones, carboxylic groups, lactones etc. [Akhter et al., 1985a, 1985b], [Smith and Chughtai, 1995], [Muckenhuber and Grothe, 2006], which are the reactive surface sites for the interaction with NO₂, as proven from formation of surface nitrate and nitrite species, [Al-Abadleh and Grassian, 2000], [Jeguirim et al., 2004]

3. Results and discussion

It is also known that these oxygen containing groups have different thermal stabilities and, upon heating, can decompose and release CO₂ or CO, or both, depending on temperature. [Muckenhuber and Grothe, 2006]. Summarised the decomposition temperature (obtained from TPD-MS measurements) of the most common O-containing groups on the soot surface is represented in Figure 3.2-5 [Figueiredo et al., 1999]. It can be seen that with decreasing acidity of the groups their thermal stability increases and they can be decomposed, respectively, at higher temperatures.

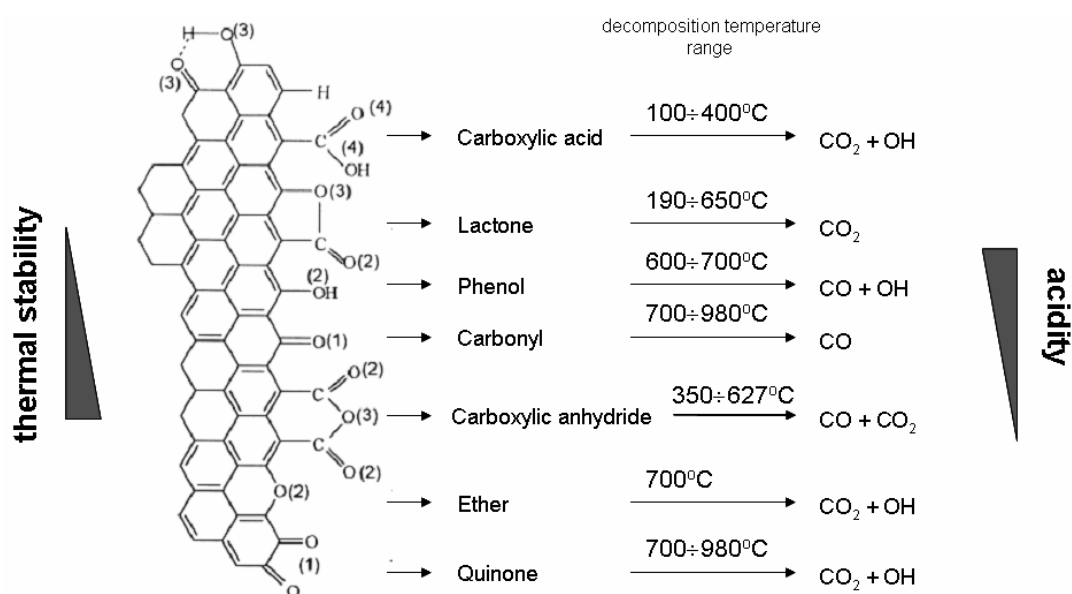


Figure 3.2-5: Thermal decomposition of oxygen-containing groups on the soot surface [Muckenhuber and Grothe, 2006]

Having in mind these findings, during the preheating procedure we have followed the signals for m/e 44 (CO₂), m/e 28 (CO) and m/e 18 (H₂O). In Figure 3.2-6 a typical preheating experiment is represented. It can be clearly seen that during the preheating CO₂ and H₂O have been released into the gas phase. Our preheating temperature is only 573 K and this means that the oxygen containing groups such as carboxylic acid, lactone or eventually carboxylic anhydride (Figure 3.2-5) decompose at our conditions.

It is also known that in these O-containing groups, the carbon atom has different oxidation numbers. For example in the carboxylic group, carboxylic anhydride or in the lactone group the oxidation number of carbon is +III, in the carbonyl group - +II, in phenol - +I. According to the thermal stability of the groups (Figure 3.2-5) we can say that those with oxidation number of +III are most unstable, they decompose at lower temperatures than the groups with

3. Results and discussion

C-oxidation number of +II or +I, and that due to our preheating procedure such groups are not present at the surface of the sample before the experiment with NO_2 .

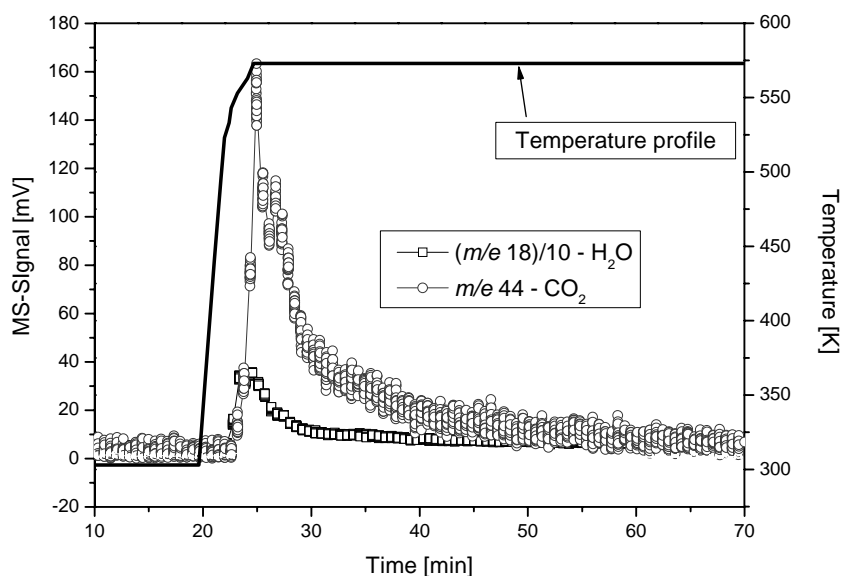


Figure 3.2-6: Preheating of a soot sample up to 570 K

Consequently, we assume that on the surface of the sample basically two types of active sites are present:

- $\{C_{\text{ox}}\}$ – oxidised surface sites with oxidation number of the C-atom of +III
- $\{C_{\text{red}}\}$ – reduced surface sites with oxidation number of the C-atom less than +III,

Due to the heating procedure we should have present only $\{C_{\text{red}}\}$ surface sites before the beginning of the experiment.

3.2.2.2 General calculations

A typical raw measurement for $T = 300$ K, gas phase concentration of NO_2 $C_0 = 4.89 \cdot 10^{11}$ molecules cm^{-3} and soot sample mass $m_s = 6.7$ mg, is shown in Figure 3.2-7. Four different masses have been recorded with the mass spectrometer during this measurement:

- m/e 46 – for NO_2 , as a reactive species,
- m/e 44 – for CO_2 as an eventual gas phase product of the reaction,
- m/e 47 – for HONO as an eventual gas phase product of the reaction,
- m/e 30 – for NO as an eventual gas phase product of the reaction, or for a fragmentation of NO_2 in the mass spectrometer, or for a fragmentation of HONO in the mass spectrometer.

3. Results and discussion

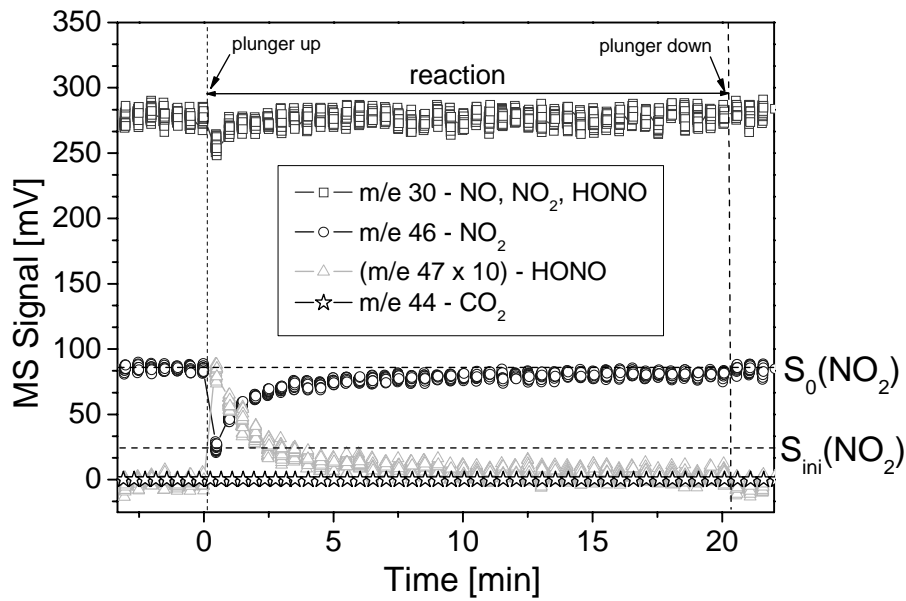


Figure 3.2-7: Typical temporal signal profile for the reaction between NO_2 and ethylene soot at 300K. The trace for m/e 47 (HONO) has been magnified ten times for clarity

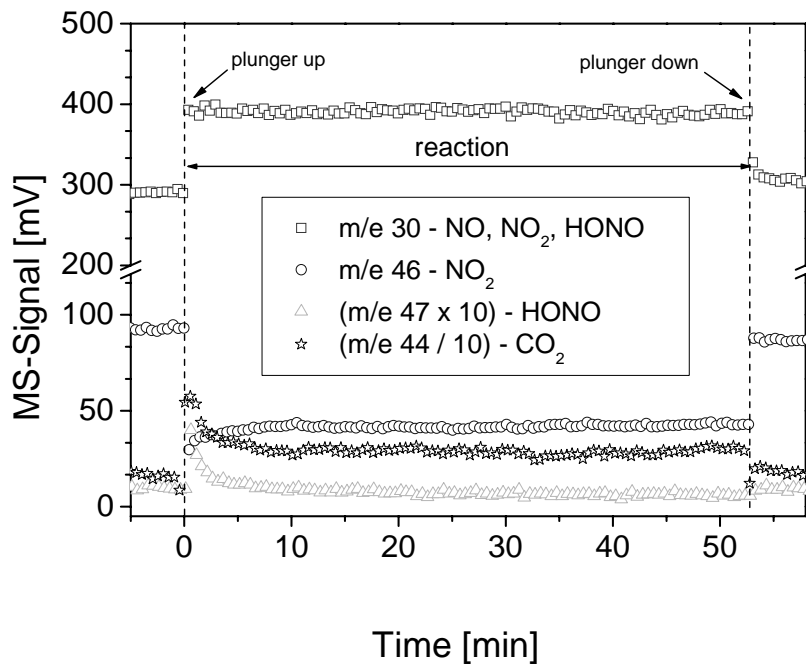


Figure 3.2-8: Typical temporal signal profile for the reaction between NO_2 and ethylene soot at 570K. The trace for m/e 47 (HONO) has been magnified ten times and the trace for m/e 44 (CO_2) has been reduced ten times for clarity

At the beginning of each experiment a constant flow of NO_2 , corresponding to a steady signal S_0 , is introduced into the Knudsen cell, while the sample surface is isolated (plunger down). At time $t = 0$ min the plunger is lifted and the fresh sample surface is exposed to the reactive gas species which results in an immediate decrease of the signal for m/e 46 to the value S_{ini} ,

3. Results and discussion

followed by a constant increase, indicating the constant saturation of the soot surface, and after about 10 min the uptake is reduced to only around 10% of its initial value. The reaction has been followed for about 20 min, after which the sample has been isolated again, the reaction stopped and the signal has taken its initial value $-S_0$.

The behaviour of the NO_2 uptake on soot for the higher temperatures is totally different. In Figure 3.2-8 is represented a measurement for 570 K. The reaction conditions were similar to those for 300 K (gas phase concentration of NO_2 $C_0 = 5.4 \cdot 10^{11}$ molecules cm^{-3} and soot sample mass $m_s = 5.9$ mg) and the same four masses have been followed with the mass spectrometer during the measurement.

Here also a constant flow of NO_2 is introduced into the cell and at time 0 min the plunger is lifted and the sample exposed to the reactive gas. At time $t = 53$ min plunger is closed and the reaction is stopped.

The major differences between 300 K and 570 K measurements can be summarized as follows:

- Evident by the measurement at 570 K is the different behaviour of m/e 46, during the reaction. Here about 10 min after opening the plunger, a steady state is reached and the signal remains constant with time even up to 53 min. In comparison to the measurement at 300K the reaction has been followed only for 20 min and after approximately 10 min exposure we could observe fast complete saturation.

- at 570 K we could observe formation of gas phase CO_2 , indicated from the rise of the signal for m/e 44 which was not the case for the lower temperature.

- at 570 K the signal for m/e 30 has also completely different behaviour after the start of the reaction, which is not the case for 300 K

- From the comparison of the signals for m/e 47 can be estimated that much less HONO is produced at 570 K compared to 300 K.

As already stated before for the interaction of water and mineral dust (soot), the reaction order should be first investigated, in order to be able to implement for further calculations the theory already described in Chapter 2.1.2.

3. Results and discussion

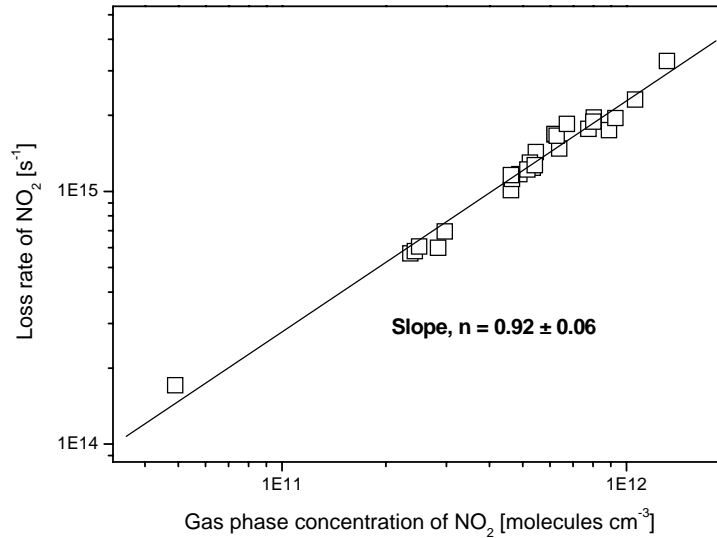


Figure 3.2-9: Reaction order for the interaction of NO₂ and ethylene soot

As it can be seen in Figure 3.2-9, representing the double logarithmic plot of loss rate of NO₂ as a function of gas phase NO₂ concentration, the initial uptake has proved to follow a first order process given from the slope of the fitted line.

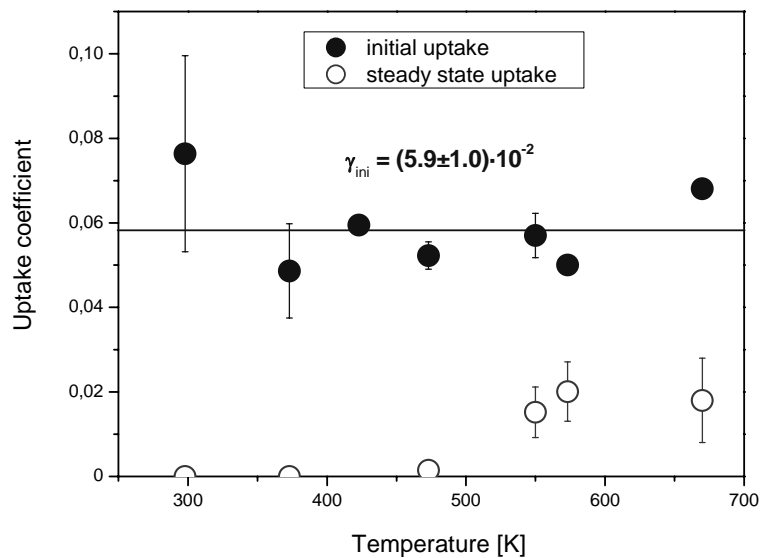


Figure 3.2-10: Initial and steady state uptake as a function of temperature for the reaction of NO₂ and ethylene soot

For the calculation of the uptake coefficients (initial – for the whole temperature interval measured, and steady state – for highest temperatures only) we have used again Equation 2.1-11 and Equation 2.1-12. The calculated initial uptake coefficients have proved to be independent of temperature as can be seen in Figure 3.2-10, resulting in a mean value of $\gamma_{ini} = (5.9 \pm 1) \cdot 10^{-2}$ for the temperature interval measured. On the other hand the steady state uptake

3. Results and discussion

coefficients, calculated for temperatures 470K and above, increase slightly with increasing temperature. Their value is, however, around 3 times lower compared to the value for the initial uptake coefficient.

The initial uptake coefficient has shown also no significant mass dependence, as represented in Figure 3.2-11. For the interval of sample masses measured this means that diffusion of the gas phase molecules into the bulk of the sample can not be observed at our experimental conditions.

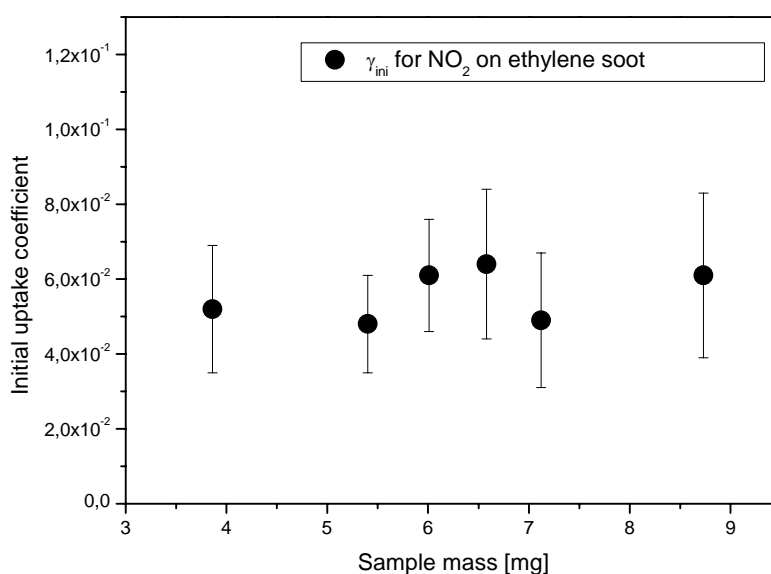


Figure 3.2-11: Initial uptake coefficients for NO₂ on ethylene soot as a function of the sample mass

3.2.2.3 Signal evaluation and product study

As it can be seen from Figure 3.2-7 and Figure 3.2-8 at room temperature no formation of CO₂ is observed, in contrast to 570 K where CO₂ is clearly produced during the reaction. HONO was observed as a gas phase product, indicated from the rise of its signal (*m/e* 47) at both temperatures. But for 300 K the amount of HONO produced is much more than at 570 K, indicated from the area under the peak of the signal during the reaction.

It is clear that the evaluation for the signal at *m/e* 30 is of a great importance in order to assess if NO is formed as a gas phase product due to the reaction between soot and NO₂, or the signal at *m/e* 30 represents only fragmentations from NO₂ and HONO.

3. Results and discussion

In Figure 3.2-12 are represented the main mass peaks for the three gas phase substances (NO_2 , NO and HONO) in our system, and the ratio between them, as we have measured it with our QMS. It can be seen very clearly that they all (NO_2 , NO and HONO) contribute to m/e 30.

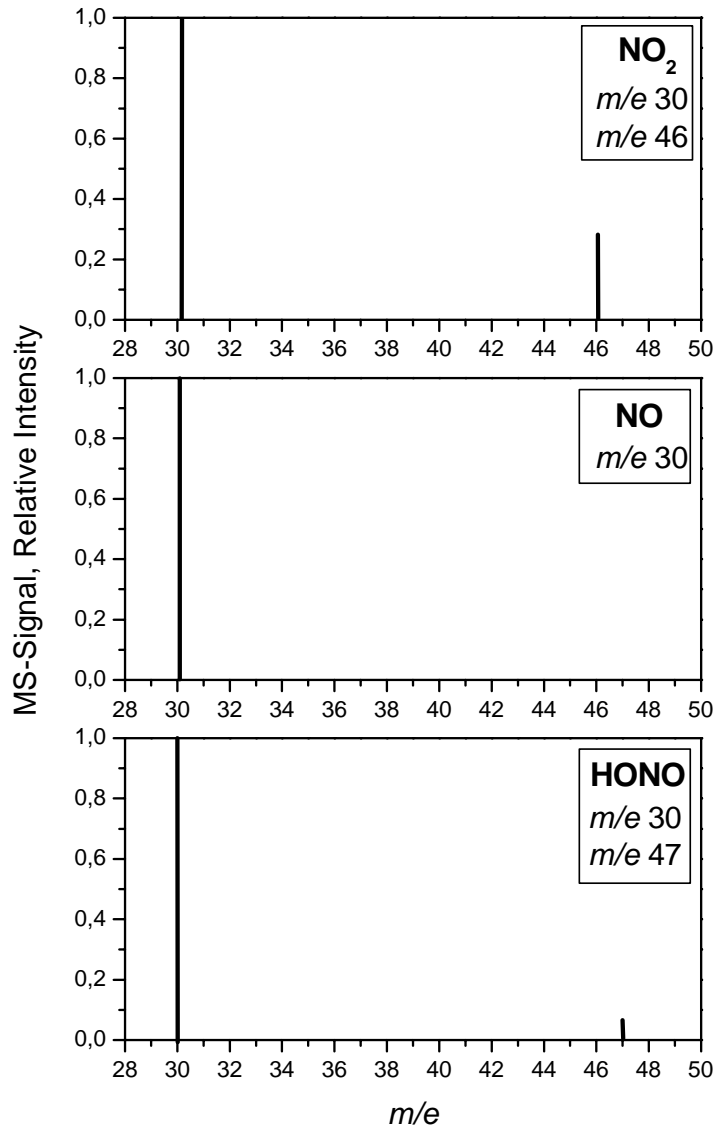
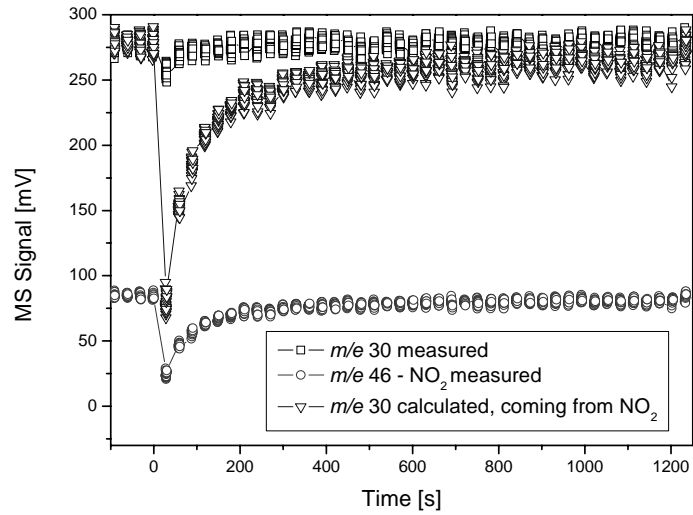
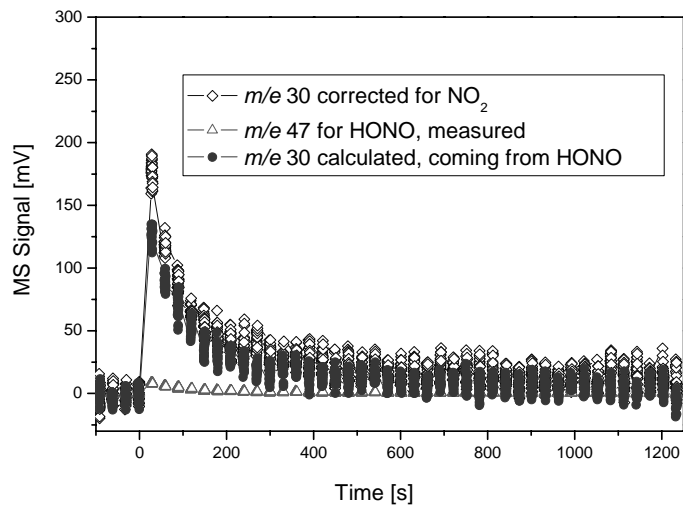


Figure 3.2-12: Mass spectra of NO_2 , NO and HONO and their relative peak intensities

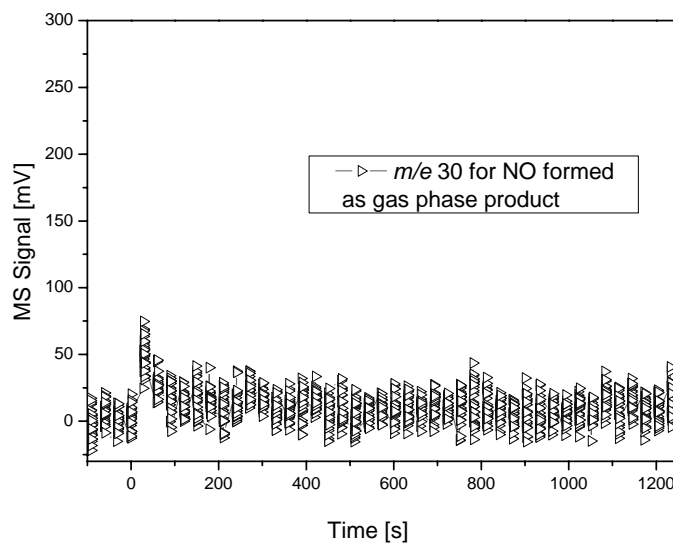
3. Results and discussion



a/.



b/.



c/.

Figure 3.2-13: Evaluation procedure for m/e 30 for the measurement at room temperature in Figure 3.2-7

3. Results and discussion

An example for the procedure we have used for evaluation of m/e 30 is given for the measurement at 300K shown in Figure 3.2-7: As it can be seen, before the reaction (for times from -3 to 0 min) the signal for m/e 46 is accompanied always with a signal for m/e 30, due to the fragmentation of NO_2 in the mass spectrometer and the ratio between these two signals can be calculated before the start of the reaction for each measurement at each temperature. Having in mind this ratio before the reaction, the signal for m/e 30 coming as a fragmentation from NO_2 , during the reaction (0 to 20 min) can be theoretically calculated.

From the experiment shown in Figure 3.2-7, the calculated signal of m/e 30, coming from NO_2 , is given with the open triangles in Figure 3.2-13 a/. Further this theoretical signal can be subtracted from the signal for m/e 30, recorded during the measurement (Figure 3.2-13 a/, open squares). The result (Figure 3.2-13 b/, open diamonds) represents m/e 30, corrected for NO_2 , but still not corrected for HONO. In order to estimate the fragmentation of m/e 30 and m/e 47 in HONO, it has been calibrated separately. The procedure has already been described in detail in Chapter 2.5.4. Knowing the ratio of m/e 30 to m/e 47 in HONO, the signal for m/e 30, coming from HONO could also be calculated (Figure 3.2-13 b/, open circles), and subtracting it from the corrected already for NO_2 signal for m/e 30 (Figure 3.2-13 b/, open diamonds), the signal for m/e 30, coming only from the formation of NO due to the reaction, could be calculated. It is represented in Figure 3.2-13 c/.

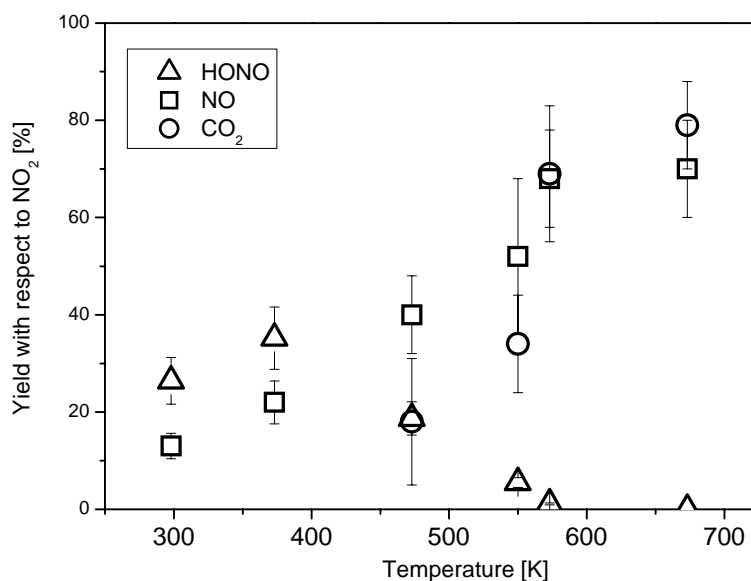


Figure 3.2-14: Yields in % of NO, HONO and CO_2 as a function of the sample temperature for the interaction of NO_2 with ethylene soot

3. Results and discussion

A summary of the product study is represented in Figure 3.2-14 in the form of yields in %, with respect to NO₂ taken up, as a function of temperature. It can be seen the strong temperature dependence of the NO (squares) and HONO yields (triangles). With increasing temperature the NO yield constantly increases, while the HONO yield decreases above 370K with temperature. The formation of CO₂ as a gas phase product can be observed above 470K (circles), and its yield increases with increasing surface temperature, and for the highest temperature it is around unity.

The HONO yields obtained here are relative low, but for the room temperature measurements they are in agreement with literature [Salgado and Rossi, 2002], [Lelievre et al., 2004], [Al-Abadleh and Grassian, 2002]. In good agreement with literature is also the increase of the HONO yield with temperature up to 370 K [Lelievre et al., 2004], [Longfellow et al., 1999]. For the higher temperature measurements no literature data have been found to which we could compare our results.

3.2.2.4 Ion chromatography (IC) results

In Figure 3.2-14 the yields of the products detected only in the gas phase with mass spectrometry are shown. After the end of the experiment in the Knudsen cell, however, the samples have been analysed ion chromatographically, in order to estimate the N-contents of the sample (in the form of nitrate and nitrite) after the reaction with NO₂. For the purpose, before each measurement the sample was diluted in 5 ml slightly alkaline deionised water and then homogenised 30 min up to 1 hour in an ultrasound bath.

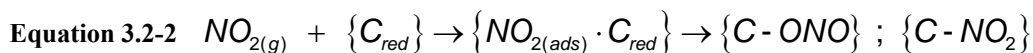
In order to estimate the N-content of the sample before reaction with NO₂, we have performed several IC measurements with not reacted samples. Unfortunately we were able to detect in these reference samples large quantities of nitrite and nitrate, $2.7 \cdot 10^{18} \text{ g}^{-1}$ and $1.3 \cdot 10^{19} \text{ g}^{-1}$ respectively. This is probably due to way of production of the soot samples in the capillary burner, where ethylene is burned in synthetic air, containing of 80 % N₂ and 20 % O₂.

The values of the found nitrate and nitrite species in the reference samples were too high in order to be able to accurately estimate the quantities of N-containing species formed and remaining on the surface due to the reaction with NO₂.

3.2.2.5 Mechanistic interpretation of the reactions

In this Chapter the results are summarised in terms of the mechanistic interpretation of the reaction. We propose the following mechanism, based on our findings:

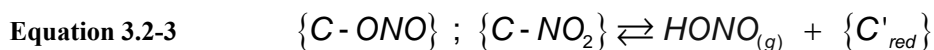
The first step is the irreversible adsorption of NO₂ on the soot surface given by the process:



where {} represent surface species, (ads) – adsorbed species, (g) – gas phase species and {C-ONO}, {C-NO₂} – N containing surface species formed. After the preheating procedure, performed before each experiment, we assume that we have only active oxygen-containing surface sites with oxidation number of +II or +I of the carbon atom, which we have indicated as reduced surface sites {C_{red}}. NO₂ is adsorbed irreversibly on such sites because for all the temperatures measured no desorption of NO₂ from the sample surface could be observed, after the end of the experiment and re-opening the plunger. The formation of N – containing surface groups have been observed via DRIFTS [Al-Abdaleh and Grassian, 2000], [Kirchner et al., 2000]. This first step we can characterise very well with the initial values of the uptake coefficient. γ_{ini} represents the adsorption rate constant of the process on a fresh sample surface, immediately after opening the plunger.

As a next step we assume that the adsorbed NO₂ species reacts further on the soot surface. There are two competitive possibilities depending on temperature:

i. For the lower temperatures (< 470K), we assume that the adsorbed NO₂, in the form of the N containing surface species {C-ONO} and {C-NO₂}, can be converted to HONO (detected in the gas phase), due to a surface reaction:



One modified reduced surface site is released {C'_{red}}, which is not reactive further to NO₂, because for T < 470K we observe fast saturation of the sample surface (Figure 3.2-7), and the uptake of NO₂ is irreversible and ceases with the consumption of all reactive {C_{red}} on the sample surface. We have represented this step as an equilibrium process because there are some literature data about the interaction of HONO and soot leading to NO/NO₂ formation [Alcala-Jornod, 2000], [Stadler and Rossi 2000].

3. Results and discussion

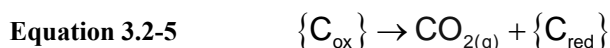
ii. For the higher temperatures ($> 470\text{K}$) we assume that the adsorbed NO_2 , in the form of the N containing surface species $\{\text{C-ONO}\}$ and $\{\text{C-NO}_2\}$, can undergo the following process leading to the oxidation of the sample surface with the reduction of NO_2 to NO :



Here NO is produced in the gas phase, detected mass spectrometrically, and one oxidized surface site $\{\text{C}_{\text{ox}}\}$ is produced.

The branching ratio between i. and ii., as already mentioned, depends on temperature. For the lower temperatures (below 470K) the reaction goes mainly into the i) channel, and then the HONO yield is larger than the NO yield. But with increasing temperature (470K and above) HONO yield decreases, and the reaction goes mainly into the ii) channel, leading to the production of more NO than HONO. The yields of HONO and NO (and their sum) obtained as a function of temperature are relatively low and below 100% (Figure 3.2-14). However, we assume that the rest of the N – yield remains on the surface in the form of surface N – containing groups in agreement with [Al-Abdaleh and Grassian, 2000] and [Kirchner et al., 2000]. We have tried to prove this assumption, by analysing the sample ion chromatographically after the end of the interaction. Unfortunately, as already discussed in Chapter 3.2.2.4, the N-contents of the sample could not be determined free of substantial errors.

For the temperatures of 470 K and above we assume a parallel step leading, eventually, to the consumption of the soot sample:



The released new oxidized surface site $\{\text{C}_{\text{ox}}\}$ from Step ii) decomposes at the higher temperature with the formation of CO_2 , detected with MS, leaving a reduced surface site $\{\text{C}_{\text{red}}\}$ which can react from the beginning with another gas phase NO_2 . For every consumed $\{\text{C}_{\text{ox}}\}$, one CO_2 molecule is produced and one $\{\text{C}_{\text{red}}\}$ is generated, which can react further with one NO_2 molecule, which explains the 100% CO_2 yield with respect to NO_2 at the higher temperatures.

With this process (Equation 3.2-5) the fact can be also explained that at the higher temperatures we observe the formation of steady state, because every released $\{\text{C}_{\text{red}}\}$ reacts

3. Results and discussion

with one NO_2 and the surface is not saturated - the reactive sites are not used with time, but regenerated due to the reaction, which was not the case for temperatures below 470 K.

3.2.3 Discussion

What should be noted here is the completely different behaviour of the two types of soot investigated. Whereas we could observe uptake of NO_2/SO_2 on ethylene soot at our experimental conditions, it was completely inactive towards water, as discussed in Chapter 3.1.1. On the other hand no uptake of NO_2/SO_2 has been observed on kerosene soot, but it was found to be reactive towards water. These findings suggest that the active surface sites, responsible for the interaction of NO_2/SO_2 , are not the same, responsible for the observed uptake of water. Whereas NO_2/SO_2 adsorbs on reduced surface sites $\{C_{red}\}$ and NO_2 is able to oxidize ethylene soot, water should adsorb on oxidised surface sites $\{C_{ox}\}$ present on the sample surface. These findings also implement that the two types of soot have different level of oxidized sites on the surface, due probably to the different way of production, and from atmospheric point of view this means that the freshly produced soot particles in the atmosphere may have completely different behaviour depending very much on the burning conditions and the type of fuel used.

4 SUMMARY AND CONCLUSIONS

Having in mind the aims of this work, postulated previously, we can summarize the obtained results as follows:

Regarding the hydrophilicity of atmospheric aerosol particles we have studied the interaction of mineral dust and soot surfaces with water vapour in the temperature interval $203 \text{ K} < T < 298 \text{ K}$ using a Knudsen cell reactor. For the uptake of water on mineral dust an initial uptake coefficient of $\gamma_{ini} = (6.3 \pm 0.7) \cdot 10^{-2}$ independent of temperature has been determined. In contrast, a strongly temperature dependent desorption rate has been found with desorption rate constants decreasing from $1 \cdot 10^{-3}$ at 265 K to $1 \cdot 10^{-4}$ at 223 K. In addition, relatively high surface coverages have been determined from which an adsorption enthalpy of -40 kJ mol^{-1} is inferred. For the uptake of water on soot the initial uptake coefficient has been found to be independent of temperature with a value of $\gamma_{ini} = (4.7 \pm 0.2) \cdot 10^{-2}$, similar to the case of mineral dust. However, the corresponding desorption rate constants have been found to be three orders of magnitude larger than for mineral dust. Consistent with this finding, low surface coverage with an adsorption enthalpy of -27 kJ mol^{-1} has been derived. A comparison of the uptake kinetics and adsorption enthalpies of water on mineral dust and soot leads to the conclusion that water is much stronger interacting with mineral dust than with soot. In terms of a concept the results suggest, that mineral dust may be regarded as hydrophilic whereas soot is hydrophobic and that fundamental kinetic and thermo-chemical parameters may be used to quantify such concept as hydrophilicity.

Regarding the reactivity of atmospheric aerosol particles we have investigated two different types of soot samples (kerosene and ethylene) and their behaviour towards NO_2 and SO_2 in a wide temperature interval $180 \text{ K} < T < 670 \text{ K}$. It has been found that under these conditions SO_2 undergoes only reversible adsorption/desorption mechanism on the surface, whereas for temperatures above 300 K NO_2 adsorbs irreversibly on the surface, and reacts further leading to formation of NO and HONO as gas phase products with strongly temperature dependent yields. With increasing surface temperature the yield of NO increases gradually, whereas

4. Summary and conclusions

HONO yield decreases. Complementary, for temperatures above 470 K the formation of CO₂ as gas phase product is observed also with gradually increasing yield with increasing temperature. For the mechanistic interpretation of the reaction we have found that NO₂ adsorbs irreversibly on the surface, followed by further formation of HONO or reduction to NO (depending on temperature). Additionally for the higher temperatures, due to the reduction to NO, a new oxidised surface site is formed which releases CO₂ into the gas phase, indicating the ability of NO₂ to oxidize the soot sample followed by its consumption.

REFERENCE LIST

- Aguzzi A. and M. Rossi, (1999), "The Kinetics of the Heterogeneous Reaction of BrONO₂ With Solid Alkali Halides at Ambient Temperature. A Comparison with the Interaction of ClONO₂ on NaCl and KBr", *Physical Chemistry Chemical Physics*, 1(18), 4337-46
- Akhter M., A. Chughtai and D. Smith, (1984), "Reaction of hexane soot with nitrogen dioxide/nitrogen oxide (N₂O₄)", *Journal of Physical Chemistry*, 88(22), 5334-42
- Akhter M., A. Chughtai and D. Smith, (1985a), "The structure of hexane soot I: spectroscopic studies", *Applied Spectroscopy*, 39, 143-153
- Akhter M., A. Chughtai and D. Smith, (1985b), "The structure of hexane soot I: extraction studies", *Applied Spectroscopy*, 39, 154-167
- Akhter M., A. Chughtai and D. Smith, (1991), "Spectroscopic studies of oxidized soots", *Applied Spectroscopy*, 45(4), 653-65
- Al-Abadleh H. and V. Grassian, (2000), "Heterogeneous Reaction of NO₂ on Hexane Soot: A Knudsen Cell and FT-IR Study", *Journal of Physical Chemistry A*, 104(51), 11926-11933
- Alcala-Jornod C., H. Van Den Bergh, M. Rossi, (2000), "Reactivity of NO₂ and H₂O on soot generated in the laboratory: a diffusion tube study at ambient temperature", *Physical Chemistry Chemical Physics*, 2(24), 5584-5593
- Alcala-Jornod C., H. Van Den Bergh and M. Rossi, (2002), *Geophysical Research Letters*, 29, DOI: 10.1029/2001 GL014115
- Alcala-Jornod C. and M. Rossi, (2004), "Chemical kinetics of the interaction of H₂O vapor with soot in the range 190 K ≤ T ≤ 300 K: A diffusion tube study", *Journal of Physical Chemistry A*, 108(48), 10667-10680
- Ammann M., M. Kalberer, D. Jost, L. Tobler, E. Rossler, D. Piguet, H. Gaggeler and U. Baltensperger, (1998a), "Heterogeneous production of nitrous acid on soot in polluted air masses", *Nature (London)*, 395(6698), 157-160

Reference list

- Ammann M., M. Kalberer, F. Arens, V. Lavanchy, H. Gaggeler and U. Baltensperger, (1998b), "Nitrous acid formation on soot particles: surface chemistry and the effect of humidity", *Journal of Aerosol Science*, 29(Suppl. 1, Pt. 2), S1031-S1032
- Arnold F., K. Wohlfrom, M. Klemm, J. Schneider and K. Gollinger, (1998), „First gaseous ion composition measurements in the exhaust plume of a jet aircraft in flight: implications for gaseous sulfuric acid, aerosols, and chemiions”, *Geophysical Research Letters*, 25(12), 2137-2140
- Baldwin A., (1982), "Heterogeneous reactions of sulphur dioxide with carbonaceous particles", *International Journal of Chemical Kinetics*, 14(3), 269-77
- Berresheim H. and W. Jaeschke, (1983), "The contribution of volcanoes to the global atmospheric sulphur budget", *Journal of Geophysical Research*, Vol.88, pp 3732-3740
- Bian H. and Ch. Zender, (2003), "Mineral dust and global tropospheric chemistry: relative roles of photolysis and heterogeneous uptake", *Journal of Geophysical Research – Atmospheres*, 108(D21), ACH 8/1-ACH 8/14
- Blake D. and K. Kato, (1995), "Latitudinal distribution of black carbon soot in the upper troposphere and lower stratosphere", *Journal of Geophysical Research – Atmospheres*, 100(D4), 7195-7202
- Börensén C., U. Kirchner, V. Scheer, R. Vogt and R. Zellner, (2000), "Mechanism and Kinetics of the Reactions of NO₂ or HNO₃ With Alumina As a Mineral Dust Model Compound", *Journal of Physical Chemistry A*, 104(21), 5036-45
- Börensén C., (2001), "Kinetische Und Mechanistische Untersuchungen Der Heterogenen Reaktionen Von Stickoxiden an Mineralstaub-Oberflächen", *Dissertation, Universität Essen*
- Brasseur G., J. Orlando, G. Tyndall, (1999), "Atmospheric chemistry and global change", *Oxford University Press*
- Caloz F., F. Fenter, K. Tabor, and M. Rossi ,(1997), "Paper I: Design and construction of a Knudsen cell reactor for the study of heterogeneous reactions over the temperature range 130-750 K: Performances and limitations", *Review of Scientific Instruments*, 68 (8), 3172-3179
- Caloz F., S. Seisel, F. Fenter and M. Rossi,(1998), „Reactivity of BrNO₂ and ClNO₂ with solid alkali salt substrates”, *Journal of Physical Chemistry A*, 102(38), 7470-7479
- Cantrell W. and G. Ewing, (2001), "Thin Film Water on Muscovite Mica", *Journal of Physical Chemistry B*, 105(23), 5434-5439

Reference list

- Cases J., I. Berend, M. Besson, J. Uriot, F. Thomas and J. Poirier, (1992), "Mechanism of adsorption and desorption of water vapour by homoionic montmorillonite. 1. The sodium-exchanged form", *Langmuir*, 8(11), 2730-9
- Cantrell W. and G. Ewing, (2001), "Thin Film Water on Muscovite Mica", *Journal of Physical Chemistry B*, 105(23), 5434-39
- Chase M., C. Davies, J. Downey, D. Frurip, R. McDonald and A. Syverud, (1985), "JANAF Thermochemical Table, Third Edition, Part I: aluminum-cobalt; Part II: chromium-zirconium", *Journal of Physical and Chemical Reference Data, Supplement*, 14(1), Part I:1-926, Part II: 927-1856
- Chughtai A., W. Welch, M. Akhter, D. Smith, (1990a), "A spectroscopic study of gaseous products of soot-oxides of nitrogen/water reactions", *Applied Spectroscopy*, 44(2), 294-8
- Chughtai A., W. Welch and D. Smith, (1990b), "A spectroscopic and gravimetric study of the soot-nitrogen dioxide/dinitrogen tetroxide reaction at various temperatures", *Carbon*, 28(2-3), 411-21
- Chughtai A., S. Gordon and D. Smith, (1994), "Kinetics of the hexane soot reaction with NO₂/N₂O₄ at low concentration", *Carbon*, 32(3), 405-16
- Chughtai A., N. Miller, D. Smith and J. Pitts, (1999a), "Carbonaceous particle hydration III", *Journal of Atmospheric Chemistry*, 34(2), 259-279
- Chughtai A., G. Williams, M. Atteya, N. Miller and D. Smith, (1999b), "Carbonaceous particle hydration. *Atmospheric Environment*, 33(17), 2679-2687
- Chughtai A., J. M. Kim and D. M. Smith, (2002), "The Effect of Air/Fuel Ratio on Properties and Reactivity of Combustion Soots", *Journal of Atmospheric Chemistry*, 43(1), 21-43
- Czarnetzki A., (2005), "Aufnahme von Wasserdampf auf Salz- und Mineralstauboberflächen", Diplomarbeit, Universität Koblenz – Lindau
- d'Almedia G., (1986), "A model for Saharan dust transport", *Journal of Climatology and Applied Meteorology*, 25, 903-916
- Dandekar A., R. Baker and M. Vannice, (1998), "Characterization of activated carbon, graphitized carbon fibers and synthetic diamond powder using TPD and DRIFTS", *Carbon*, 36(12), 1821-1831
- De Boer J., (1968), "The Dynamical Character of Adsorption", 2nd ed, 240 pp

Reference list

- Delville A., (1995), "Monte Carlo Simulations of Surface Hydration: An Application to Clay Wetting", *Journal of Physical Chemistry*, 99(7), 2033-7
- DeMott P., D. Cziczo, A. Prenni, D. Murphy, S. Kreidenweis, D. Thomson, R. Borys, D. Rogers, (2003a), "Measurements of the concentration and composition of nuclei for cirrus formation", *Proceedings of the National Academy of Sciences of the United States of America*, 100(25), 14655-60
- DeMott P., K. Sassen, M. Poellot, D. Baumgardner, D. Rogers, S. Brooks, A. Prenni and S. Kreidenweis, (2003b), *Geophysical Research Letters*, 30, DOI: 10.1029/2003GL017410
- Desboeufs K., L. Remi, V. Francoise, Ch. Sylvain, (1999), "The pH-dependent dissolution of wind-transported Saharan dust", *Journal of Geophysical Research, [Atmospheres]*, 104(D17), 21287-21299.
- Dios Cancela G., F. Huertas, Taboada, E. Romero, F. Sanchez-Rasero and A. Hernandez Laguna, (1997), "Adsorption of water vapor by homoionic montmorillonites. Heats of adsorption and desorption", *Journal of Colloid and Interface Science*, 185(2), 343-354
- Donaldson K., V. Stone, A. Seaton, and W. MacNee, (2001), "Ambient Particle Inhalation and the Cardiovascular System: Potential Mechanisms", *Environmental Health Perspectives Supplements*, 109(4), 523-527
- Egli R. (1990), "Nitrogen oxide emissions from air traffic", *Chimia*, 44(11), 369-371
- Fahey D., E. Keim, K. Boering, C. Brock, J. Wilson, H. Jonsson, S. Anthony, T. Hanisco, P. Wennberg, et al., (1995), "Emission measurements of the Concorde supersonic aircraft in the lower stratosphere", *Science (Washington, D. C.)*, 270(5233), 70-4
- Figueiredo J., M. Pereira MFR, Freitas M. and Orfao J., (1999), "Modification of the surface chemistry of activated carbons", *Carbon*, 37 (9), 1379-1389
- Finlayson-Pitts B. and J. Pitts Jr., (1986), "Atmospheric Chemistry: Fundamentals and experimental Techniques", John Wiley & Sons, ISBN-0-471-88227-5
- Gerecke A., A. Thielmann, L. Gutzwiller, M. Rossi, (1998), "The chemical kinetics of HONO formation resulting from heterogeneous interaction of NO₂ with flame soot", *Geophysical Research Letters*, 25(13), 2453-2456
- Ginoux P., M. Chin, I. Tegen, J. Prospero, B. Holben, O. Dubovik and S. Lin, (2001), "Sources and distributions of dust aerosols simulated with the GOCART model" *Journal of Geophysical Research – Atmospheres*, 106, 20255-20273

Reference list

- Gleitsmann G. and R. Zellner, (1999), „The aerosol dynamics of H₂O-H₂SO₄-HNO₃ mixtures in aircraft wakes. A modeling study”, *Physical Chemistry Chemical Physics*, 1(24), 5503-550
- Global NEST – Global Network for Environmental Science and Technology, (2006), “Discussion on global issues – Aerosol particles and global climate change”, http://www.gnest.org/Global_Issues/Aerosol.htm
- Golden D., G. Spokes and S. Benson (1973), "Pyrolyse Bei Sehr Kleinem Druck (VLPP): Eine Vielseitige Kinetische Methode", *Angewandte Chemie*, no. 85, 602-14
- Gomes L. and D. Gillette, (1993), “A comparison of characteristics of aerosol from dust storms in Central Asia with soil-derived dust from other regions”, *Atmospheric Environment, Part A: General Topics*, 27A(16), 2539-44
- Granier C., P. Artaxo, C. Reeves, (2004), “Advances in global research, Vol. 18: Emissions of atmospheric trace compounds”, Kluwer Academic Publishers
- Grassian, V. (2001), “Heterogeneous uptake and reaction of nitrogen oxides and volatile organic compounds on the surface of atmospheric particles including oxides, carbonates, soot and mineral dust: implications for the chemical balance of the troposphere”, *International Reviews in Physical Chemistry*, 20(3), 467-548
- Goodman A., P. Li, C. Usher and V. Grassian, (2001), "Heterogeneous Uptake of Sulfur Dioxide on Aluminum and Magnesium Oxide Particles", *Journal of Physical Chemistry A*, 105(25), 6109-20
- Guelle W, Y. Balkanski, M. Schulz, B. Marticorena, G. Bergametti, C. Moulin, R. Arimoto, K. Perry, (2000) “Modeling the atmospheric distribution of mineral aerosol: comparison with ground measurements and satellite observations for yearly and synoptic timescales over the North Atlantic”, *Journal of Geophysical Research – Atmospheres*, 105(D2), 1997-2012
- Hagen D., M. Trueblood, D. White, (1989), “Hydration properties of combustion aerosols”, *Aerosol Science and Technology*, 10(1), 63-9
- Hanisch F. and J. Crowley, (2003), "Heterogeneous Reactivity of NO and HNO₃ on Mineral Dust in the Presence of Ozone", *Physical Chemistry Chemical Physics*, 5(5), 883-87.
- Haywood J. and K. Shine, (1995), “The effect of anthropogenic sulfate and soot aerosol on the clear sky planetary radiation budget”, *Geophysical Research Letters*, 22, 603–606
- Hendricks J., B. Karcher, A. Doppelheuer, J. Feichter, U. Lohmann, D. Baumgardner, (2004), “Simulating the global atmospheric black carbon cycle: a revisit to the contribution of aircraft emissions” *Atmospheric Chemistry and Physics*, 4, 2521-2541

Reference list

- Hensen E., T. Tambach, A. Bliok and B. Smit, (2001), "Adsorption isotherms of water in Li-, Na-, and K-montmorillonite by molecular simulation", *Journal of Chemical Physics*, 115(7), 3322-3329
- Hernandez M., (1996), "Distribution and dynamics of inorganic nitrogen compounds in the troposphere of continental, coastal, marine and Arctic areas", *Reports on polar research*, 184
- Hesse D., (1988), "Analyse der Abgase russender Kohlenwasserstoff-luft-flammen", Dissertation, George-August University, Göttingen, Germany
- Horvath H., (1993), "Atmospheric Light Absorption – A Review", *Atmospheric Environment*, 27A, 293–317
- Hung H., A. Mlinowski, S. Martin, (2003), "Kinetics of heterogeneous ice nucleation on the surfaces of mineral dust cores inserted into aqueous ammonium sulfate particles", *Journal of Physical Chemistry A*, 107(9), 1296-1306
- Husar R., D. Tratt, B. Schichtel, S. Falke, F. Li, D. Jaffe, S. Gasso, T. Gill, N. Laulainen, F. Lu, M. Reheis, Y. Chun, D. Westphal, B. Holben, C. Gueymard, I. McKendry, N. Kuring, G. Feldman, C. McClain, R. Frouin, J. Merrill, D. DuBois, F. Vignola, T. Murayama, S. Nickovic, W. Wilson, K. Sassen, N. Sugimoto, W. Malm, (2001), "Asian dust events of April 1998", *Journal of Geophysical Research - Atmospheres*, 106(D16), 18317-18330
- ICAL, (2005), Image and Chemical Analysis Laboratory at Montana State University, Department of Physics. <http://www.physics.montana.edu/ICAL/ical.html>
- Israel G., C. Schlums, R. Treffeisen and M. Pesch, (1996), „Rußimmissionen in Berlin – Herkunftsbestimmung, KFZ-Flottenemissionsfaktoren, Vergleichbarkeit von Probenahmemethoden“, *Abschlußbericht B281KF*, VDI Verlag, Düsseldorf
- Jacob D., (1999), "Introduction to atmospheric Chemistry", Princeton University Press
- Jacquot F., V. Logie, J. Brilhac and P. Gilot, (2002), "Kinetics of the oxidation of carbon black by NO₂. Influence of the presence of water and oxygen", *Carbon*, 40(3), 335-343
- Jaenicke R., (1993), "Tropospheric aerosols. In: Hobbs PV (ed) *Aerosol-Cloud-Climate Interactions*", Academic Press, San Diego, California, pp 1-31
- Jeguirim M., V. Tschamber, J. Brilhac, and P. Ehrburger, (2004), „Interaction mechanism of NO₂ with carbon black: effect of surface oxygen complexes", *Journal of Analytical and Applied Pyrolysis*, 72(1), 171-181

Reference list

- Johnson K., B. Zuberi, L. Molina, M. Molina, M. Iedema, J. Cowin, D. Gaspar, C. Wang, A. Laskin, (2005), "Processing of soot in an urban environment: case study from the Mexico City Metropolitan Area", *Atmospheric Chemistry and Physics Discussions*, 5, 5585-5614
- Jonas P. and H. Rohde, (1995), "Climate Change", Editor J. Houghton, Cambridge University Press, New York
- Kalberer M., M. Ammann, H. Gaggeler and U. Baltensperger, (1999), "Adsorption of NO₂ on carbon aerosol particles in the low ppb range", *Atmospheric Environment*, 33(17), 2815-2822
- Kandylas I., O. Haralampous and G. Koltsakis, (2002), "Diesel Soot Oxidation with NO₂: Engine Experiments and Simulations", *Industrial & Engineering Chemistry Research*, 41(22), 5372-5384
- Karagulian F., C. Santschi, M. Rossi, (2006), "The heterogeneous chemical kinetics of N₂O₅ on CaCO₃ and other atmospheric mineral dust surrogates", *Atmospheric Chemistry and Physics*, 6(5), 1373-1388
- Khalfi A. and P. Blanchart, (1999), "Desorption of water during the drying of clay minerals. Enthalpy and entropy variation", *Ceramics International*, 25(5), 409-414
- Kirchner U., V. Scheer and R. Vogt, (2000), "FTIR Spectroscopic Investigation of the Mechanism and Kinetics of the Heterogeneous Reactions of NO₂ and HNO₃ with Soot", *Journal of Physical Chemistry A*, 104(39), 8908-8915
- Kleffmann J., K. Becker, M. Lackhoff, and P. Wiesen, (1999), "Heterogeneous conversion of NO₂ on carbonaceous surfaces", *Physical Chemistry Chemical Physics*, 1(24), 5443-5450
- Kleffmann J. and P. Wiesen, (2005), "Heterogeneous conversion of NO₂ and NO on HNO₃ treated soot surfaces: Atmospheric implications", *Atmospheric Chemistry and Physics*, 5(1), 77-83
- Köhler B., V. Nicholson, H. Roe and E. Whitney, (1999), "A Fourier transform infrared study of the adsorption of SO₂ on n-hexane soot from -130 degrees to -40 degrees C", *Journal of Geophysical Research – Atmospheres*, 104 (D5), 5507-5514
- Kortüm G., (1969), "Reflectance Spectroscopy. Principles, Methods, Applications", Springer Verlag, Berlin and New York, 366 pp
- Kreyling W. and G. Scheuch, (2000), "Clearance of particles deposited in the lungs", In: *Particle-Lung Interactions*, pp. 323–376, P. Gehr and J. Heyder
- Kubelka P. and F. Munk, (1931), *Zeitschrift für Technische Physik*, 12, 593
- Kubelka P. (1948), *Journal of Optical Society of America*, 38, 448

Reference list

- Kureti S., S. Nobst and H. Bockhorn, (2003a), "Catalyzed simultaneous conversion of soot and nitrogen oxides to nitrogen and carbon dioxide in the exhaust gas of diesel engines", *Chemie Ingenieur Technik*, 75(8), 1050-1051
- Kureti S., K. Hizbullah and W. Weisweiler, (2003b), „Simultaneous catalytic removal of nitrogen oxides and soot from diesel exhaust gas over potassium modified iron oxide”, *Chemical Engineering & Technology*, 26(9), 1003-1006
- Kureti S., W. Weisweiler and K. Hizbullah, (2003c), "Simultaneous conversion of nitrogen oxides and soot into nitrogen and carbon dioxide over iron containing oxide catalysts in diesel exhaust gas", *Applied Catalysis, B: Environmental*, 43(3), 281-291
- Lammel G. and T. Novakov, (1995), "Water nucleation properties of carbon black and diesel soot particles", *Atmospheric Environment*, 29(7), 813-23
- Lelievre S., Y. Bedjanian, G. Laverdet, G. Le Bras, (2004), "Heterogeneous Reaction of NO₂ with Hydrocarbon Flame Soot", *Journal of Physical Chemistry A*, 108(49), 10807-10817
- Longfellow C., A. Ravishankara, D. Hanson, (1999), "Reactive uptake on hydrocarbon soot: Focus on NO₂", *Journal of Geophysical Research – Atmospheres*, 104(D11), 13833-13840
- Mertes S. and A. Wahner, (1995), "Uptake of Nitrogen Dioxide and Nitrous Acid on Aqueous Surfaces", *Journal of Physical Chemistry*, 99(38), 14000-14006
- Mochida M., J. Hirokawa and H. Akimoto, (2000), "Unexpected Large Uptake of O₃ on Sea Salts and the Observed Br₂ Formation", *Geophysical Research Letters*, 27(17), 2629-32
- Muckenhuber H. and H. Grothe, (2006), "The heterogeneous reaction between soot and NO₂ at elevated temperature", *Carbon*, 44(3), 546-559
- Nelson P. and B. Haynes, (1994), "Hydrocarbon-NO_x interactions at low temperatures - 1. conversion of NO to NO₂ promoted by propane and the formation of HNCO", *Symposium (International) on Combustion*, [Proceedings], 25th, 1003-10
- Newman A., (1983), "The specific surface of soils determined by water sorption", *Journal of Soil Science*, 34(1), 23-32
- Novakov T., (1982), "Soot-catalyzed atmospheric reactions in heterogeneous atmospheric chemistry", *Geophys. Monogr. Serv.*, vol., edited by D.R. Schryer, pp. 215-220, AGU, Washington, D.C.

Reference list

- Olivier J., A. Bouwmann, C. Van der Maas, J. Berowski, C. Veldt, J. Bloos, A. Visschedijk, P. Zandveld and J. Haverlag, (1996), "Description of EDGAR Version 2.0: A set of global emission inventories of greenhouse gases and ozone depleting substances for all anthropogenic and most biogenic sources on a per country basis and on 1° x 1° grid" RIVM, Bilthoven, December 1996, RIVM report nr. 771060 002 / TNO-MEP report nr. R96/119
- Olivier J., A. Bouwmann, J. Berowski, C. Veldt, J. Bloos, A. Visschedijk, P. Zandveld, C. Van der Maas, (1999), "Sectoral emission inventories of greenhouse gases for 1990 on a per country basis as well as 1° x 1°" *Environmental Science and Policy*, 2, 241 – 246
- Olivier J. and J. Berowski, (2001), "Global Emissions sources and sinks. In: *The Climate System*", Editors J. Berowski, R. Guicherit, and B. Heij, pp 33-78. A.A. Balkema Publishers/Swets&Zeitlinger Publishers, Lisse, The Netherlands, ISBN 90 5809 255 0, 2001
- Olivier J., J. Berowski, J. Peters, J. Bakker, A. Visschedijk, and J. Bloos, (2001), "Applications of EDGAR. Including a description of EDGAR v3.0: reference database with trend data for 1970-1995", RIVM report 773301 001 / NRP report 410200 052
- Otake T., S. Tone, Y. Yokota and K. Yoshimura, (1971), "Kinetics of sulfur dioxide oxidation over activated carbon", *Journal of Chemical Engineering of Japan*, 4(2), 155-9
- Petzold A., J. Strom, S. Ohlsson, F. Schroder, (1998), "Elemental composition and morphology of ice-crystal residual particles in cirrus clouds and contrails", *Atmospheric Research*, 49(1), 21-34
- Petzold A., A. Döpelheuer, C. Brock and F. Schröder, (1999), "In situ observations and model calculations of black carbon emission by aircraft at cruise altitude", *Journal of Geophysical Research – Atmospheres*, 104(D18), 22171-22181
- Picaud S., P. Hoang, S. Hamad, J. Mejias and S. Lago, (2004), "Theoretical study of the adsorption of water on a model soot surface: II. Molecular dynamics simulations", *Journal of Physical Chemistry B*, 108(17), 5410-5415
- Pope C. and D. Dockery, (1999), "Epidemiology of Particle Effects, in: *Air Pollution and Health*", Edited by: S. Holgate, J. Samet, H. Koren, and R. Maynard, pp. 673–705, Academic Press
- Popovitcheva O., M. Trukhin, N. Persiantseva and N. Shonija, (2001), "Water adsorption on aircraft-combustor soot under young plume conditions", *Atmospheric Environment*, 35(9), 1673-1676
- Popovicheva O., N. Persiantseva, N. Shonia, N. Zubareva, A. Starik, E. Loukhovitskaya, A. Secundov, D. Usenko, V. Zakharov, J. Suzanne, D. Ferry and B. Demirdjian, B., (2003a), "Aircraft engine soot: characteristic properties as cloud condensation nuclei in upper troposphere", *Combustion and*

Reference list

- Atmospheric Pollution, International Symposium on Combustion and Atmospheric Pollution, St. Petersburg, Russian Federation, July 8-11, 2003
- Popovicheva O, N. Persiantseva, B. Kuznetsov, T. Rakhmanova, N. Shonija, J. Suzanne and D. Ferry, (2003b), "Microstructure and Water Adsorbability of Aircraft Combustor Soots and Kerosene Flame Soots: Toward an Aircraft-Generated Soot Laboratory Surrogate", *Journal of Physical Chemistry A*, 107(47), 10046-10054
- Popovicheva O., N. Persiantseva, E. Lukhovitskaya, N. Shonija, N. Zubareva, B. Demirdjian, D. Ferry, J. Suzanne, (2004), "Aircraft engine soot as contrail nuclei", *Geophysical Research Letters*, 31(11), L11104/1-L11104/4
- Pruppacher H. and Klett, (1980), "Microphysics of clouds and precipitation", Reidel Publishing Company, Dordrecht, Boston, London
- Reimer L., (1998), "Scanning Electron Microscopy: Physics of Image Formation and Microanalysis", 2nd Edition, Springer, ISBN-3-540-63976-4
- Rogaski C., D. Golden and L. Williams, (1997), "Reactive uptake and hydration experiments on amorphous carbon treated with NO₂, SO₂, O₃, HNO₃, and H₂SO₄", *Geophysical Research Letters*, 24(4), 381-384
- Rose D., B. Wehner, M. Ketzler, C. Engler, J. Voigtländer, T. Tuch, A. Wiedensohler, (2005), "Atmospheric number size distributions of soot particles and estimation of emission factors", *Atmospheric Chemistry and Physics Discussions*, 5, 10125-10154
- Prack E., (1993), "An introduction to process visualisation capabilities and considerations in the Environmental Scanning Electron Microscope (ESEM)", *Microscopy Research and Technique*, 25, 4887-492
- Projekt PAZI, Partikel aus Flugzeugtriebwerken und ihr Einfluss auf Kondensstreifen, Zirruswolken und Klima (PAZI), Endbericht, Deutsches Zentrum für Luft- und Raumfahrt (DLR), Cologne, 2003, <http://www.pa.op.dlr.de/pazi/pazi-end.pdf>.
- Raschke E. and K. Warrach, (2001), „Water cycles in the climate system“, *Wissenschaftliche Auswertungen: Climate of the 21st century – changes and risks*, Editors: J. Lozàn, H. Graßl and P. Hupfer, 184-189
- Reinhardt H. and R. Zellner, (2003) "DRIFTS-Studies of the Interactions of HNO₃ With Ice and HCl (HNO₃)-Hydrate Surfaces at Temperatures Around 165 K", *Journal of Molecular Structure*, 661, 567-77
- Rognon P., G. Coude-Gaussen, M. Revel, F. Grousset and P. Pedemay, (1996), "Holocene Saharan dust deposition on the Cape Verde Islands: sedimentological and Nd-Sr isotopic evidence", *Sedimentology*, 43(2), 359-366

Reference list

- Russel A., G. McRae, G. Cass, (1985), "The dynamics of nitric acid production and the fate of nitrogen oxides", *Atmospheric Environment*, Vol. 19, No. 6, pp. 893-903
- Saathoff H., K. Naumann, N. Riemer, S. Kamm, O. Mohler, U. Schurath, H. Vogel, B. Vogel, (2001), "The loss of NO₂, HNO₃, NO₃/N₂O₅, and HO₂/HOONO₂ on soot aerosol: a chamber and modeling study", *Geophysical Research Letters*, 28(10), 1957-1960
- Salgado M. and M. Rossi, (2002), "Flame soot generated under controlled Combustion conditions: heterogeneous reaction of NO₂ on hexane soot", *International Journal of Chemical Kinetics*, 34(11), 620-631
- Schütz L. and M. Seibert, (1987), "Mineral aerosols and source identification", *Journal of Aerosol Science*, 18(1), 1-10
- Schulz M., (2001), "Role of the Natural and Anthropogenic Tropospheric Aerosols in Climate Evolutions", *Wissenschaftliche Auswertungen*, ISBN 3-00-006227-0
- Schumann U., J. Stroem, R. Busen, R. Baumann, K. Gierens, M. Krautstrunk, F. Schroeder and J. Stingl, (1996), "In situ observations of particles in jet aircraft exhausts and contrails for different sulfur-containing fuels", *Journal of Geophysical Research – Atmospheres*, 101(D3), 6853-6869
- Schurath U. and K. Naumann, (1998), "Heterogeneous processes involving atmospheric particulate matter", *Pure & Applied Chemistry*, 70, 1353-1361
- Seinfeld J. and S. Pandis, (1998), "Atmospheric chemistry and physics: From air pollution to climate change", John Wiley, New York
- Seisel S., B. Flueckiger and M. Rossi, (1998), "The heterogeneous reaction of N₂O₅ with HBr on ice. Comparison with N₂O₅+HCl", *Berichte der Bunsen-Gesellschaft*, 102(6), 811-820
- Seisel S., Y. Lian, T. Keil, M. Trukhin and R. Zellner, (2004a), "Kinetics of the interaction of water vapour with mineral dust and soot surfaces at T = 298 K", *Physical Chemistry Chemical Physics*, 6(8), 1926-1932
- Seisel S., C. Börensen, R. Vogt and R. Zellner, (2004b), "The Heterogeneous Reaction of HNO₃ on Mineral Dust and Gamma-Alumina Surfaces: a Combined Knudsen Cell and Drifts Study", *Physical Chemistry Chemical Physics*, 6(24), 5498-508
- Seisel S., T. Keil, Y. Lian and R. Zellner, (2006), "Kinetics of the uptake of SO₂ on mineral oxides: Improved initial uptake coefficients at 298 K from pulsed Knudsen cell experiments", *International Journal of Chemical Kinetics*, 38(4), 242-249

Reference list

- Setiabudi A., M. Makkee and J. Moulijn, (2004), "The role of NO₂ and O₂ in the accelerated combustion of soot in diesel exhaust gases", *Applied Catalysis, B: Environmental*, 50(3), 185-194
- Sheridan P. and I. Musselman, (1985), "Characterization of aircraft-collected particles present in the Arctic aerosol; Alaskan Arctic, spring 1983", *Atmospheric Environment (1967-1989)*, 19(12), 2159-66
- Singh H. B., (1987), "Reactive nitrogen in the troposphere. Chemistry and transport of NO_x and PAN", *Environmental Science & Technology*, 21(4), 320-327
- Smith D. and A. Chughtai, (1995), "The surface structure and reactivity of black carbon", *Colloids and Surfaces A: Physicochemical and Engineering Aspects*, 105(1), 47-77
- Stadler D. and M. Rossi, (2000), "The reactivity of NO₂ and HONO on flame soot at ambient temperature: The influence of combustion conditions", *Physical Chemistry Chemical Physics*, 2(23), 5420-5429
- Tabazadeh A., M. Jacobson, H. Singh, O. Toon, J. Lin, R. Chatfield, A. Thakur, R. Talbot, J. Dibb, (1998), "Nitric acid scavenging by mineral and biomass burning aerosols", *Geophysical Research Letters*, 25(22), 4185-418
- Tabor K., L. Gutzwiller, M. Rossi, (1993), "The heterogeneous interaction of nitrogen dioxide with amorphous carbon", *Geophysical Research Letters*, 20(14), 1431-4
- Tabor K., L. Gutzwiller, M. Rossi, (1994), "Heterogeneous Chemical Kinetics of NO₂ on Amorphous Carbon at Ambient Temperature", *Journal of Physical Chemistry*, 98(24), 6172-86
- Tegen I. and I. Fung, (1994), "Modeling of mineral dust in the atmosphere – sources, transport and optical thickness", *Journal of Geophysical Research Atmospheres*, 99 (D11): 22897-22914
- Toon O., Miake-Lye, and C. Richard, (1998), "Subsonic Aircraft: Contrail and Cloud Effects Special Study (SUCCESS)", *Geophysical Research Letters*, 25(8), 1109-1112
- Ullerstam M., M. Johnson, R. Vogt and E. Ljungstroem, (2003), "DRIFTS and Knudsen Cell Study of the Heterogeneous Reactivity of SO₂ and NO₂ on Mineral Dust", *Atmospheric Chemistry and Physics*, 3, 2043-51
- Umann B, Arnold F, Schaal C, M. Hanke, J. Uecker, H. Aufmhoff, Y. Balkanski, R. Van Dingenen, (2005) "Interaction of mineral dust with gas phase nitric acid and sulfur dioxide during the MINATROC II field campaign: first estimate of the uptake coefficient γ_{HNO_3} from atmospheric data", *Journal of Geophysical Research – Atmospheres*, 110(D22), Art. No. D22306/1-D22306/17

Reference list

- Vogt R. and B. Finlayson-Pitts, (1994), "A Diffuse-Reflectance Infrared Fourier-Transform Spectroscopic (DRIFTS) Study of the Surface-Reaction of NaCl With Gaseous NO₂ and HNO₃", *Journal of Physical Chemistry*, 98(14), 3747-55
- Warneck P., (1988), "Chemistry of the natural atmosphere", *Internat. Geophysic. Ser.*, 41, Academic Press, New York
- Wayne R. et al., (1990), "The nitrate radical: physics, chemistry and the atmosphere", *Air Pollution Research report 31*, Commission of the European Communities
- Wayne R., (1991), "Chemistry of atmospheres", Second Edition, Clarendon Press – Oxford
- Weingartner E, C. Keller and W. Stahel, (1997), "Aerosol emission in a road tunnel", *Atmospheric Environment*, 31(3), 451-462
- Weiss J. and T. Weiss, (2004), "Handbook of Ion Chromatography", Third, Completely Revised and Enlarged Edition, Two Volumes, ISBN: 3-527-28701-9
- Wuebbles D., D. Maidn, R. Selas Jr, S. Baughcum, M. Metwally, A. Mortlock, (1993), "Emission scenarios development: Report of the emissions scenarios committee. In: The Atmospheric effect of Stratospheric Aircraft: A Third Programm report", Editors R. Stolarski, H. Wesocky, NASA Reference publication 1313, NASA Office of Space Science and Applied, Hampton VA, USA.
- Ye S., W. Zhou, J. Song, B. Peng, D. Yuan, Y. Lu, and P. Qi, (1999), "Ambient Particle Inhalation and the Cardiovascular System: Potential Mechanisms", *Atmospheric Environment*, 34, 419–429
- Yu F. and Turco, R, (1997), "The role of ions in the formation and evolution of particles in aircraft plumes", *Geophysical Research Letters*, 24(15), 1927-1930
- Zellner R., (1999), "Global Aspects of atmospheric Chemistry", *Topics in Physical Chemistry 6*, Guest Editor Zellner R, edited by Baumgärtel H., Grünbein W., Hensel F., Springer, Darmstadt
- Zettlemoyer A. and K. Narayan, (1966), "Adsorption from solution by graphite surfaces", *Chemistry and Physics of Carbon*, 2, 197-224

CURRICULUM VITAE

Personal data

Name	Aneta Kirilova Pashkova
Birth date	August, 10th 1977
Birth place	Asenovgrad, Bulgaria
Citizenship	Bulgarian
E-mail	ani@argon.acad.bg

Education

2002 – 2006	Scientific coworker (PhD student) at the University of Duisburg-Essen
1996 – 2001	Master's degree in chemistry at University of Plovdiv, Bulgaria
1991 – 1996	High school with humanitarian profile, Plovdiv, Bulgaria

Research interests

Atmospheric chemistry
Surface chemistry
Heterogeneous processes – kinetic and thermodynamic

Languages

Bulgarian	native speaker
English	fluent
German	fluent
Russian	good
Spanish	beginner

PC skills

Standard software	Windows 98/NT/2000/XP, MS Office
Special software	Microcal Origin® - data analysis OPUS – spectroscopy software

PUBLICATIONS

Peer-Reviewed Papers

1. Sabine Seisel, Aneta Pashkova, Yu Lian, and Reinhard Zellner, *Water Uptake on Mineral Dust and Soot: A Fundamental View on the Hydrophilicity of Atmospheric Particles*, Faraday Discussions, 130, 437-451, (2005).
2. Sabine Seisel, Aneta Pashkova, and Reinhard Zellner, *The formation of NO and HONO in the reaction of NO₂ with soot surfaces at elevated temperatures*, in preparation.

Oral presentations

1. Sabine Seisel, Thorsten Keil, Aneta Pashkova, Maxim E. Trukhin, and Reinhard Zellner, *Kinetic and Mechanistic Studies of the Uptake of H₂O and NO_y on Soot Surfaces*, 17th International Symposium on Gas Kinetics, Essen, Germany, August 2002.
2. Sabine Seisel, Yu Lian, Aneta Pashkova, and Reinhard Zellner, *Water Uptake, Hydrophilicity and Cloud Condensation Properties of Mineral Dust and Soot Particles*, ISAIE 2004 - Ice, Soot and Aviation: what Impact on the Environment, La Londe, France, May 2004.
3. Sabine Seisel, Aneta Pashkova, and Reinhard Zellner, *Water Uptake on Soot Particles: A Molecular View on Hydrophilicity*, 8th International Conference on Carbonaceous Particles in the Atmosphere, Vienna, Austria, September 2004.
4. Aneta Pashkova, Sabine Seisel and Reinhard Zellner, *Reaktion von NO₂ auf Rußoberflächen im Temperaturbereich von 300 bis 700 K*, Bunsentagung 2006, Erlangen, Germany, May 2006.

Poster presentations

1. Sabine Seisel, Thorsten Keil, Maxim E. Trukhin, Aneta Pashkova, and Reinhard Zellner, *Kinetics of the Interaction of Atmospheric Trace Gases with Soot Surfaces*, International Symposium on Combustion and Atmospheric Pollution, St. Petersburg, Russia, July 2003.
2. Aneta Pashkova, Sabine Seisel and Reinhard Zellner, *The Heterogeneous Reactions of NO₂ and SO₂ with Soot in the Temperature Range 200 K to 700 K*, General Assembly of the European Geosciences Union, Vienna, Austria, April 2006